Master's thesis

NTNU
Norwegian University of Science and Technology
Faculty of Natural Sciences
Department of Materials Science and Engineering

Solveig Høgåsen

The effect of compaction and thermal treatment in the recovery of coated aluminium scrap through FTIR off-gas analysis and remelting in molten heel

Master's thesis in Chemical Engineering and Biotechnology
Supervisor: Gabriella Tranell
Co-supervisor: Anne Kvithyld and Alicia Vallejo-Olivares
June 2022

Tom Gertjegerdes (RWTH Aachen)

NTNU
Norwegian University of
Science and Technology

Solveig Høgåsen

The effect of compaction and thermal treatment in the recovery of coated aluminium scrap through FTIR off-gas analysis and remelting in molten heel

Master's thesis in Chemical Engineering and Biotechnology
Supervisor: Gabriella Tranell
Co-supervisor: Anne Kvithyld and Alicia Vallejo-Olivares
June 2022

Norwegian University of Science and Technology
Faculty of Natural Sciences
Department of Materials Science and Engineering

NTNU
Norwegian University of
Science and Technology

Preface

This master's thesis was written and submitted in the course "TMT4900: Material Chemistry and Energy Technology, Master's Thesis" as the final fulfilment of the five-year master's degree program in Chemical Engineering and Biotechnology at the Norwegian University of Science and Technology (NTNU).

The thesis work was performed from January to June 2022 as a continuation of work conducted by the author during a specialisation project in the autumn of 2021. Experimental work was performed at laboratories at the Department of Material Science (NTNU) and IME Process Metallurgy and Metal Recycling RWTH Aachen University (RWTH Aachen). The author performed all laboratory work partly in collaboration with Alicia Vallejo-Olivares (NTNU) and Tom Gertjegerdes (RWTH Aachen).

I declare that this is independent work according to the exam regulations of NTNU.

Trondheim, June 2022
Solveig Høgåsen

Acknowledgements

First of all, I would like to show my gratitude for five memorable and instructive years in Trondheim at the Norwegian University of Science and Technology. The experience and knowledge I have gained and the friends I have made will stick with me long after departing from this city when heading toward new adventures.

I would like to thank NTNU, the Alpakka project, and the EXTREME projects for allowing me to immerse myself in the field of aluminium recycling and the possibility of travelling to Aachen in Germany for the conduction of experiments at RWTH Aachen. I would like to thank Tom Gertjegerdes (RWTH Aachen) and Prof. Bernd Friedrich (RWTH Aachen) for the hospitality and help during the stay. A special thanks to Tom for the collaboration in trial planning and execution of FTIR analysis and remelting trials. I must also thank Pål Skaret (NTNU) for help and facilitation during the compaction of briquettes for sample preparation and Anders Brunsvik (SINTEF) for conducting the GC/MS analysis.

Finally, I would like to thank my supervisor Prof. Gabriella Tranell (NTNU), and my co-supervisors Senior Research Scientist Anne Kvithyld (SINTEF), and PhD candidate Alicia Vallejo-Olivares (NTNU), for their great support and help during this master's thesis, and also during previous projects in the summer and autumn of 2021. I have appreciated our discussions and your feedback during our meetings and I have learned a great deal through your knowledge. I will forever look back on our collaboration in gratitude.

Abstract

With increasing focus on global warming, all technological fields need to rethink their current situation and find solutions to energy consumption and emission problems. As for the aluminium industry, increasing primary production leads to proportional end-of-life waste generation, which requires proper recycling. Varied types of aluminium scrap demand different treatments. Regarding coated packaging post-consumer products, thermal treatment for decoating and compaction for reduced metal oxidation can be applicable. However, burning the coating can increase oxidation and lead to environmentally unfriendly off-gassing. Oxidation can lead to metal loss and dross formation.

This master thesis has explored the combination of compaction and thermal treatment for optimised aluminium recycling. A coated aluminium 8111-alloy of thickness 600 µm was shredded into chips, and equal parts of the resulting material were compacted with uniaxial pressure (100 kN), compacted with uniaxial pressure (100 kN) and torque (MPT), or kept as chips. Half of the material was thermally treated in a closed furnace with FTIR off-gas analysis with a heating rate of 350 °C/h and a target temperature of 550 °C. A nitrogen atmosphere with 5 % oxygen was used. Thermally treated and not thermally treated samples were remelted in a molten aluminium heel in an argon atmosphere. The samples were de-drossed before casting. One series with remelting of uncoated alloy chips was also conducted. Coated material was analysed with TGA and DSC, and a pyrolysis condensate was analysed with GC/MS.

The FTIR trials found increased off-gassing from the coated chips compared to the briquettes in terms of integrated and maximum values. The uniaxial briquettes had a higher off-gassing compared to the MPTs. The calculated mass loss during thermal treatment was largest for chips, corresponding to the higher off-gassing. Less oxygen was consumed during the treatment of briquettes, suggesting less combustion and possible increased oxidation. Thermal treatment did not impact dross amounts, but the MPT briquettes generated more dross than the uniaxial briquettes and the chips. Remelting of uncoated chips resulted in the least dross. DSC analysis indicated one endothermic and one exothermic peak, and the pyrolysis condensate was found to consist of various organic compounds. The mass loss from FTIR thermal treatment was lower than that from TGA analysis. Unfortunately, some planned trials were not completed due to repairs on the FTIR equipment. Nevertheless, the obtained results show the most off-gassing and least dross formation for loose or loosely compacted material, but thermal pretreatment did not influence the dross generation.

Sammendrag

Økt fokus på global oppvarming har medført at alle teknologiske sektorer ser etter løsninger på problemer tilknyttet energibruk og utslipp. Aluminiumsektoren har de siste tiårene opplevd en økt primærproduksjon noe som også fører til økte mengder med avfall, for eksempel fra brukt matemballasje. Denne typen emballasje er ofte lakkert og kan derfor trenge varmebehandling før den smeltes for å fjerne urenheter. Forbrenning av lakk kan føre til økt oksidasjon av metallet under, samt utslipp av miljøfiendtlig gass. Oksidasjonen kan også resultere i økt metall-tap ved omsmeltning da aluminiumsoksider ikke kan gjenvinnes, men fører til store mengder generert slagg.

Denne masteroppgaven har undersøkt kombinasjonen av kompaktering og varmebehandling for best mulig aluminiumresirkulering. En 600 µm tykk og lakkert 8111-legering av aluminium ble kuttet opp i små flak og like store mengder av materialet ble deretter presset til briketter med uniaksialt trykk (100 kN) eller presset med uniaksialt trykk (100 kN) og torsjon (MPT). En tilsvarende mengde materiale forble også som flak. Halvparten av materialet ble varmebehandlet i en lukket ovn med FTIR avgassmåling. Ovnen var fylt av en nitrogenatmosfære med 5 % oksygen. Oppvarmingshastigheten var satt til 350 °C/t og slutt-temperaturen 550 °C. Materialet ble holdt ved 550 °C i 30 minutter. Både varmebehandlede og ikke varmebehandlede prøver ble smeltet i flytende aluminium under en argonatmosfære og slagg ble fjernet før støpning. En serie med omsmelting av rene legeringsflak ble også gjennomført. Det ble gjennomført TGA- og DSC-analyse av lakkert materiale og et pyrolysekondensat ble analysert med GC/MS.

Forsøkene med FTIR ga høyere integrerte og maksimale avgassverdier for løst lakkert materiale enn for presset, og de uniaksiale brikettene ga mer gass enn MPT brikettene. Det målte vekttapet etter varmebehandling var også større for løst materiale enn for briketter. I forsøkene for briketter ble det konsumert mindre oksygen, noe som kan tyde på lavere forbrenning og et større potensiale for oksidasjon. Varmebehandlingen hadde ingen påvirkning på genererte mengder slagg, men MPT brikettene frembrakte mer slagg enn de andre lakkerte materialene. Det ulakkerte løse materialet frembrakte minst slagg. DSC analysen indikerte en endoterm og en eksoterm reaksjon, og TGA analysen viste at høyere vekttap var mulig enn det som ble oppnådd ved FTIR varmebehandling. Pyrolysekondensatet besto av ulike komplekse organiske forbindelser. Dessverre ble et par planlagte forsøk ikke gjennomført på grunn av reparasjon på FTIR apparatet. Likevel tyder resultatene på at løst eller løst presset materiale gir best resultater for økte avgassmengder og mindre slagg, men varmebehandling minsket ikke mengden slagg.

Contents

List of Figures

List of Tables

Table of abbreviations

Table 0.1: Table of abbreviations

Abbreviation	Explanation
BADGE/DGEBA	Bisphenol-a-diglycidyl ether
CO_2-e	CO_2-equivalents
DSC	Differential Scanning Calorimetry
DTA	Differential Thermal Analysis
EGA	Evolved Gas Analysis
EPMA	Electron Probe Microanalysis
FTIR	Fourier-Transform Infrared spectroscopy
GC	Gas Chromatograph
GHG	Green House Gas
GWP	Global Warming Potential
ICP	Inductively Coupled Plasma
LIBS	Laser-Induced Breakdown Spectroscopy
Mmt/Mt	Million metric tonnes
MPT	Medium Pressure Torsion
MRF	Municipal Recycling Facility
MS	Mass Spectrometer
MSD	Mass Selective Detector
NMP	Non-Metallic Products
OM	Optical Microscopy
PE	Polyethylene
PET	Polyethylene terephthalate
RSA	Spectral Resolution Analysis
TG	Thermogravimetry
TGA	Thermogravimetric Analysis
UBC	Used Beverage Cans
VOC	Volatile Organic Compounds
WGSR	Water-Gas Shift Reaction
XRD	X-Ray Diffraction
XRT	X-Ray Transmission

1 Introduction

1.1 Background and motivation

Aluminium is used in various spreads of products, and the high technology society of 2022 is partly based on the use of this particular metal. The application areas of aluminium spread from transportation and electrical equipment, building, construction, and machinery materials, to consumer durables and packaging. Aluminium is a light metal and thus reduces the energy consumption and demand in transportation as aluminium products have low weight. At the same time, the production of aluminium from bauxite ore is very energy-intensive. Recycling can reduce energy consumption and Green House Gas (GHG) emissions by up to 90 %. Aluminium metal is also, in theory, 100 % recyclable. The reduction in GHGs occurs, among other things, because 2/3 of the electricity used for primary aluminium electrolysis is fossil-based [1]. Reducing the total GHG emissions is essential for slowing down the increasing greenhouse effect and global warming. Between 1970 and 2010, the GHG emissions in the world increased as observed in Figure 1.1 and this trend has to be reversed [2].

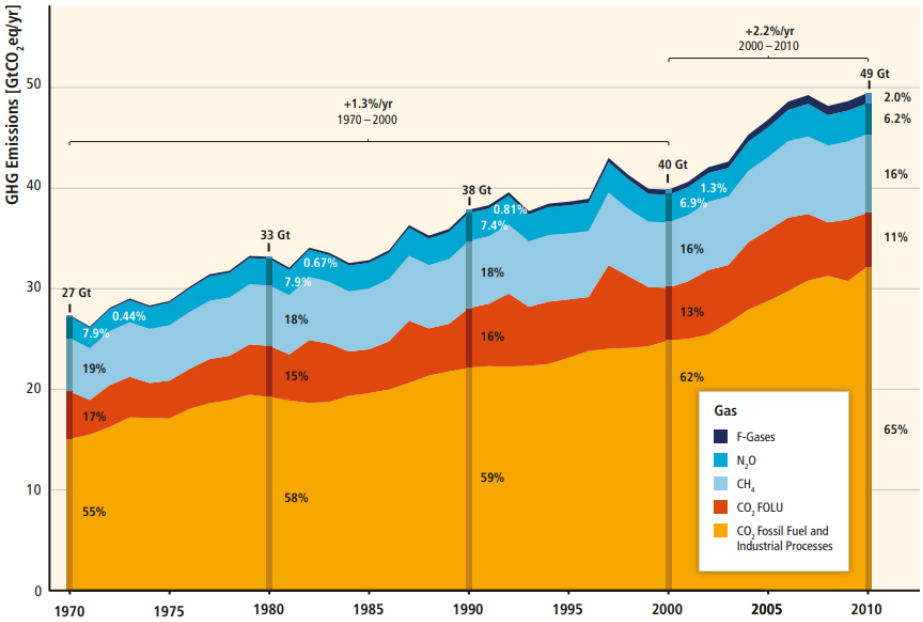

Figure 1.1: Total annual GHG emissions by groups of gasses 1970-2010 [2]

The recycling rate of different aluminium products is constantly increasing. Therefore, the aluminium scrap market is growing like the entire aluminium market. The available amount of aluminium scrap increased from 18 Million metric tonnes (Mmt) in 2018 to 33 Mmt in 2019, and the amount of available aluminium scrap is predicted to double by 2050. The amount of recycled aluminium metal increased from one Mmt in 1980 to 20 Mmt in 2019 [1]. Variations in metal content and product lifetime will affect the recycling

processes regarding raw material availability and complexity. Construction materials are infrequently recycled, but the metal content and scrap amount are significant when first available. On the other hand, packaging materials have short product life, so the availability is large. However, the metal content is small, and the materials are often coated with paints and coatings to protect the contents inside the packaging, thus improving preservation properties and storage time[3].

The coatings are essential for food and beverage conservation, but at the same time, they challenge the recycling process. The coatings should thus be removed before recycling since the content is regarded as contaminants during remelting[4]. Thermal treatment is the used industry practice today, but the method needs optimisations to improve coating removal while reducing oxidation. Metal oxidation can lead to direct metal loss since oxides cannot be recycled and lead to increased dross formation during remelting. Compaction has been suggested as a method for preventing oxidation by reducing the surface-to-volume ratio of the aluminium[5]. Kvithyld et al. explored the optimised operating window for thermal decoating. They found this to be narrow since the difference between too much and too little treatment was small[6].

Variations in organic components in the coating and the coating thickness can influence the proper temperature and duration for the thermal treatment. The organic composition of the coating will also determine the type of off-gassing during thermal treatment. The atmosphere in which the material is treated does also influence the reaction products. During treatment in an oxygen-rich atmosphere, combustion will occur, and combustion products will evolve. Treatment in an oxygen-reduced atmosphere, or total absence of oxygen, will result in pyrolysis and generation of pyrolysis gases[7]. Pyrolysis gases can have useful heating values regarding the heat of combustion but also have higher values for global warming potential. Different analysis methods can be used to measure and characterise the gases.

1.2 Aim and scope of the work

This master thesis is the continuation of two projects previously conducted by A. Vallejo-Olivares, S. Høgåsen, G. Tranell, and A. Kvithyld during the summer and autumn of 2021. The objective of both earlier projects has been to investigate coated aluminium scrap and how thermal pretreatment can affect the recyclability of the metal. The first project also investigated the effect of compaction before remelting in salt flux.

This master thesis aims to further increase the insight into the thermal decoating process, and the influence compaction has on gas evolution and remelting behaviour on coated materials. Thermal treatment pyrolysis experiments will be executed with FTIR off-gas analysis, where the gas amount, composition, and temperature will be measured. Two types of compacted material, as well as loose chips, will be investigated. The three coated material groups, both decoated and not, will be remelted under a molten aluminium heel to examine the dross generation and inspect differences between material groups and pretreatment. A trial of uncoated non-treated loose chips will also be remelted as a comparison to the coated materials. By increasing the insight on the influence of pretreatment steps with compaction and thermal treatment, and the influence in off-gassing and dross formation, the overall recycling processes can be improved. With increasing scrap generation and the need for reduced energy consumption and GHG emissions, improved recycling processes can be one step toward a more sustainable future.

2 Theory and Literature survey

2.1 Chemical and physical properties of aluminium

Aluminium is the 13th element of the periodic table and is classified as a metal. The low density of 2.7 g/cm^3 makes it very suitable as a construction and manufacturing material, and it is also used in transportation. Aluminium is used as a conductor for electricity and heat. As a ductile metal with high formability in its pure form, it is suitable for rolling films and drawing wires. Therefore, it is often used as a packaging material, and for food packaging, this will usually be in the form of foils or cans [8]. Aluminium quickly oxidises in contact with oxygen due to a high oxygen affinity. Therefore, aluminium is not found in nature in its pure form, only as an oxide. The cause is the spontaneous reaction between oxygen and aluminium having a Gibbs free energy (ΔG°) below zero. The Ellingham diagram, presented in Figure 2.1, illustrates the oxygen affinity of a variety of elements [9]. Aluminium is observed as the third bottom line.

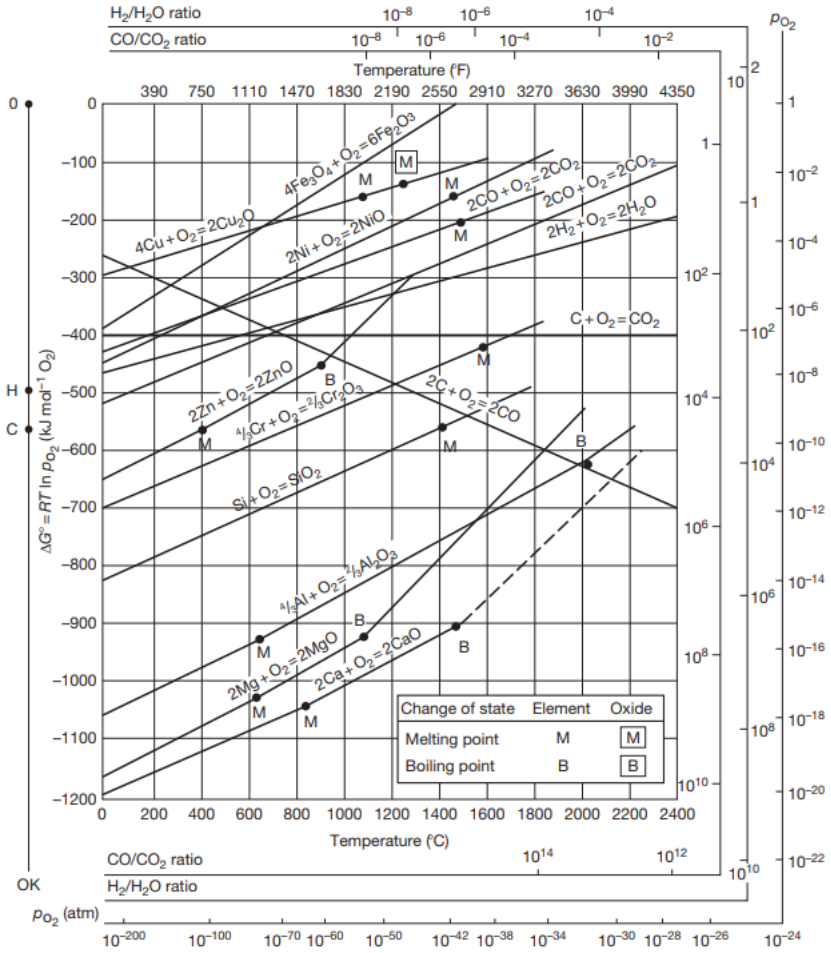

Figure 2.1: The Ellingham diagram [9]

To adjust the properties of aluminium, elements such as silicon, manganese, magnesium, copper, and sink are typically used as alloying elements. The alloy number specifies the alloying materials where an alloy with 8 as the first digit represents an alloy with several main components, a distinctive main element, or a combination. In pure form, the melting point of aluminium is 660 °C[8].

2.2 Primary aluminium production

Since the 17th century, the Hall-Héroult electrolysis process has been the sole approach for primary aluminium production[3]. The raw material of the process is bauxite ore, an aluminium-rich rock containing 30-60 % of aluminium oxide (Al_2O_3, alumina). The bauxite is treated by the selective leaching Bayer process, which processes bauxite into purified alumina. A by-product of the process is large amounts of red mud, which causes problems with handling and storage due to high alkaline properties[10]. The purified alumina is further used as raw material in the Hall-Héroult electrolysis process. The reaction is conducted inside an electrolysis cell with molten cryolite. A direct electrical current of 100-300 kA flows from a carbon anode through the melt to a carbon cathode at the furnace bottom. The reactor voltage is 4-5 V. The overall reaction equation is given by Equation 2.1. The reaction is carried out at 960 °C.

$$\frac{1}{2}Al_2O_3(s) + \frac{3}{4}C(s) \longrightarrow Al(l) + \frac{3}{4}CO_2(g) \tag{2.1}$$

If the products of the Hall-Héroult process are discharged at 1000 °C, the theoretical energy consumption of the process is 6.37 kWh/(kg of aluminium produced)[10]. However, the actual consumption is higher and varies from production site to production site. The aluminium factory of Hydro at Karmøy is reported to have an energy demand of 12,000 kWh/(tonne of aluminium produced), corresponding to 12 kWh/(kg of aluminium produced)[11]. The higher actual energy demand is caused by, for instance, the high affinity to oxygen[8]. The products may also deviate from the ideal, and high amounts of gases such as fluorides, sulfur dioxide, and carbon monoxide are produced in addition to the carbon dioxide. Primary produced aluminium generates about 12-16.5 tonnes of GHGs per tonne of metal produced, including methane, nitrous oxides, hydrofluorocarbons, perfluorocarbons and sulphur hexafluoride[1] .

2.3 Secondary aluminium production

2.3.1 An overview to aluminium recycling

Unlike primary metal production, which uses mineral ore as raw material, secondary metal production uses scrap, and the new material is produced through recycling[3]. The advantages of secondary aluminium production are many, including reduced energy consumption and costs. If only considering primary energy demands, the needed energy for remelting aluminium scrap may be as low as 5 % of the energy needed for primary production. However, this is regarding ideal melting without material or energy losses; thus, the actual energy demand will vary[12].

Costs for secondary aluminium production can be reduced by 80-85 % if compared to primary production[13]. Recycling will also result in less waste generation, for instance, by reducing salt cake generation and no formation of red mud. The total CO_2 emissions can be reduced by 90 %. However, dust generation and emissions of chlorine gases and Volatile Organic Compounds (VOCs) are typical at scrap processing- and melting facilities[14]. Closed furnaces with off-gas circulation, scrubbers and bag houses are used to control the emissions. Post-consumer scrap and industrial wastes are typical sources of input material for aluminium recycling, and in Europe today, 36 % of the aluminium supply is secondarily produced[13]. By the mid-century, it is estimated that half of the aluminium supply is secondarily produced, and this trend is illustrated in Figure 2.2.

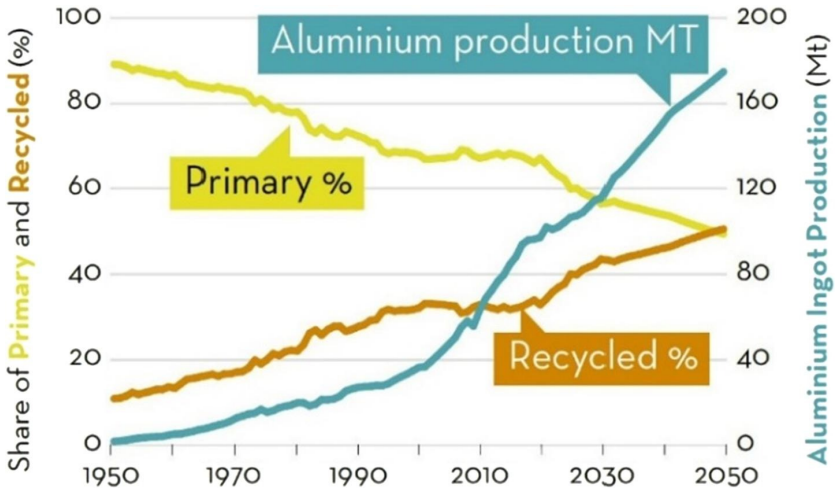

Figure 2.2: Share in primary and secondary produced aluminium towards 2050[1]

Some European countries have established very effective collection and recycling systems resulting in recycling rates up to 99 %, while the global average is estimated to be approximately 40 %[15][1]. Theoretically, aluminium is 100 % recyclable, but a metal loss will occur during remelting due to oxidation and impurities. However, some state that when the metal is collected, the scrap-based aluminium recycling industry has a yield of

98 %[1]. Remelting different alloys simultaneously can lower the quality due to new and undesired compositions. Short-lived products such as Used Beverage Cans (UBCs) or other packaging products are, therefore, recycled to new equivalent products directly[1]. To secure a sustainable and effective recycling process, sorting and pretreatment may be necessary before remelting.

2.3.2 The variation in scrap types

Aluminium scrap is differentiated into groups depending on the origin and purity. Scrap consisting of primarily aluminium alloys, such as UBCs and construction materials, is named liberated scrap since it is free of attached pieces of other metals and thus needs no dismantling before recycling[3]. One can also differentiate between new and old scrap. New scrap is typically leftover material generated from primary production and origins directly from the manufacturing and fabrication process[16]. This scrap will usually be in the form of ingots, billet croppings, or edge trimmers which are easily remelted as they are liberated and of known composition. The term in-house scrap can also be used on new scrap since it origins from inside a factory[3]. Dross generated in aluminium production, which is the oxide slag phase formed during remelting, is also included in the term new scrap[1].

Another scrap type is old scrap, which originates from various sources such as consumer products taken out of service. UBCs, foils, other food packaging, and electronic, automobile, aerospace, and construction waste can be examples of old scrap. It is typically contaminated with impurities and organics[3][1][16]. The scrap feed used for secondary aluminium production is hence a complex combination of varying type, size, shape, composition, and contamination[16]. Aluminium in the form of oxides, nitrides, chlorides and carbides can not be used as input materials in the recycling processes as they cannot be reprocessed into metallic aluminium[1].

2.3.3 Scrap collection and sorting

The available amount of scraps for recycling depends on collection rates, and the possible re-gained metal amount depends on the purity and metal content of the scraps[3]. Collection and remelting of new scrap are usually dealt with at the site. In contrast, old scrap must be collected and transported to a recycling site, sometimes via a sorting facility[3]. The collection is conducted in several ways, for instance, at the consumer's house by curbside separation or brought to a facility or reversed vending machine by the consumer either sorted or unsorted. Unsorted scrap can be sorted at a Municipal Recycling Facility

(MRF) by various machines[3].

The sorting machines can separate scraps by different properties such as density, magnetism, conductivity, and alloy type. Air- and rising current separators can separate light and heavy scraps such as rubber and metal from plastics and paper. A magnetic separator can further separate rubber and non-ferrous metals such as aluminium from ferrous metals such as nickel and iron, taking advantage of magnetic properties. An eddy-current separator can further separate aluminium from other metals. The principle of eddy-current separation is based on magnets of altering polarity, deflecting some types of materials while not affecting others. Due to the high ratio between conductivity and density of aluminium, it will be deflected. At the same time, stainless steel, nickel, brass, and copper, which have smaller ratios due to high densities, will not deflect. However, copper is less affected; in some cases, hand sorting can be necessary to sort aluminium from copper. Magnesium has a ratio close to aluminium making eddy-current separation difficult[3].

New sensor technology, such as X-Ray Transmission measurement (XRT) with Spectral Resolution Analysis (RSA), is making it possible to separate different aluminium alloys[1]. The two main aluminium alloy groups, wrought alloys and cast alloys, can be differentiated as low alloys and high alloys, respectively, based on their amounts of alloying components[8]. During XRT, heavy alloying elements will appear dark and thus make it possible to separate the different types of alloys based on colour. This is feasible as refining will be easier if similar alloys are remelted simultaneously. Laser-Induced Breakdown Spectroscopy (LIBS) can be used to separate alloys with different amounts of alkali metals and alkaline earth metals as the LIBS is especially sensitive to these components[17]. A LIBS separator is illustrated together with an eddy-current separator in Figure 2.3.

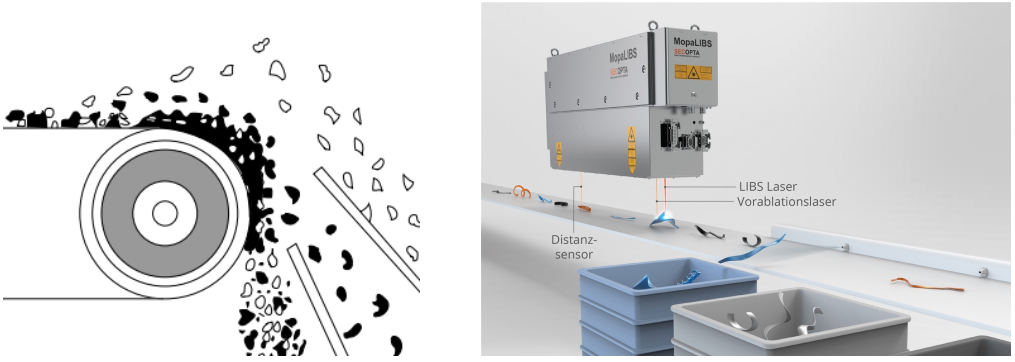

(a) Eddy current separation **(b)** LIBS separation

Figure 2.3: Sorting machines for aluminium separation[3] [18]

During the LIBS scan, a pulsed laser is focused on the sample surface, which generates a plasma, and the optical plasma emission will detect the components and their concentrations. An air jet then separates the pieces into different fractions. For these scans, a clean sample surface is required.

2.3.4 Shredding and compaction of aluminium scrap

After collection and separation, scraps may be shredded into smaller pieces. Some examples of shredders are the hammer mill, and the rotary shredder [3]. Smaller aluminium chips are also generated through the whole production cycle as edge trimmers, machining components, or from profile, plate, and sheet production [5]. Sometimes the shredded scrap is further compacted into bales, logs, or briquettes. The compaction can be conducted to reduce the volume to ease transportation or reduce the possibility of oxidation.

While loose chip can have bulk weights between 0.14 and 0.25 g/cm^3, compacted chips can have bulk densities between 2.2 and 2.4 g/cm^3 [5]. For thin scrap such as foils, compaction is favourable since it decreases the area-to-volume ratio, which reduces the possibility of oxidation and burn-off. On the other hand, having large balers can make direct feeding to a remelting furnace difficult. Too intense compaction can make it challenging to reshred the material before remelting. A small compacted log or briquette can therefore be preferred [3] [5]. As the average aluminium alloy density lies at 2.35 g/cm^3, a briquette with a 2.2 to 2.4 g/cm^3 will hardly float during remelting and thus reduce both burn-off and oxidation. Therefore, some refiners have reported 2-7 % higher yields when remelting compressed material [5]. Figure 2.4 illustrates two machines used for the compaction of briquettes.

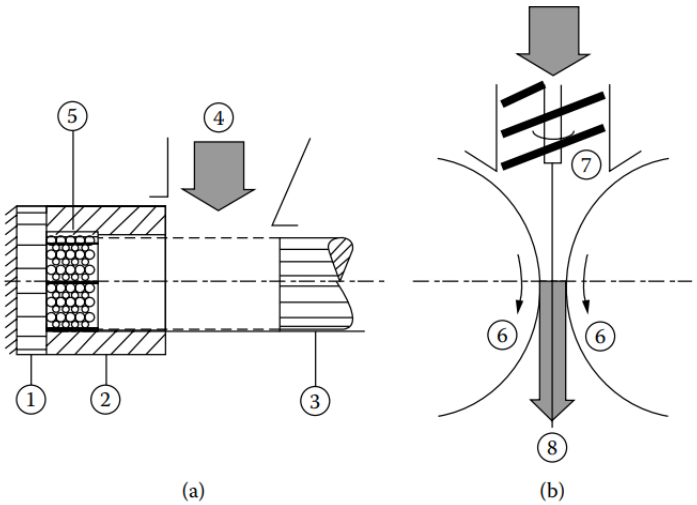

Figure 2.4: Illustration of compaction machinery: (a) Punch-and-die and (b) Roller press [3]

2.3.5 Aluminium scrap remelting

Aluminium scraps are further remelted, and an efficient remelting step is critical for achieving high aluminium recovery, low energy consumption, and low environmental impact. Aluminium melts are, such as solidified aluminium, highly reactive with oxygen and oxidation of aluminium melts occurs excessively from 727 °C, and it increases strongly above 780 °C. The oxidation particularly occurs in an oxygen-rich and humid atmosphere. However, pure aluminium can also react with oxides in the melt, such as iron oxide or silicon dioxide, or with combustion gases such as carbon dioxide, further forming aluminium oxides. Proper control over input materials and melting temperature conditions, and oxygen availability are, therefore, essential to prevent melt oxidation. Because the oxide layer is dense, it will protect the melt underneath from further oxidation [1].

Remelting furnaces can be differentiated by their heat generation, whereas gas-fired and electrical furnaces are two options. Natural gas is typically used as fuel in a gas-fired furnace, and required temperatures typically vary between 650 and 850 °C. To increase the flaming temperature, the inlet air can be pre-mixed with oxygen as an increased oxygen concentration will increase the combustion energy. Increased oxygen concentrations will also reduce the heat loss in the off-gas as the inert nitrogen concentration of the air will be diminished, and less heat will be consumed by compounds that do not contribute to the process. Reducing nitrogen in the inlet air will also reduce the production of hazardous NOx gases. An example of a gas-fired furnace is the reverberatory furnace [3].

The other choice is electrical furnaces, where induction furnaces are most common. The heat is generated by electricity, which is favourable if electricity is cheap. If the electricity is produced from a renewable source, electrical furnaces will also have a much lower carbon footprint than gas-fired furnaces. Nevertheless, electrical furnaces have lower remelting emissions regardless of power source as no combustion products are generated. This also produces a cleaner metal since no combustion products can contaminate the melt. Electrical furnaces often have better stirring properties than gas-fired ones, but effective stirring can entrap inclusions and oxides in the melt. Possible high electricity costs compared to natural gas can make gas-fired furnaces more economically competitive. Therefore, electrical furnaces are more often used for small-scale remelting than large-scale, and the fraction of remelted metal from these furnaces is consequently small. However, increased focus on emission and clean metal can increase this fraction rapidly [3]. An example of a reverbaratory gas-fired furnace and a core-less electrical induction furnace can be seen in Figure 2.5.

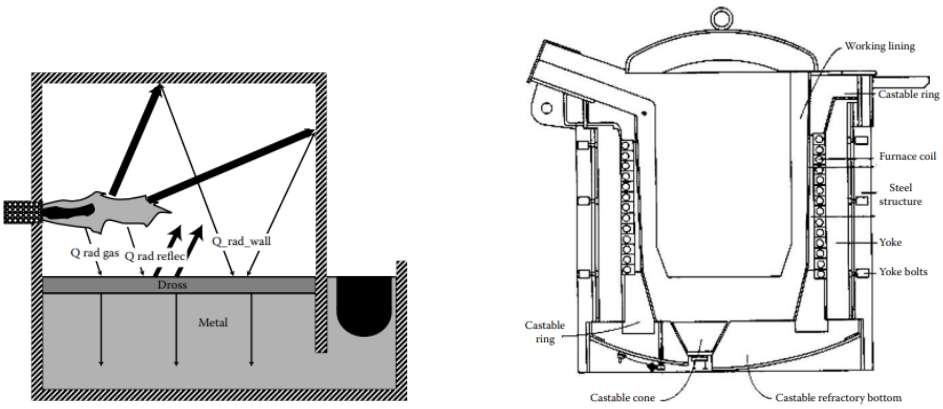

(a) Reverbaratory furnace **(b)** Core-less induction furnace

Figure 2.5: Aluminium melting furnaces[3]

2.3.6 Aluminium scrap remelting under salt-flux

Aluminium scraps can also be remelted under a molten salt layer, for instance, in a rotary melting furnace[16]. This can be extra favourable when melting highly oxidised scrap or other low-quality scraps with high amounts of oxides, and impurities[4]. At the same time, as the salt layer can protect the metal underneath from further oxidation, it can extract impurities, inclusions, and oxides from the melt and extract metal entrapped in the dross. The choice of salts should regard toxicity, density, vapour pressure, and costs. Reduced toxic properties and low vapour pressure will result in improved process conditions, and costs are essential for competitiveness[3]. Sodium and potassium chlorides are typical fluxing salts as they are cheap, and fluorides, such as Na_3AlF_6, NaF or KF, are often added to enhance coalescence. The fluorides help strip and break up the oxide layers so that imprisoned metal droplets can be accessed, and coalescence improved[19].

After fluxing, the salt cake is removed and treated to extract trapped metal and reduce the number of solid waste[14]. The treatment can either be conducted immediately after skimming as a hot treatment or after cooling as a cold treatment. First, a concentration process is executed by crushing, milling and screening to separate solids with high aluminium content from oxidised aluminium, salts, and contaminants. The larger metallic particles are remelted while smaller particles are processed to extract salt for reuse[14].

2.3.7 Remelting behaviour of some aluminium scraps

Yang et al. investigated the melting behaviour of ten different aluminium scraps (cast ingots, profiles, rolling mill cuttings, printing plates, fridge shreds, bottle caps, car plates, granulates, turnings, and margarine foils), and the recyclability was examined. Remelting

trials were executed in a laboratory-scale electrical resistance chamber furnace in a nitrogen atmosphere, with temperatures between 800 and 900 °C, and a NaCl-KCl-Na_3AlF_6 salt system was used for fluxing[16].

The results confirmed that scrap type, surface conditions, size, and contaminants significantly influence metal yield and thus the scrap recyclability. Properties which seemed to increase the recyclability included stirring, increased metal content in the scrap, low contamination, and increased cryolite concentrations in the salt flux. Cast ingots were thus ranked best. On the other hand, properties which seemed to decrease the recyclability were; low metal content in the scrap and high levels of contamination. Margarine foils were thus ranked worst. Scrap characteristics regarding metal content, size, surface-to-volume ratio, and contamination were specified to be of high importance since coalescence and recovery rates would be improved with increased scrap size, cleanliness, and a salt composition high in cryolite[16].

2.4 Coatings

Some aluminium products require resistance from chemical attacks, such as corrosion and excessive oxidation, and protection in the form of a coating is necessary. For instance, waterborne epoxy, polyester, and acrylic polymer resins are widely used as beverage can coatings[20]. In a study by Li and Qui, the coating on Coca-Cola beverage cans was investigated using pyrolysis and leaching. Phenol, 2-methyl-phenol, 2,2-dimethyl-1,3-propanediol, benzonitrile, and 2,3,5-trimethyl-phenol were found to be the main organic components[21]. Other organic compounds can also be used, such as painting materials, waxes, inks, oils, and types of vinyl[22]. Figure 2.6 shows the cross-section of a coated aluminium coffee capsule[23].

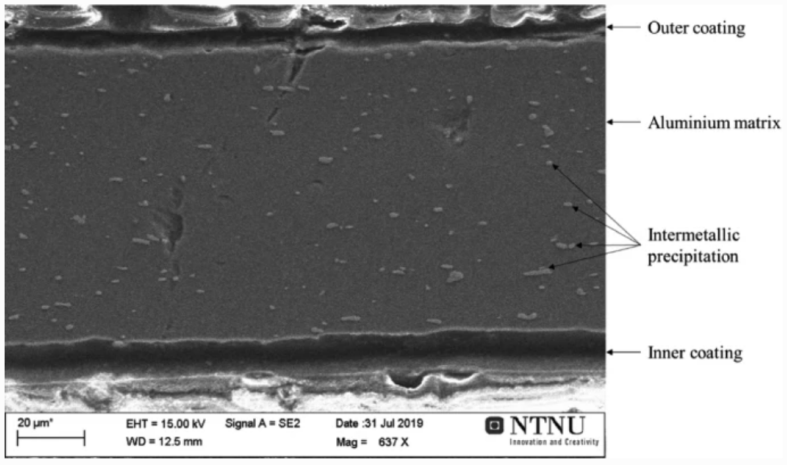

Figure 2.6: Cross sectioned wall of a coffee capsule[23]

2.4.1 Composition of coatings

Most coatings are constructed as a mixture of organic and inorganic compounds, whereas the organic compound is referred to as the coating vehicle. The vehicle enables the coating to convert from a mobile liquid to a solid film and serves as the film-forming ingredient. The other coating part is the inorganic particles, often referred to as pigments. A pigment particle is usually smaller than 25 µm. As solid particles, the organic vehicle will serve as the carrier to spread the pigments out on the metal surface[22]. The pigments can serve as colouring agents, and different types of pigments can be added to achieve specific colours. A typical white pigment is titanium oxide, while brown and red pigments are often based on iron oxides. Pigment orange 23:1 contains insoluble barium sulphate by-products.

2.4.2 Necessary coating properties and typical organic vehicles

Coatings may serve decoratively, but in addition to being attractive, a proper coating should be washable, waterproof, durable, and resistant to its environment. A food packaging container must thus withstand the chemical properties of its contents and the outside world. The coating must have good printability, block resistance and scratch resistance for food packaging purposes, and it must also withstand sterilisation and changes in temperature and acidity. The coating must be non-toxic and neutral regarding odour and taste. It is also crucial that the coating is elastic in the case of ruptures such that the food does not come in contact with the metal[22].

Some materials are naturally better suited, and polyesters have excellent balance in elasticity and surface hardness and have a good surface adhesion. Polyesters are also resistant to yellowing, making them very suitable for packaging purposes as the decorative properties will withstand for a long time[22]. Polyester has the chemical formula $C_8H_6O_4$ and can have several structural formulas. The two possibilities, therephthalic acid and isophthalic acid, are shown in Figure 2.7.

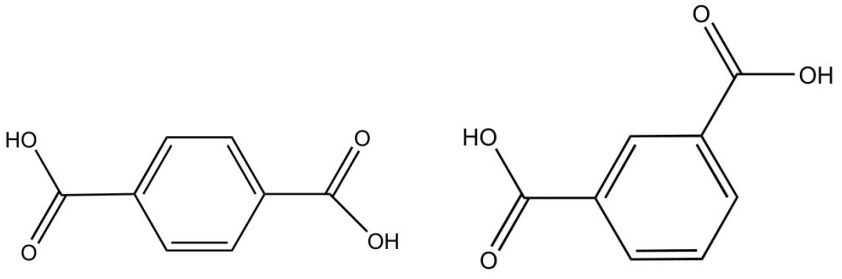

(a) Polyester: Therephthalic acid **(b)** Polyester: Isophthalic acid

Figure 2.7: Structural formulas for polyester

Bisphenol-a-diglycidyl ether-based epoxy resins (BADGE/DGEBA) are also common in the beverage can industry[24]. The chemical formula of BADGE is $C_{21}H_{24}O_5$ and the structural formula is illustrated in Figure 2.8 together with the structural formula of a PET monomer. Polyethylene terephthalate (PET) has the chemical formula $C_{10}H_8O_4$ and is another typical coating compound.

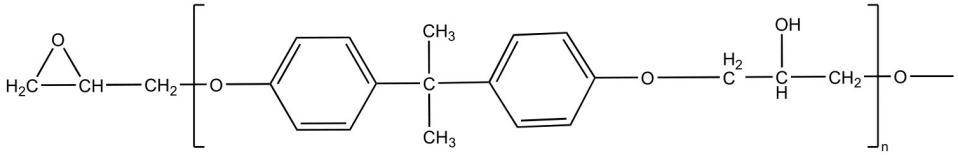

(a) BADGE/DGEBA epoxy

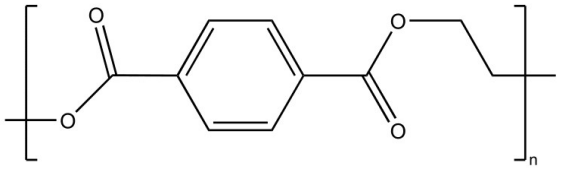

(b) PET monomer

Figure 2.8: Structural formulas of BADGE epoxy and PET monomer

2.4.3 Application of coatings

Application of a coating to a metal surface can be conducted in a variety of ways, and some possibilities for application are spray, brush, roller coating, direct gravure, screen printing, or ink-jet printing. An adhesive is often used before applying the actual coating; if not, a primary substrate could be embossed instead. The total matrix of the coating would then combine a base sheet, the adhesive or primary substrate, the coating, and a release liner. When choosing an application method, several concerns have to be made, such as the viscosity of the organic vehicle, the desired film thickness, and the substrate shape. Cost and versatility of use can also be of importance. Coatings on flexible products are often applied by grauve coater. To solidify the coating, it can be cured at medium-high temperature. Waterborne resins have typical curing temperatures between 150 and 200 °C, but the specific temperature will depend on the exact resin-cure system and the curing time[22].

2.5 Thermochemical conversion of organic material

Coatings consists, as stated in Section 2.4, of some organic material and can thus be classified as carbonaceous materials. Thermochemical conversion, or thermolysis, is the

standard description of processes that convert carbonaceous materials, such as organic material, into valuable and convenient gaseous fuels or chemical feed-stock. Thermochemical conversion can thus be relevant in an aluminium recycling perspective, specifically related to the decoating processes, due to the thermal conversion of the organic mass and the impact the treatment may have on the aluminium metal. Further introduction to specific thermal treatment of coated aluminium surfaces will be given in Section 2.6. Various pathways of thermochemical conversion exist which can be differentiated related to thermodynamic and atmospheric conditions that results in varied reaction products [7]. This section will focus on combustion and pyrolysis.

When thinking of thermochemical conversion of organic mass, burning might be the first reaction that comes to mind. Burning of organics, that is combustion, releases heat in an exothermic process by breaking chemical bonds of organic matter in reaction with oxygen, resulting in combustion products without useful heating values [7]. Such products can be carbon dioxide and steam, and a general combustion reaction is given in Equation 2.2. When combusting a coated aluminium surface excess oxygen can lead to harmful oxidation [3].

$$\mathrm{CxHy}(s/l/g) + z\mathrm{O}_2(g) \longrightarrow x\mathrm{CO}_2(g) + \frac{y}{2}\mathrm{H}_2\mathrm{O}(g) \tag{2.2}$$

2.5.1 Pyrolysis

Another thermochemical conversion method, which occurs in an oxygen-deficient environment, is pyrolysis. Pyrolysis reactions are endothermic and occurs at relatively low temperatures between 300 and 650 °C and in a total absence of oxygen, if concerning ideal conditions. However, under some terms, oxygen is allowed in small concentrations to provide the needed thermal energy, but the oxygen level will nevertheless be lower than during combustion. In all pyrolysis processes, large hydrocarbons are broken down into smaller hydrocarbons of gas, liquid, or a solid-state of char. The product will depend on the pyrolysis temperature, heating rate, and holding time [7].

The initial pyrolysis product can be a condensable gas of heavier molecules which condense upon cooling, a non-condensable gas, a liquid of bio-oil, tar, bio-crude, or a solid char. The condensable gases or liquid and solid products can further undergo secondary cracking and break down into non-condensable primary gases such as CO, CO_2, H_2, methane, ethane, and ethylene, which do not condense upon cooling. This gives a final non-condensable gas product consisting of a mixture of primary and secondary gas. Decomposition through gas-phase homogeneous reactions and gas-solid-phase heterogeneous

thermal reactions follows Equation 2.3[7].

$$\mathrm{CnHmOp(solid\ mass)} \xrightarrow{\mathrm{heat}} \Sigma_{\mathrm{liquid}}\mathrm{CxHyOz} + \Sigma_{\mathrm{gas}}\mathrm{CaHbOc} + \mathrm{H_2O} + \mathrm{C(char)} \tag{2.3}$$

Several variations of pyrolysis exist which can be differentiated as slow pyrolysis or fast pyrolysis. Slow pyrolysis will give reaction products of gases and solids, while fast pyrolysis only results in liquids. Conventional slow pyrolysis is characterised by residence times of 5 to 30 minutes, low heating rates, and pyrolysis temperatures around 600 °C. On the contrary, fast pyrolysis will have residence times of about 2 seconds, very high heating rates and temperatures around 500 °C. The heating process can be divided into four stages; 1) a drying phase occurring up to 100 °C, which frees moisture and loosely bound water, 2) an initial step between 100 and 300 °C where exothermic dehydration takes place, resulting in the formation of CO, CO_2, and H_2O, 3) an intermediate phase of primary pyrolysis occurring above 200 °C where large hydrocarbons decompose, and 4) secondary cracking between 300 and 900 °C. In an aluminium decoating perspective, pyrolysis temperatures above 660 °C will be unpractical as the metal will start to melt, and high temperatures are disadvantageous regarding oxidation[7].

The pyrolysis product yield varies with the pyrolysis parameters, and rapid heating will yield VOCs and higher amounts of reactive char. In contrast, slow heating and prolonged residence times result in secondary char formation from reactions between the primary char and the VOCs. The reaction products will further depend on the possibility of secondary reactions, which are correlated to rapid or slow removal of the primary gas formation. This dependence on mass transport is due to the presence of secondary reactions between gases and gases, liquids, char products, and raw materials. A suction or a gas sweep can remove condensable and non-condensable gases and minimise secondary cracking and re-condensation[7].

2.5.2 Stoichiometric thermolysis

Stoichiometric thermolysis is described as a combustion reaction without excess available oxygen, but only the stochiometric needed amount for a specific combustion reaction to happen[24]. The lambda ratio (λ), given in Equation 2.4, describes the ratio of available oxygen to the required amount of oxygen for stoichiometric combustion. The ratio has a significant effect on coating removal and corresponding remaining residues. A ratio above 1 will result in exothermic combustion with CO_2 and H_2O formation. A ratio below 1 will, on the other hand, result in endothermic decomposition and formation of CO, CxHy,

H_2O, and CO_2. With a ratio equalling zero, endothermic pyrolysis will occur, resulting in CxHy gas and solid carbon residue. In all cases, inorganic pigments and metal oxides in the coating will be left on the metal surface as they do not form volatile components such as the organics[1].

$$\lambda = \frac{\text{Available oxygen}}{\text{Stoichiometric required oxygen}} \tag{2.4}$$

2.6 Thermal treatment and decoating

Until the 1980s, it was standard procedure to charge and remelt greased and coated scrap directly, while nowadays, thermal pretreatment of post-consumer scrap is most common[3]. The coating is regarded as contamination, and if not removed, it can cause impurities in the melt and the new products, which will lower the quality and value of the recycled goods. Problems and safety hazards of soot and smoke evolution can also be avoided, and oxidation of the metal can be prevented due to controlled treatment temperatures. The percentage of metal that is converted to oxides inside the remelting furnace is called the burn-off, and the level of burn-off can be increased when the coatings burns. Therefore, it is feasible to remove the coating before charging to the remelting furnace and hence increase the recycling yield[4].

2.6.1 Industrial practices

Industrial decoating is often conducted in either a separated rotary kiln with temperatures between 450 and 600 °C or in a combined multi-chamber furnace with temperatures between 600 and 750 °C[25]. In the rotary kiln, short heating durations are typical, and the heat is provided from process gases of VOCs and air with a combined oxygen concentration below 8 %. The low oxygen concentration can reduce the possibility of oxidation[3]. In the rotary-kiln, a separate afterburner is provided to burn excess VOCs before releasing the off-gas out of the furnace[3]. Other possible reactors are the packed-bed reactor and the belt de-coater, heating the scrap at lower temperatures but longer durations. Fluidised bed de-coaters using long heat exposure times and low temperature can also be used. In the fluidised bed, inert particles are fluidised by the process gas, heating the scrap together with the gas, resulting in a more efficient heating[3]. An illustration of a rotary-kiln is shown in Figure 2.9.

High temperatures can result in increased operating costs and complexity. Therefore, two strategies have been established to optimise the thermal treatment process while

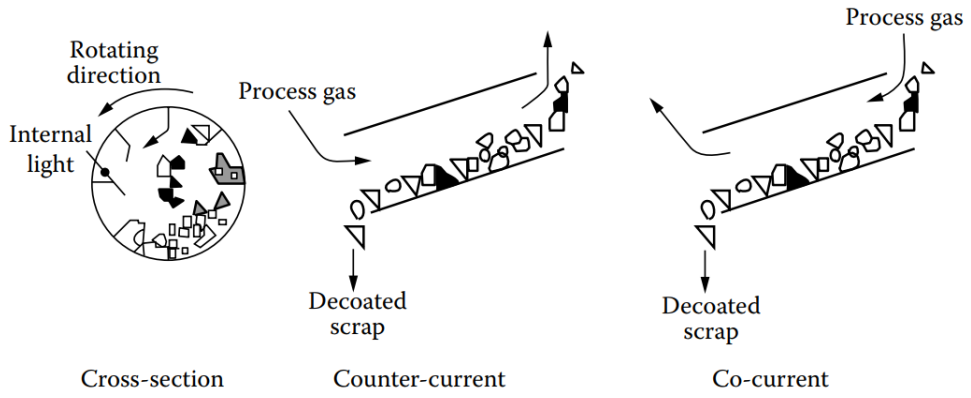

Figure 2.9: Rotary-kiln decoating furnace[3]

lowering the oxidation and operation costs. For instance, operating temperatures between 480 and 520 °C are desirable to minimise oxidation. The low temperature will require prolonged treatment time, so higher temperatures between 590 and 620 °C can be applied to reduce the time demand. On the other hand, the higher temperature might enhance oxidation, and a compromise between optimal temperature and duration must be found. However, short treatment times at high temperatures can ensure complete decoating without excessive oxidation due to the short exposure. The choice of temperature can also concern the organic components in the coating as different organic components will have different combustion temperatures[3].

2.6.2 Coating decomposition mechanisms

The coating decomposition will be initiated by degassing, and the formation of pores in the coating[24]. When the curing temperature of the coating is exceeded, the polymer network starts to degrade, resulting in reduced polymer lengths and decomposition. This phenomenon is called scission and will result in reduced elasticity and hardness of the coating[20]. The scission is the first of two or three thermal effects a coating will undergo during thermal treatment[3]. In the second step, VOCs will be formed, and char and inorganic particles will be left on the metal surface[6]. In an oxygen-containing atmosphere, a third step will also arise, where the residue char will be oxidised and combusted. A higher temperature increases the reaction time, but for aluminium decoating a high temperature is not always desired as this might cause oxidation or melting. Figure 2.10 illustrates the two steps of scission and combustion on a coated metal substrate.

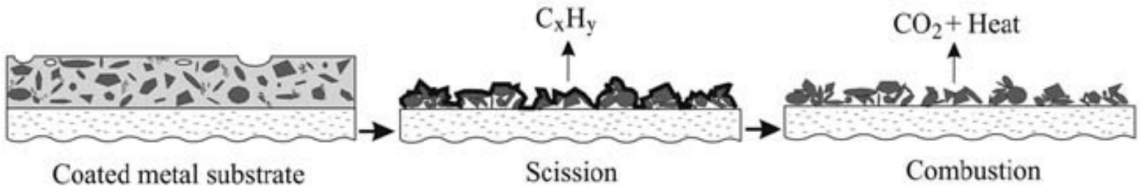

Figure 2.10: Illustration of the scission and combustion steps during decoating of a metal substrate[6]

There are several mechanisms for polymer decomposition. Decomposition of polymers may proceed either thermally, by an oxidative process, or with a combination of the two. Thermal degradation is generally accelerated in the presence of oxygen, lowering the minimum thermal decomposition temperature. In most cases, the solid polymer will break down into a variety of smaller chemical species, and when heat is applied, these will vaporise immediately. During random-chain scission, scission occurs at unspecified locations in the polymer, while scission occurs at the polymer end during end chain scission. During chain-stripping, atoms and molecule groups which are not part of the main polymer chain will be removed[26].

Different polymers undergo different mechanisms, which further result in varied decomposition products. Regarding the polymer PET, decomposition is initiated by random-chain scission of alkyl-oxygen bonds. The main observed gaseous products are acetaldehyde, water, carbon monoxide, carbon dioxide, and compounds with acid and anhydride end groups[26]. As for epoxy resins, the wide variety of compositions results in several possible complex mechanisms and decomposition products. However, the most common epoxy resins are based on Bisphenol A (such as BADGE epoxy), yielding phenolic decomposition products. Steglich et al. described the char residue of an amine cured BADGE epoxy resin which was heated to 800 °C in a N_2-flow for Thermogravimetric Analysis (TGA). The results displayed 84 wt% carbon, 11 wt% oxygen, and 2 wt% nitrogen. There were no traces of sulphur or phosphor[20]. Several polyesters exist, and polyethylene (PE) is one. In an inert atmosphere, PE will start to decompose at 292 °C and extensive weight loss will occur above 372 °C. The decomposition products include a wide variety of alkanes and alkenes such as propane, propene, ethane, ethene, buthene, hexene-1, and butene-1, which are formed during scission of week links in the polymer[26].

2.6.3 Studies investigating thermal decoating

The project work before this master thesis analysed the thermal decoating of coated 8111-aluminium alloy sheets by heating the sheets in air in a Nabertherm Muffle Furnace. Two series of thermal treatments were conducted, where one series consisted of constant temperature at 550 °C and treatment duration between 5 and 60 minutes. The other

series included temperatures between 450 and 600 °C and treatment duration of 5 and 10 minutes. For these trials, the coated aluminium alloy was cut to sheet samples of size 10x5 cm^2, weighting 8-9 g each, and three sheets were treated with the same parameters.

As a result of thermal treatment, the front side coating thickness was reduced from an initial average of 24.71 µm to an average of 14.43 µm. Changes in the colours upon thermal treatment were also observed, and the coating would start to loosen and flake off. Sheets treated for prolonged times or at higher temperatures would obtain brighter colours. This colour change correlated well with the mass loss; thus, bright colours were a sign of successful decoating. On the other hand, dark colours were a sign of incomplete decoating. Shades of black were not observed. Examples of colour changes in the first series of constant temperature can be found in Figure 2.11.

(a) Front side coating

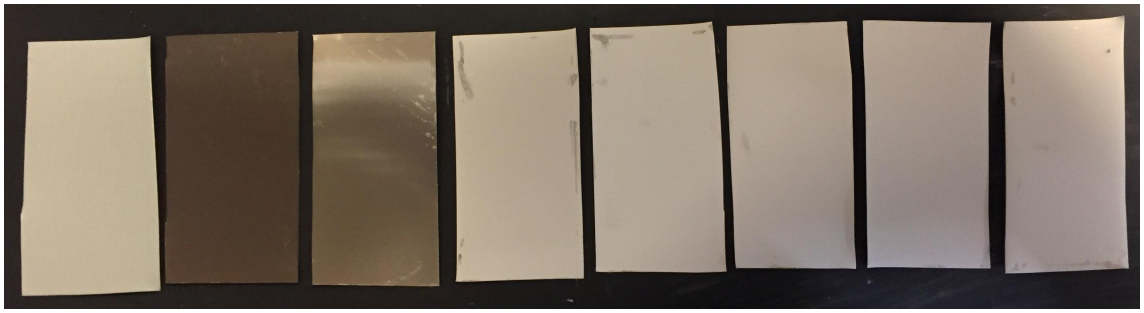

(b) Backside coating

Figure 2.11: Variations in front side and backside coating colour after thermal treatment at 550 °C. From left to right: No heat treatment, 5 min, 10 min, 20 min, 30 min, 40 min, 50 min, and 60 min of treatment

Regarding weight losses, the thermal treatments resulted in weight reductions between 1.08 and 1.80 % measured by weighing the sheets before and after thermal treatment. The smallest weight reduction was obtained by heating at 450 °C for 5 minutes and the highest for heating at 550 °C for 20 minutes. The weight reductions corresponded to decoating efficiencies of 45.03 and 74.52 %, calculated as the ratio between the weight loss and the initial total coating weight of each sheet (including both organic and inorganic components of the coating). It was found that the material had 0.0241 (g of coating/g of material) based on coating amounts from one sheet. For the first series, it was observed that treatment times above 20 minutes had no increased effect on the weight loss or

decoating efficiency if compared to shorter times. For the second series, an increase in heating temperature would increase the weight loss, and so would a change from 5 to 10 minutes of treatment time.

Capuzzi et al. studied thermal treatment experiments on an AA3000 aluminium coil coated on both sides, together with a corresponding coil without coating[27]. The materials were thermally treated at 400, 500, and 600 °C with a heating rate of 10 °C/min and the coating surface and thickness were analysed before and after thermal treatment using SEM. After thermal treatment, the coating thicknesses were reduced, and differences in coating composition were suggested to explain the thickness differences between the two sides of the coating. The coating layer, which was not completely removed during thermal treatment, was very loose and could be removed by a stamping process[27].

Steglich et al. investigated the thermal treatment and decoating of Mg-Si-rich UBC can body and can end alloys. The coated alloys were annealed at 550 and 570 °C for 60-320 minutes and 7-56 minutes, respectively, and the results showed that to avoid oxidation, the thermal treatment temperature should be limited to 570 °C. Based on these results, a recommendation for industrial applications was designed with commendation to use thermal treatment temperatures between 550 and 570 °C, since a successful decoating would require temperatures of 550 °C. In comparison, a limit of 570 °C would prevent oxidation. The resulting temperature interval will require precise temperature control[25].

Steglich also recommended using shredded materials when thermally treating UBCs. The shredding will increase the surface-to-volume ratio, allowing a rapid convective heat transfer and a homogeneous temperature distribution in the material. This would also reduce the needed cycle time of the treatment, even with a temperature limit of 570 °C[25]. This is, however, conflicting advice compared to the recommendation of compaction, which could prevent oxidation by reducing the area-to-volume ratio[5]. The final recommendation of Steglich was to perform spot sample measurements on the effective scrap temperature during the thermal pretreatment. This recommendation was based on the need for reasonable temperature control, and spot measurements can help detect locally exceeding temperatures caused by combustion of organic contamination[25].

2.6.4 Studies investigating thermal treatment and compaction

Vallejo-Olivares et al. conducted thermal treatment on coated aluminium alloy in the form of chips and two types of compacted briquettes. The alloy sheet was shredded into chips and sieved into fractions for sample preparation. Chips in sizes 2-5 mm were compacted into briquettes in a hydraulic press using uniaxial pressure (100 kN), Medium

Pressure Torsion (MPT)(70 kN), and MPT with heating at 450 °C (70 kN). All samples weighed 20 g. The density of coated uniaxial briquettes was 1.90 g/cm^3 ± 0.18 and the density of coated MPT briquettes was 2.19 g/cm^3 ± 0.09. Half of the prepared samples were thermally treated at 550 °C for 1 hour, and the weight was measured before and after treatment to calculate the weight change. On average, for three trials of coated material, the uniaxial briquettes had a weight decrease of -1.70 % ± 0.01, the chips -1.66 % ± 0.05, and the MPT briquettes -1.52 % ± 0.05. The heated MPT briquettes were not thermally treated[28].

Steglich et al. examined the recyclability of coated and baled aluminium UBC scrap of different densities and purity. Three types of UBC material were used (A, B, and C), and the different samples' properties are found in Table 2.1. Note that UBC C had three different densities.

Table 2.1: Properties of Steglich's UBC materials

Sample type	Density [g/cm^3]	Organic content [wt%]
UBC A	0.45	2.8 ± 0.3
UBC B	0.91	8.4 ± 4.0
UBC C	1.11 / 0.81 / 0.69	10.0 ± 2.6

UBC B also had a higher moisture content than UBC A and UBC C and impurities of plastic, iron, and copper. The carbon and oxygen concentrations in the UBC samples were measured with Leco TC600 and Leco TO800. The UBC materials A and B were thermally treated at 550 °C in a closed furnace for 30 minutes in different atmospheres of pure argon, an argon and oxygen mix, and air. Other process parameters can be found in the original article[20]. The treatment of UBC material C is presented in Section 2.6.5.

The results indicated a substantial carbon and oxygen content reduction for UBC A for all temperature and atmosphere variations. Pyrolysis in an argon atmosphere led to the highest remaining concentrations of oxygen and carbon. In contrast, thermal treatment in air at 550 °C led to the highest removal of carbon and reduced oxygen concentrations compared to the raw material. Regarding UBC B, all variations in temperature and atmosphere would result in decreased concentrations of carbon but increased oxygen concentrations due to oxidation. For UBC B, the highest reduction in carbon was obtained by thermal treatment in air at 550 °C, but this also resulted in the most excessive oxidation. The increased oxygen content of UBC B was assumed to be caused by oxidation due to exothermic reactions during burning of plastics and contamination. However, the reactor or the off-gas temperature was not measured to determine this. Lower oxygen content in the materials treated at 450 °C could, however, support the hypothesis[20].

2.6.5 Studies investigating stoichiometric thermolysis

The prepared samples of UBC C, as described in Section 2.6.4, were thermally pretreated under stoichiometric thermolysis [24]. The oxygen demand for the process was calculated using the organic mass of the samples, the molecular weights of BADGE epoxy, polyester, and PET monomer, and a simplified combustion calculation for thermolysis conditions. Equations 2.5, 2.6, and 2.7 were used as the stoichiometric chemical reactions. It was assumed formation of $\frac{2}{3}$ CO_2 and $\frac{1}{3}$ CO in addition to water vapour. The emission of hydrocarbons was neglected.

$$\text{Epoxy: } C_{21}H_{24}O_5 + 21O_2 \longrightarrow 14CO_2 + 7CO + 12H_2O \tag{2.5}$$

$$\text{Polyester: } C_8H_6O_4 + 6O_2 \longrightarrow 5CO_2 + 3CO + 3H_2O \tag{2.6}$$

$$\text{PET monomer: } C_{10}H_8O_4 + 8O_2 \longrightarrow 6CO_2 + 4CO + 4H_2O \tag{2.7}$$

The stoichiometric thermolysis resulted in the best decoating results while also reducing aluminium oxidation.

2.6.6 Studies investigating thermal treatment with off-gas analysis

Gökelma et al. explored the recyclability of used aluminium coffee capsules with and without residue. Pyrolysis in an argon atmosphere was executed in a resistance furnace at 800 °C with a heating rate of 300 °C/h and a holding time of 30 minutes. Off-gas analysis was executed with an FTIR analyser where the main pump was set to 1.5 L/min. Gökelma et al. found that the decomposition of organic matter would happen in two periods; first, a dehydration process with water vapour formation and then a degradation process in which the organic material would degrade into volatile components and char. Some specific compounds were measured to indicate the degradation mechanism. In the second cracking step, methane (CH_4), ethane (C_2H_6), ethylene (C_2H_4) and butane (C_4H_{10}) were detected as probable degradation products from longer organic hydrocarbon chains. Also, possible oxidation reactions were evident with the formation of reaction products such as CO_2, CO and H_2O. Ethane (C_2H_6) was detected between 300 °C and approximately 470 °C, while above 470 °C, the formation of hydrogen and methane was favoured compared to ethane. Figure 2.12 illustrates the formation of generated gases during pyrolysis [23].

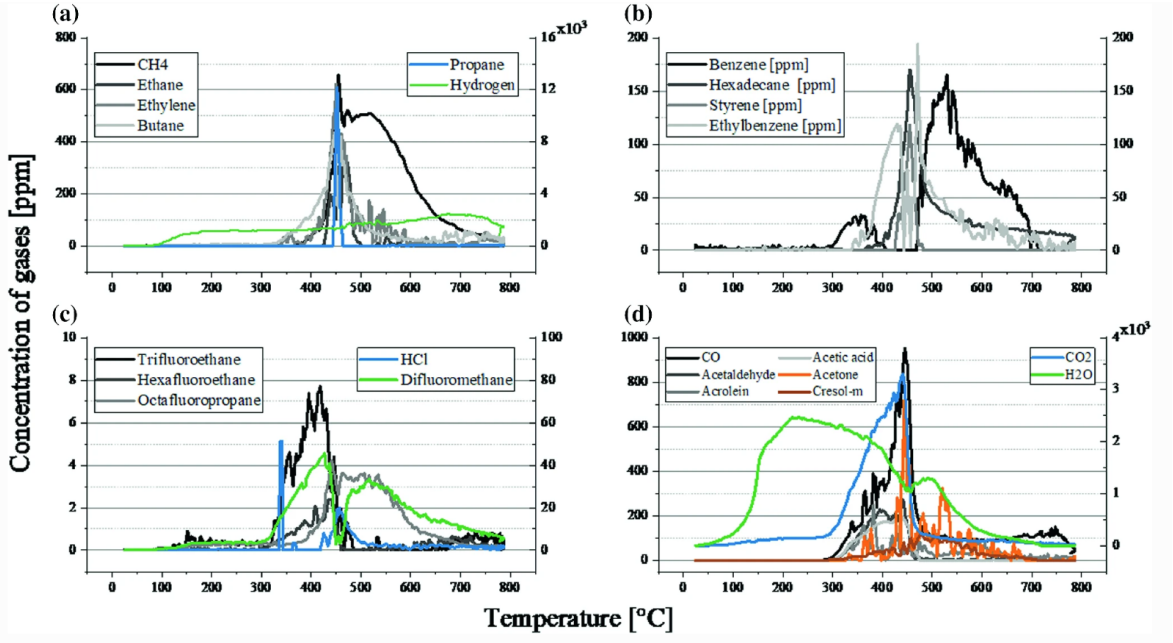

Figure 2.12: Composition of generated gas during pyrolysis of used (wet and yellow type) capsules versus temperature: (a) permanent hydrocarbons and hydrogen, (b) condensable hydrocarbons, (c) halogenated compounds, and (d) oxygen containing compounds

Meskers et al. investigated the decoating process of four painted magnesium automobile objects. Two objects had rough and thick paint layers (A and B), while the others had shiny and smooth surfaces (C and D). The organic coating resin was suggested to be polyester, epoxy, or polyester-epoxy mix as this is typical for these products. The four objects were cut to sizes of 5-10 mm^2 and decoated in a Seiko EXSTAR 6300 Thermogravimetry (TG)/Differential Thermal Analysis (DTA) machine in atmospheres of air and argon. A Gaslab 300 mass spectrometer was used for Evolved Gas Analysis (EGA) and it was set to detect CO_2, acetylene, 1-butene, butanal, acetaldehyde, pentadiene, and phenol ions[29].

For treatments in air, materials A, B, and C obtained one single decomposition peak at approximately 430 °C when using a heating rate of 20 °C/min. EGA showed the release of light hydrocarbons at temperatures between 290 and 380 °C and the release of light and heavier hydrocarbons above those temperatures. Material D had three mass loss peaks when heated at 10 °C/min, and the release of heavier molecules was only obtained at the last peak. Overall, light hydrocarbons were released at lower temperatures than heavier ones. After scission, a brown-black residue of carbon, pigments, and fillers remained, but the materials were almost entirely decoated[29].

For the treatments in an argon atmosphere, no materials were completely decoated. Compared to treatment in air, the mass loss peaks were shifted towards higher temperatures which indicate that scission occurred at lower temperatures if oxygen was present. From

DTA, it was observed that in the first mass loss peak, a small amount of heat was generated, and in the second peak, a significant amount of heat was generated. The peak could thus be characterised as exothermic, and the EGA detected CO_2. The EGA detected lighter hydrocarbons in the first scission peak and heavier hydrocarbons in the second. The four materials could be derived into two groups; those which decoat during the heating rate section (A and B) and those which decoat during the holding time section (C and D). Object C would also decoat later than object D and was, therefore, the worst material type. Materials A and B were easy to decoat and, thus, the preferred materials from a recycling point of view[29].

Kvithyld et al. examined thermal decoating by decomposition in a thermogravimetric furnace while measuring the Differential Thermal Gravimetry (DTG) curve, and the evolved gases with Mass Spectrometer (MS)[30]. The mass loss curve had two peaks, one corresponding to the scission regime and one corresponding to the combustion regime, as observed in Figure 2.13.

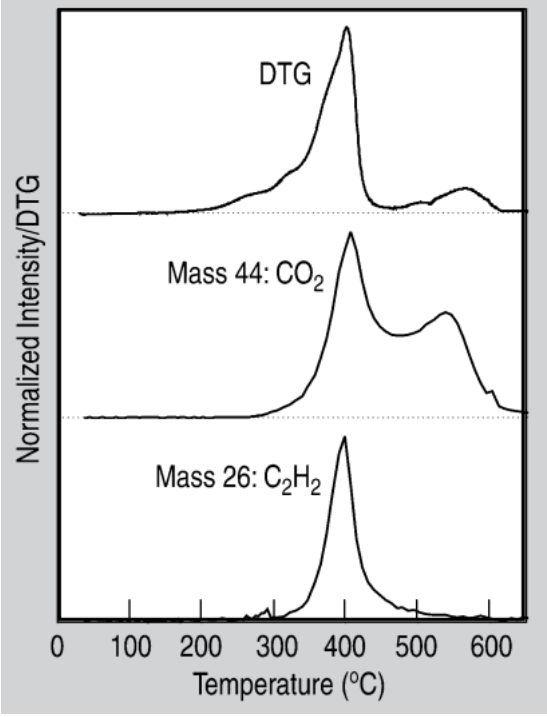

Figure 2.13: Mass-loss curve (DTG) and corresponding intensity curves for evolved CO_2 and C_2H_2 gas from a typical hydrocarbon for acrylic coated aluminium[6]

Hydrocarbon gases and CO_2 were observed simultaneously as the first peak, which indicates chemical degradation of the coating in the scission regime. The second peak of the DTG corresponds to further CO_2 evolution, which indicates that combustion gases are the only components in the combustion regime, also observed in Figure 2.13. Kvithyld also used hot stage microscopy and observed colour changes in the coating upon thermal treatment. In the scission regime, the coating turned black, while after combustion,

the surface regained a white colour. The black colour was explained to be due to the formation of char, and tar[30].

2.6.7 Studies investigating thermal decoating and coalescence

The compacted aluminium samples of Vallejo-Olivares, described in Section 2.6.4, were remelted under a salt flux consisting of NaCl, KCl, and CaF_2. The study concluded that the coating significantly affected the coalescence of the metal during remelting, while metal yields were relatively similar for all trials. Thermal decoating in advance of the remelting improved the coalescence for the coated material, while compaction alone did not improve the coalescence. Compaction with MPT made the thermal treatment less effective as a lower amount of coating was removed, resulting in a lower coalescence[28].

Capuzzi et al. studied the coalescence upon remelting of clean, coated, and decoated aluminium and found a positive effect on the coalescence after thermal pretreatment at 400, 500, and 600 °C[4]. The decoating removed the organic fraction in the coating while oxides and other impurities were left behind. The oxides and pollutants would negatively affect the scrap quality upon remelting, but a positive effect was observed on the metal recovery, and coalescence due to the decoating[4].

2.6.8 Possible side reactions during thermal treatment

During thermolysis of organic material, several chemical reactions may occur, not only the main reactions. It can thus be relevant to have an overview of the possibilities to be able to predict which compounds that will react and to explain possible irregularities. The Water-Gas Shift Reaction (WGSR) is a reaction between an equimolar mixture of steam and carbon monoxide, given in Equation 2.8[31]. The reaction is moderately exothermic with an enthalpy of ΔH = -41 kJ/mol; therefore, high conversion is favoured at low temperatures. However, reaction kinetics dominates at higher temperatures. High concentrations of carbon monoxide and water vapour will, by the Le Châteliers principle, push the reaction to the right. The reverse WGSR will, naturally, have the opposite chemical equation and enthalpy of ΔH = +41 kJ/mol.

$$CO(g) + H_2O(g) \longrightarrow CO_2(g) + H_2(g) \tag{2.8}$$

Methanation converts COx gases to methane and water vapour in a reaction with hydrogen gas. The reaction with CO_2 is given in Equation 2.9 and has an enthalpy of ΔH =

-165 kJ/mol, and the reaction with CO is given in Equation 2.10 and has an enthalpy of ΔH = -206 kJ/mol. The two exothermic reactions are thermodynamically favoured by relatively low temperatures[32].

$$CO_2(g) + 4H_2(g) \longrightarrow CH_4(g) + 2H_2O(g) \tag{2.9}$$

$$CO(g) + 3H_2(g) \longrightarrow CH_4(g) + H_2O(g) \tag{2.10}$$

The Boudouard reaction, describing the equilibrium between carbon, carbon monoxide and carbon dioxide, is given in Equation 2.11. The reaction is endothermic at all temperatures[7].

$$C(s) + CO_2(g) \longrightarrow 2CO(g) \tag{2.11}$$

2.6.9 Alternative methods for decoating and a comparison to thermal treatment

Thermal treatment for coating removal is not the only option in the field of decoating. A set of various spread techniques, including decoating by solvent extraction, decoating by sandblasting, and decoating by firing, was investigated by Rabah[33]. Both solvent concentration and treatment time would increase the decoating efficiency during solvent extraction, which was concluded to be the best technique with a 100 % decoating efficiency. Vacuum pyrolysis and stripping with H_2SO_4, HNO_3, and distilled water were studied by Li and Qui[21]. UBCs were thermally treated at temperatures between 300 and 650 °C for 30 minutes to remove organic components before the materials were leached in acid or distilled water. The leaching was applied to remove inorganic compounds. The best operation was concluded to be thermal treatment vacuum pyrolysis at 650 °C and 20 minutes treatment time, combined with leaching by 5 % H_2SO_4 for 60 seconds.

Wang et al. studied the effects of thermal decoating compared to the efficiency of using chemical agents such as thick sulphuric acid[34]. The results showed benefits of using chemical agents, which would result in a 100 % decoating efficiency, where the decoating efficiency was calculated as the ratio in weight of the pieces before and after thermal treatment[34]. Thermal treatment at 540 °C for 20 minutes would only result in a decoating efficiency of 93 %, and for treatment duration longer than 20 minutes, the decoating efficiency decreased. Varying temperatures were used for thermal treatments of 5 and

10 minutes, and the longer time would increase the decoating efficiency. It was observed that the thermal treatments at high temperatures and short treatment times obtained lower decoating efficiencies than treatments at 540 °C from 20 and up to 40 minutes. The decoating efficiencies for thermal treatments with variation in temperature and time are shown in Figure 2.14.

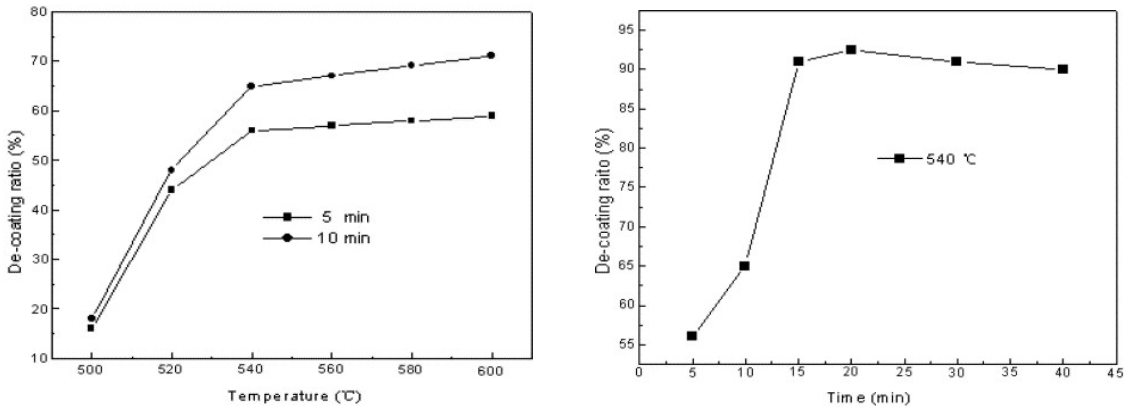

(a) Decoating efficiency with varying temperatures

(b) Decoating efficiency with varying time

Figure 2.14: Decoating efficiencies from Wang et al.[34]

2.7 Global warming potential and heat of combustion

Some gases, such as CO_2, CO, and CH_4 have strong absorption of energy, further leading to the greenhouse effect in the atmosphere around the earth[10]. Elevated amounts of these gases contribute to an increasing greenhouse effect, and thus emissions of GHGs are monitored. The impact of the emission is commonly expressed in terms of CO_2-equivalents (CO_2-e) or as a Global Warming Potential (GWP). The GWP reflects the emitted gasses contribution to global warming compared to CO_2, and the GWP of some common gases is presented in Table 2.2. Values for CO_2 and N_2O are given as direct GWP, while the rest is given as indirect GWP. Numbers are found from the IPCC's Fourth Assessment Report[35].

Table 2.2: GWP for a selection of gases

Species	Chemical formula	GWP [-]
Carbon dioxide	CO_2	1.0
Carbon monoxide	CO	1.9
Propane	C_3H_8	3.3
Ethane	C_2H_6	5.5
Methane	CH_4	25.0
Nitrous oxide	N_2O	298.0

A species' heat of combustion can either be measured calorimetrically or be calculated theoretically as the reaction enthalpy from ideal combustion of that species in reaction with oxygen gas[36]. The heat of combustion for a reaction is thus the energy transferred as heat at standard conditions for temperature and pressure (25 °C, 1 atmospheric pressure) and where the products are carbon dioxide gas and water vapour. Calculated values for the heat of combustion for a selection of gas species are presented in Table 2.3. Reaction equations and calculations can be found in Appendix B.

Table 2.3: Heat of combustion (ΔH_c) for a selection of gases

Species	Chemical formula	ΔH_c [MJ/kg]
Carbon monoxide	CO	10.1
Methane	CH_4	50.1
Ethane	C_2H_6	47.7
Ethene	C_2H_4	47.2
Propane	C_3H_8	46.4
Propene	C_3H_6	40.1

2.8 Remelting and dross formation

During aluminium remelting, the formation of aluminium oxides, that is, dross reduces the yield since the metal which is bound as oxide is lost[37]. The dross can also entrap molten metal due to its high oxide strength, which decreases the yield even more. The dross has a lower density than the molten metal, so the aluminium will sink to the bottom upon remelting, while the dross will float on top. Therefore, the dross will shield the liquid metal, preventing further oxidation. Dross has a lower thermal conductivity than liquid aluminium, so heat transfer through the dross may be a limiting factor for melting, and proper stirring can be necessary for heat transfer. Stirring can also enhance the submergence of light scrap, preventing oxidation, and it can be conducted by bubble injection, mechanical stirring, or electromagnetic stirring[3].

Promoted oxidation may have several causes, whereas high temperature is one. Steglich et al. found that UBC can-end alloys oxidise extensively within 10 minutes of thermal treatment at 570 °C, which leads to excessive dross formation upon remelting. Note that the UBC material was rich in both magnesium and silicon content. Additional oxides and metal entrapment into oxide films were proposed as reasons for the excessive oxidation. Therefore, it is desirable to have properly tempered melts and reasonable temperature control to reduce the dross formation and increase the yield. Temperature regulation can be complicated if the scrap metal is contaminated with organic residues. As the organics burn, the temperature will increase locally, promoting oxidation[25].

Stevens et al. explored the effect humidity and carbon residue have on the thermal oxidation of an aluminium alloy with 5 % magnesium. Carbon powder was used to simulate carbon residue, and dry and humid atmospheres of air, argon, and carbon dioxide gas was used. A TGA was used for off-gas analysis, and an MS was used to detect changes in mass. It was observed that a humid argon atmosphere would result in oxidised aluminium and the development of hydrogen gas. A damp air atmosphere would also produce oxidised aluminium but no hydrogen formation. An atmosphere mix of air and carbon dioxide resulted in reduced oxidation [37].

It was also observed that the carbon powder seemed to protect the aluminium surface from oxidation. In industry, the formation of oxides and dross reduces the yield in production. Stevens et al. suggested that metallic aluminium droplets are enclosed in alumina oxide layers, and when the layers break, new aluminium may be oxidised. The results indicate that some carbon residue should be left on the metal surface to protect the metal from oxidation. Therefore, a specially designed decoating procedure should be established so that these requirements can be fulfilled after the organics of the coating have decomposed [37].

In Steglich's trials on the coated UBCs, for which decoating was described in Section 2.6.4 and 2.6.5, the materials were melted in submerged salt-free remelting after the thermal pretreatment [20]. The remelting was executed in a molten aluminium heel at 750 °C in an argon atmosphere. Each experiment included 1000 ± 5 g of pre-molten aluminium heel and 100 ± 1 g of UBC sample. Visual inspection after stirring ensured complete melting, and a reaction time of 30 minutes was maintained. The dross was skimmed, cooled in argon, weighted, and analysed, and the metal was cast into a mould. The amount of formed dross was calculated by Equation 2.12.

$$\text{Dross formation in } \% = \frac{\text{Dross mass}}{\text{Dry scrap input}} \cdot 100\ \% \tag{2.12}$$

The results showed that UBC material A significantly reduced dross formation when the material was treated by thermolysis before remelting. The reduced dross amounts were suggested to be due to the decreased carbon and oxygen concentrations in the material after the treatment. For material A, all dross amounts, as calculated by Equation 2.12, would vary between 50 and 70 %. For UBC material B, dross amounts would range between 60 and 70 % depending on the pretreatment method. It was observed that, on average, all thermally treated samples of material B would result in higher dross amounts than the raw material sample without any pretreatment. This might be due to the higher contamination of carbon and oxygen in the thermally treated material. UBC material B was also more compact, and the higher density might have impeded the organic removal.

Thus, higher levels of scrap compaction and higher density might not be beneficial if organics have to be removed as gaseous products. The bales should have a low density to minimise metal loss but high enough for economical transportation and storage [20].

One third of the dross from each of Steglich's samples was remelted under a salt flux containing equimolar amounts of NaCl and KCl with 5 % Na_3AlF_6 [24]. The metallic and non-metallic contents were weighted after remelting to calculate the formation of Non-Metallic Products (NMP) by Equation 2.13.

$$\text{NMP in \%} = \frac{\text{Dross mass - Metal mass in dross}}{\text{Dross mass}} \cdot 100\ \% \tag{2.13}$$

The metal yield (η) was calculated by Equation 2.14.

$$\text{Metal yield } (\eta) \text{ in \%} = \frac{\text{Metal mass in dross + Recovered metal mass}}{\text{Dry scrap mass}} \cdot 100\ \% \tag{2.14}$$

The amounts of dross and non-metallic products from UBCs A and B can be seen in Figure 2.15.

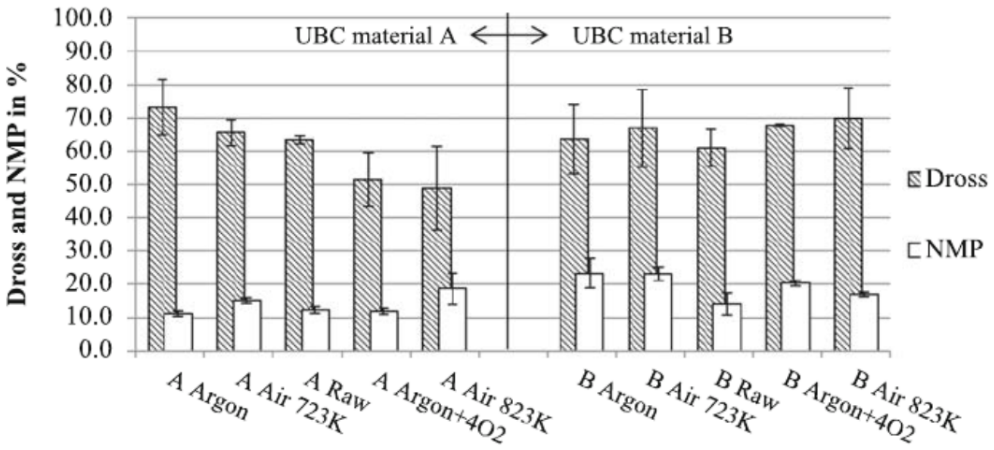

Figure 2.15: Dross formation and non-metallic products from Steglich

Reasons for metal oxidation can be several. The metal loss in the dross could originate from oxidised and entrapped metal. Oxides are hard to recover as aluminium has a high oxygen affinity, but the entrapped metal can more easily be recovered by dross processing. Oxidation could have occurred if the coating was partially removed, leaving the metal surface exposed to oxygen such that oxidation happened. Also, a higher organic content in the coating and contamination could result in intensified burning, resulting in higher temperatures and local oxidation. The oxidation would further result in enhanced dross

amounts, and metal loss[20].

Submerged melting is favourable as it will not expose the feed metal to a hot atmosphere that promotes oxidation but shield the metal completely in the melt. However, neither the submerged metal nor the argon atmosphere could prevent reactions between the melt and gaseous decomposition products from the organic contaminants on the scrap, leading to enlarged dross formation. Steglich's trials concluded that thermal pretreatment could reduce the amount of dross if stoichiometric thermolysis was applied between 550 and 570 °C for 30 minutes. Shredded or loose UBC material would also be preferable rather than bales, as small pieces promote heat transport into and gas transport out of the scrap. If the material has to be baled, lower densities are preferred. One should also take into consideration the organic content of the scrap[20].

For the UBC material C, the metal yield after remelting was highest for the medium-dense material, which was thermally treated by stoichiometric thermolysis. Metal yields for the different trials can be observed in Figure 2.16[24].

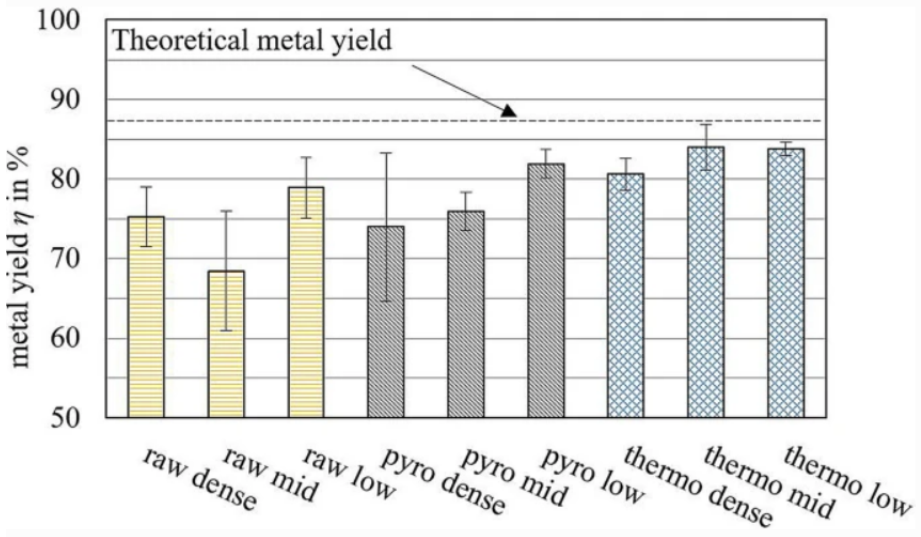

Figure 2.16: Metal yield of UBC material C with densities of 1.1 g/cm^3 (dense), 0.81 g/cm^3 (mid), and 0.69 g/cm^3 (low), without pretreatment (raw), after pyrolysis in argon at 550 °C (pyro), and stoichiometric thermolysis in air at 550 °C (thermo).

3 Method

3.1 Materials

Two different aluminium 8111-alloy sheets of thickness 600 µm were investigated, one with surface coating and one without coating. The coated alloy had a coating on both sides, one light grey and one dark grey-brown. In the project work before this master's thesis, Optical Microscopy (OM) found that the light grey coating had a thickness of 6.83 µm and the dark grey-brown 24.71 µm. Electron Probe Microanalysis (EPMA) found that the dark grey-brown coating consisted of elements such as aluminium, iron, oxygen, titanium, carbon, silicon, sulfur, and barium. X-Ray Diffraction analysis (XRD) found the best component matches for the phases $BaSO_4$, TiO_2, and SiO_2. The organic binder composition was not determined. The chemical composition of the two alloys, previously found by Inductively Coupled Plasma Mass Spectroscopy (ICP-MS) analysis, can be seen in Table 3.1. Regarding the coated alloy, the coating was removed from the alloy surface before analysis. Hydro, now Speira Holmestrand supplied both materials.

Table 3.1: Chemical composition of the two aluminium alloys

Component	Coated aluminium	Uncoated aluminium
Al [wt%)]	96.87 ± 0.94	98.10 ± 1.56
B [ppm]	7.30 ± 0.23	4.78 ± 0.13
Cd [ppm]	0.02 ± 0.00	0.10 ± 0.01
Co [ppm]	1.82 ± 0.04	2.86 ± 0.07
Cr [ppm]	7.78 ± 0.17	15.60 ± 0.16
Cu [ppm]	10.93 ± 0.40	340.00 ± 6.38
Fe [wt%]	0.75 ± 0.01	0.81 ± 0.01
Ga [ppm]	114.0 ± 1.41	106.33 ± 1.70
Mg [ppm]	6.90 ± 0.16	404.00 ± 5.35
Mn [ppm]	26.63 ± 0.49	366.00 ± 6.16
Ni [ppm]	39.80 ± 0.22	30.20 ± 0.94
P [ppm]	3.64 ± 0.41	1.93 ± 0.11
Pb [ppm]	9.53 ± 0.13	14.43 ± 0.12
Si [wt%]	0.23 ± 0.03	0.23 ± 0.02
Sn [ppm]	1.93 ± 0.01	2.45 ± 0.50
Sr [ppm]	0.15 ± 0.01	0.28 ± 0.08
Ti [ppm]	99.37 ± 1.16	53.03 ± 1.62
V [ppm]	83.77 ± 1.87	207.67 ± 0.94
Zn [ppm]	22.50 ± 1.84	74.40 ± 2.48
Zr [ppm]	15.83 ± 0.40	6.82 ± 0.27

For remelting trials, an aluminium alloy ingot of similar composition as the sheets was used as a molten heel. The specific chemical composition was unknown. The material was supplied from Speira Holmestrand and delivered as ingots of 2 kg, which were cut in quarters before use.

3.2 Equipment and procedure

3.2.1 Shredding and sieving of aluminium alloy sheets

A Getecha RS 1600-A1.1.1 machine with three blades was used to shred both coated and uncoated aluminium alloy into small chips. A grate below the blades, with circular holes of 8 mm in diameter, prevented fragments of larger sizes from passing through to the sample box underneath the machine. In advance of feeding, the alloy sheets were cut with pliers into pieces of approximately 10x10 cm, and new material was fed to the machine when the last feed was finished cut. The machine was stopped regularly to remove large pieces from the grate and cool the machinery.

The chips were further sieved into three fractions by a Retsch Rotap sieving machine. Two grates, with rectangular holes of 2 and 5 mm in size, and a solid sample holder was used to separate the chips. Portions of 500-700 g of chips were fed in batches and shaken for one minute by the Retsch Rotap. They were separated into one fraction holding chips smaller than 2 mm, one with chips in the 2-5 mm range and one with chips larger than 5 mm. The chips in the 2-5 mm range were further used for compaction of briquettes and direct thermal treatment and melting. Six portions were prepared holding 1 kg each of coated chips, and three portions were prepared holding 1 kg each of uncoated chips. The other chip fractions were saved but not used any further.

3.2.2 Compaction of briquettes

Coated chips in the 2-5 mm sieve fraction were compacted into briquettes using an MTS 311 Hydraulic press. 50 g portions of chips were weighted and filled into a mould in two doses. Between the fillings, a pressure of 20 kN was applied to slightly compress the material, which made room for the second portion. The mould had a diameter of 4 cm resulting in briquettes of that size. Two different compaction methods were used: uniaxial pressing and Medium Pressure Torsion (MPT), both at room temperature. 126 briquettes were made using each technique.

For the uniaxial pressing, briquettes were compacted with a 100 kN uniaxial pressure

load, which was held for 5 seconds. After compaction, the briquette was removed from the mould, and the height and weight of the briquette were measured. For the MPT pressing, a load of 100 kN of uniaxial pressure was applied together with torque. The pressure was held for 200 seconds while the mould rotated at a speed of 1.2 revolutions per minute (rpm), resulting in four rounds of torque. The briquette would then be removed from the mould, and the height and weight of the briquette were measured. Six sample bags, each holding 20 briquettes and equivalent of 1 kg material, were prepared for each briquette type. The six remaining briquettes of each type were saved for other purposes.

Figure 3.1 illustrates parts of the sample preparation with the Getecha RS shredding blades, shredded chips in the 2-5 mm fraction, and one compacted briquette.

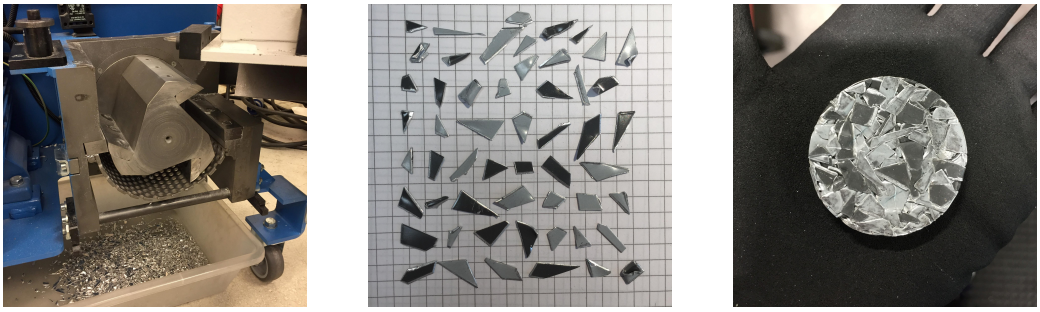

(a) Blades of the shredding machine

(b) Shredded chips in 2-5 mm fraction

(c) Compacted briquette

Figure 3.1: Shredding machine, chips, and briquette

3.2.3 Thermal treatment with FTIR analysis

Ten thermal treatment trials were conducted, seven with Fourier-Transform Infrared spectroscopy (FTIR) off-gas analysis and three for sample generation before remelting. An overview of the types of treated sample materials can be seen in Figure 3.2.

Table 3.2: Number of thermally treated samples of each material group

Material type	FTIR analysis	Sample generation
Coated chips	3	1
Uniaxial briquettes	3	1
MPT briquettes	1	1

All trials were conducted in a closed induction furnace with a Gasmet FTIR analyser. Each trial included approximately 500 g of sample material, and the exact weight was measured before treatment. Some samples were also weighed after treatment. Sample material was fed to a crucible before being inserted into the furnace chamber. Briquettes were fed lying flat on each other in a tower formation. Chips were fed with a cylindrical

filter in the middle of the crucible, making the chips lay in a doughnut formation around the filter. The furnace was closed with a lid fastened with eight nuts. The lid and furnace chamber was water-cooled, and the lid had inlets and outlets for cooling water, inlet gas, outlet gas, and a thermocouple, as shown in Figure 3.2. The excess gas outlet was connected to a scrubbing system. Two filters in the outlet gas pipes leading to the FTIR would collect particles more prominent than one micrometre. Both the filters and all other equipment were washed with ethanol between trials.

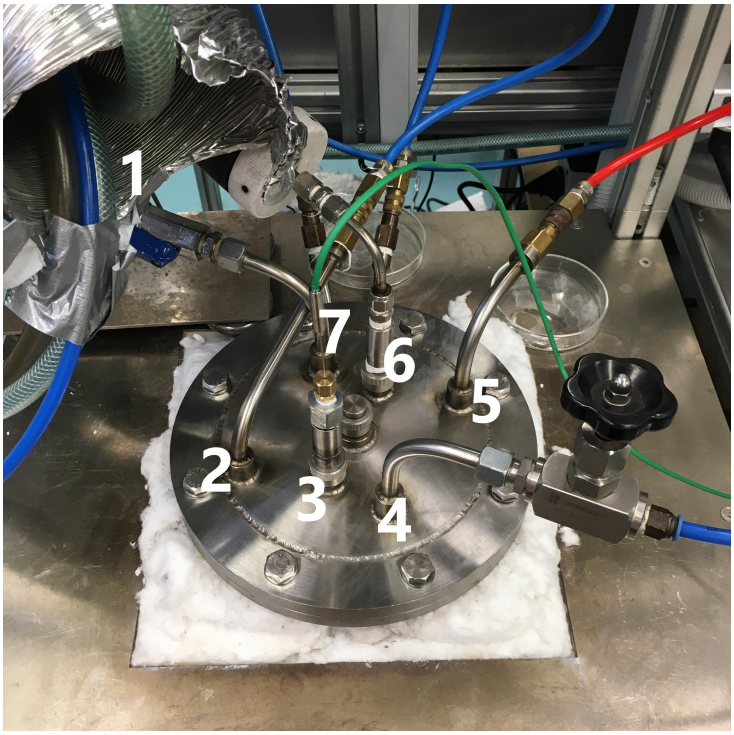

Figure 3.2: Furnace setup for thermal treatment and off-gas analysis where; 1=Exhaust pipe, 2=Water cooling inlet, 3=Thermocouple, 4=Gas inlet, 5=Water cooling outlet, 6=Gas outlet for FTIR analysis, and 7=Excess gas outlet

Samples were inserted into the furnace at room temperature, and the furnace chamber was flushed with pure nitrogen gas to zero the analyser. Before flushing, the equipment was heated to 180 °C. The reaction gas consisted of argon, nitrogen, and oxygen and the flow was set to 3 L/min. The needed oxygen concentration was calculated using Equations 2.5, 2.6, and 2.7 and set to 5 %. It was assumed that the coated material consisted of 2 wt% of organic material, based on weight losses obtained in the project work before this master thesis. The calculations were inspired by the work of Steiglich and can be found in Appendix A. A heating rate of 350 °C/h and a 650 °C target temperature were chosen. Later, the target temperature rose to 700 and then 800 °C due to large temperature differences between the furnace and the sample, whereas the thermocouple measured the actual sample temperature. When reaching a sample temperature of 550 °C, a 30 minutes holding time was conducted. The furnace was then turned off and cooled. At approximately 200 °C the crucible was removed from the furnace and cooled to room

temperature before the sample was weighted. An additional 11th trial was included as the first trial of thermal treatment of chips only reached a sample temperature of 450 °C. Initially, it was planned to conduct three FTIR and three sample generation trials of each material, but the number of trials was reduced due to repair of the equipment.

3.2.4 Remelting in molten heel

Remelting trials were executed in a water-cooled induction furnace. Table 3.3 gives an overview of the number of trials conducted for each material group.

Table 3.3: Number of samples remelted of each material group

Material type	Thermally treated	Not thermally treated
Uncoated chips	0	3
Coated chips	2	3
Uniaxial briquettes	2	3
MPT briquettes	1	3

The furnace power was set to 10 kW, the voltage was 140-250 V, and the frequency was 3.5 kHz. During experiments, the power varied between 6 and 12 kW to regulate the temperature and electromagnetic stirring in the melt. All equipment was coated with boron nitrate before the trials and dried to prevent sticking of aluminium metal or metal splashes. Two blocks of aluminium heel, in total 1 kg (1066.8 g ± 18.5), were washed with ethanol, dried, and charged to a graphite crucible placed inside the furnace's induction coil. The furnace coil was protected with heat-resistant mat covers, which also fixed the crucible. The experimental setup of the furnace is illustrated in Figure 3.3.

The heel was heated in an argon atmosphere until molten, and the argon gas flow was set to 10 L/min. A thermocouple was placed inside the molten melt. In the first experiments, the thermocouple was placed inside an alumina cover, while in the last experiments, another thick thermocouple without a cover was used. The molten heel was de-drossed at 780 °C at which the furnace was turned off. The furnace was turned on again, and when the molten and de-drossed heel re-obtained a temperature of 750 °C, 1 kg (986.6 g ± 22.7) of sample material was charged into the melt in portions using a small shovel. When charging coated material, the furnace had to be turned off two to three times, and the material had to be manually pushed into the melt using a spoon. Stirring with the spoon was conducted when all material was charged. The need for pushing and stirring was less profound for the decoated and uncoated material. Therefore, charging time would vary between 6 and 12.5 minutes. The total metal charge was heated to 780 °C and de-drossed with the spoon. Then the material was re-heated to 750 °C and cast into

a mould. Initially, three remelting trials were to be conducted for each material type, except for the unoacted material, which only had not thermally treated samples. Due to the FTIR equipment repair, a reduced amount of thermally treated samples resulted in a reduced amount of remelting trials.

Figure 3.3: Furnace setup for remelting trials where; 1=Argon gas inlet, 2=Lid, 3=Crucible, 4=Thermocouple, and 5=Exhaust pipe

3.3 Analysis

3.3.1 Analysis of pyrolysis condensate

30 mg of pyrolysis condensate, generated during FTIR thermal treatment, was dissolved in dichloromethane and analysed with a GC/MS system from Agilent Technologies, consisting of a 7890A Gas Chromatograph (GC) and a 5975C Mass Selective Detector (MSD). The GC was equipped with an Agilent 19091S-433 column of 0.5 µL injection volume. The total oven run time was 40.5 minutes, divided into four sections of 1) 40 °C for 5.7 min, 2) 8.8 °C/min to 100 °C for 1.7 min, 3) 13.3 °C/min to 220 °C for 3.4 min, and 4) 10.0 °C/min to 325 °C for 3.43 min. Scan parameters were set to low mass (35.0) and high mass (800.0).

3.3.2 TGA and DSC analysis

Three trials of TGA and DSC (Differential Scanning Calorimetry) were conducted for samples of the coated material. Each sample weighed 40-45 mg and was placed in a platinum crucible. A Linseis STA PT 1600 thermogravimetric analyser was used with a heating rate of 5 °C/min up to 550 °C where a holding time of 30 min was held. A 0.05 L/min flow of 5 % oxygen and 95 % nitrogen was applied, achieved by mixing a flow of 0.012 L/min synthetic air (21 % oxygen and 79 % nitrogen) and 0.038 L/min of nitrogen. Before each trial, the chamber was vacuumed and filled with nitrogen gas.

4 Results

4.1 Sample preparation

The weight and height of 20 briquettes from the two compaction types were measured, and their densities were calculated by Equation 4.1. For the height, three values were measured for each briquette at various positions, and the average was used in the further calculations.

$$\text{Density} = \frac{\text{Mass}}{\pi \cdot \text{Radius}^2 \cdot \text{Height}} \tag{4.1}$$

Table 4.1 shows the resulting values with standard deviations. It is observed that the MPT briquettes have an average 8.8 % higher density than the uniaxial briquettes. The uniaxial briquettes were more fragile than the MPT briquettes and fell slightly apart upon removing the mould and during transportation.

Table 4.1: Average weight, height and density of 20 briquettes

Briquette type	Weight [g]	Height [mm]	Density [g/cm^3]
Uniaxial	51.16 ± 1.27	19.60 ± 0.32	2.04 ± 0.04
MPT	50.22 ± 2.63	17.97 ± 0.08	2.22 ± 0.08

4.2 Thermal treatment

4.2.1 FTIR off-gas analysis

FTIR off-gas analysis was executed for each coated material type. At approximately 280 °C, initial gas formation was observed, and above 300 °C excessive gas formation was detected both on the analyser equipment and as cloudy gas in the scrubbing system. Each trial resulted in measured gas values (given in ppm), and the thermocouple measured the corresponding temperatures. The resulting data showed the largest gas formation of CO_2 and CO, as well as the formation of shorter hydrocarbons, H_2O, H_2, N_2O, and methanol. The oxygen concentration throughout the treatment was also measured. It was assumed that decomposition would happen from 250 °C and through the 550 °C interval. All further data is presented in the temperature interval from 250 °C up to 550 °C and through the 30 minutes holding time. The interval will be referred to as the reaction interval. MEEAPP will further be an abbreviation for methane (CH_4), ethane (C_2H_6), ethene (C_2H_4), acetylene (C_2H_2), propane (C_3H_8), and propene (C_3H_6) combined.

The measured oxygen signal was very uneven and was thus filtered with a seven-point filter equation, given by Equation 4.2. The filtered values were used for all graphical representations, while total integrated amounts were calculated from the unfiltered raw data.

$$y_n = \frac{59y_n + 54(y_{n+1} + y_{n-1}) + 39(y_{n+2} + y_{n-2}) + 14(y_{n+3} - y_{n-3}) - 21(y_{n+4} + y_{n-4})}{231} \tag{4.2}$$

In Figures 4.1, 4.2, and 4.3 graphical representations of the emergence of major gas phases in the reaction interval from the trials with loose chips can be observed. Note that there is some variation in the y-axes.

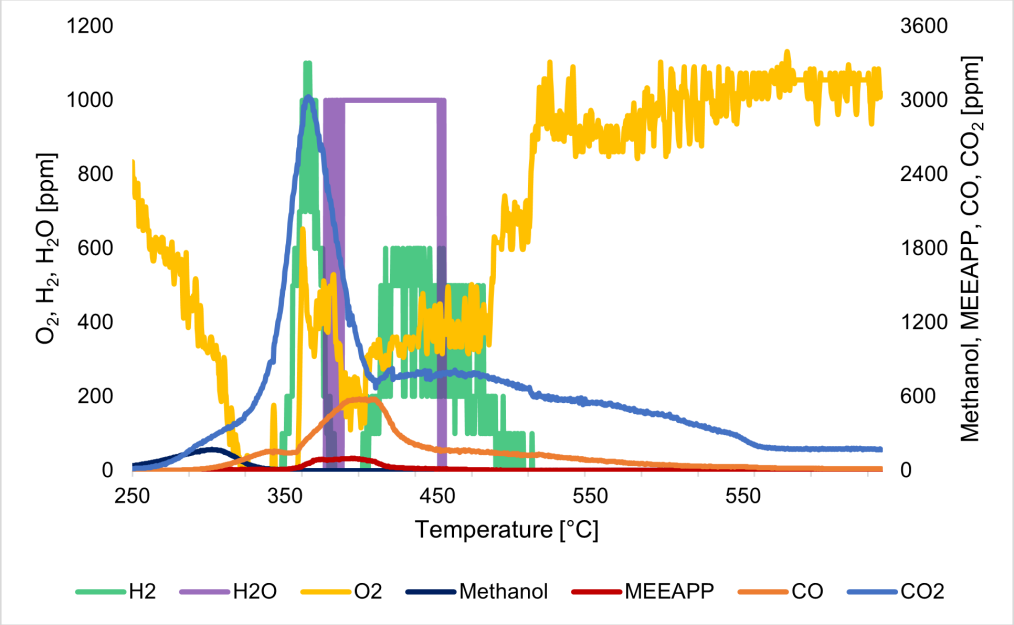

Figure 4.1: FTIR off-gas analysis loose chips (1)

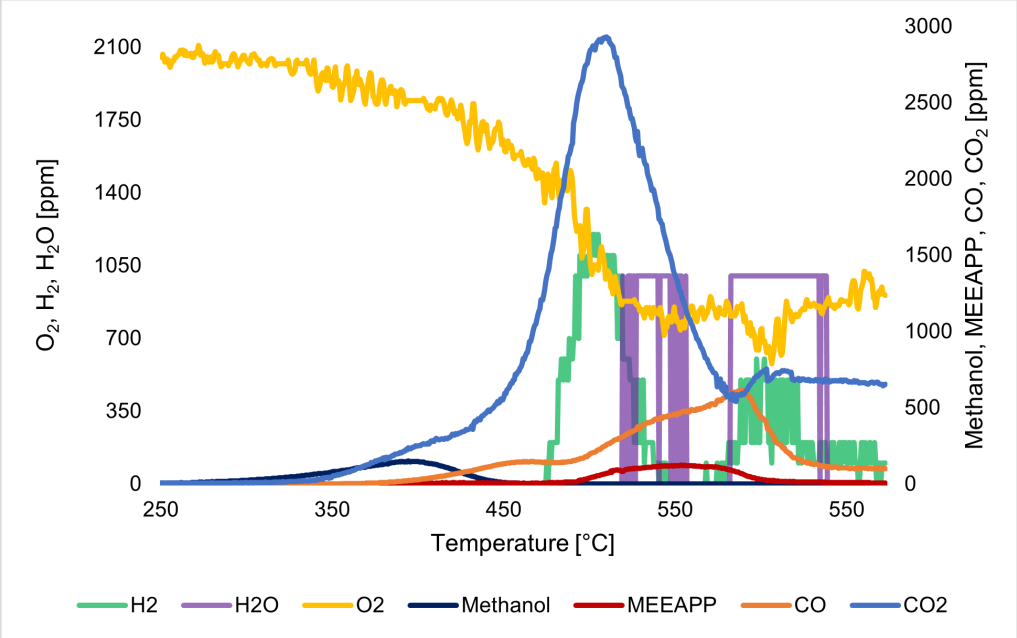

Figure 4.2: FTIR off-gas analysis loose chips (2)

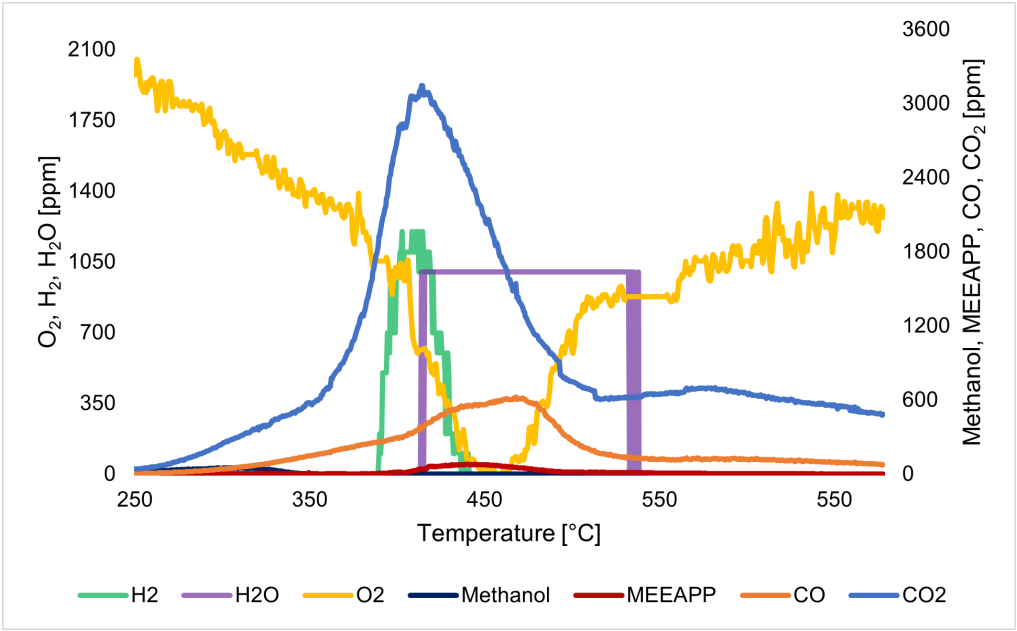

Figure 4.3: FTIR off-gas analysis loose chips (3)

The corresponding total integrated gas amounts in the reaction interval for the loose chips trials can be found in Table 4.2. Values are presented as individual values for each trial, as an average between the three trials with a percentage standard deviation (STD%) and average volume fractions of each species. The integrated value was obtained by summing all data points in the reaction interval for each species. The percentage standard deviation was calculated by Equation 4.3. The volume fractions were found by dividing each species' total integrated amount by the total average generated gas amount of the whole gas mix.

$$\text{STD\%} = \frac{\sqrt{\frac{(x-\bar{x})^2}{n}}}{\text{Average}} \cdot 100\% \tag{4.3}$$

Table 4.2: Total integrated gas values for chips in the reaction interval. Av. = Average. Vol.frac. = Volume fraction

Gas	Chips1 [Total ppm]	Chips2 [Total ppm]	Chips3 [Total ppm]	Av.±STD% [ppm±%]	Vol.frac. [%]
O_2	$98.8 \cdot 10^4$	$110.3 \cdot 10^4$	$92.4 \cdot 10^4$	$100.5 \cdot 10^4 \pm 7.4$	46.91
CO_2	$82.7 \cdot 10^4$	$49.4 \cdot 10^4$	$72.6 \cdot 10^4$	$68.2 \cdot 10^4 \pm 20.4$	31.85
CO	$16.4 \cdot 10^4$	$10.7 \cdot 10^4$	$15.6 \cdot 10^4$	$14.2 \cdot 10^4 \pm 17.7$	6.64
H_2O	$18.9 \cdot 10^4$	$13.5 \cdot 10^4$	$21.8 \cdot 10^4$	$18.1 \cdot 10^4 \pm 19.0$	8.43
H_2	$12.9 \cdot 10^4$	$10.2 \cdot 10^4$	$6.4 \cdot 10^4$	$9.9 \cdot 10^4 \pm 27.1$	4.59
Methanol	$2.4 \cdot 10^4$	$2.1 \cdot 10^4$	$0.6 \cdot 10^4$	$1.7 \cdot 10^4 \pm 45.9$	0.80
MEEAPP	16882.7	18208.0	11746.9	15612.5 ± 17.8	0.73
Methane	5334.6	5695.6	4011.4	5013.9 ± 14.4	0.23
Ethane	4729.6	5443.7	3498.8	4557.4 ± 17.6	0.21
Propane	230.0	666.7	199.1	365.3 ± 58.5	0.02
Ethene	5974.4	6014.1	3597.0	5195.2 ± 21.8	0.24
Propene	6.4	0.0	0.5	2.3 ± 126.4	< 0.00
Acetylene	607.7	387.9	440.0	478.5 ± 19.6	0.02
N_2O	1136.0	727.8	1051.1	971.6 ± 18.1	0.05

Some notable observations:

- All trials have similarities in peak shape and order of gas emergence. The first evolving peak represent methanol, followed by H_2, H_2O, CO_2, MEEAPP, and CO. In the first trial, all peaks are shifted towards a lower temperature compared to the second and third trials.
- Absolute values for CO_2 were obtained at 417 °C (3030 ppm), 540 °C (2931 ppm), and 430 °C (3144 ppm) for trials one, two, and three respectively.
- The average integrated CO_2 generation is 480 % higher than the average integrated CO generation.
- The oxygen concentration is decreasing until approximately maximum CO generation. The highest concentrations are found in the second and third trial, but it is below 2100 ppm during the whole intervals. In volume fractions of the total gas mix, oxygen is the primary compound.

Graphical representations from off-gassing of uniaxial briquettes in the reaction interval can be observed in Figures 4.4, 4.5, and 4.6. Corresponding integrated values, averages and volume fractions can be found in Table 4.3. All numbers are calculated in the same manner as for the chips.

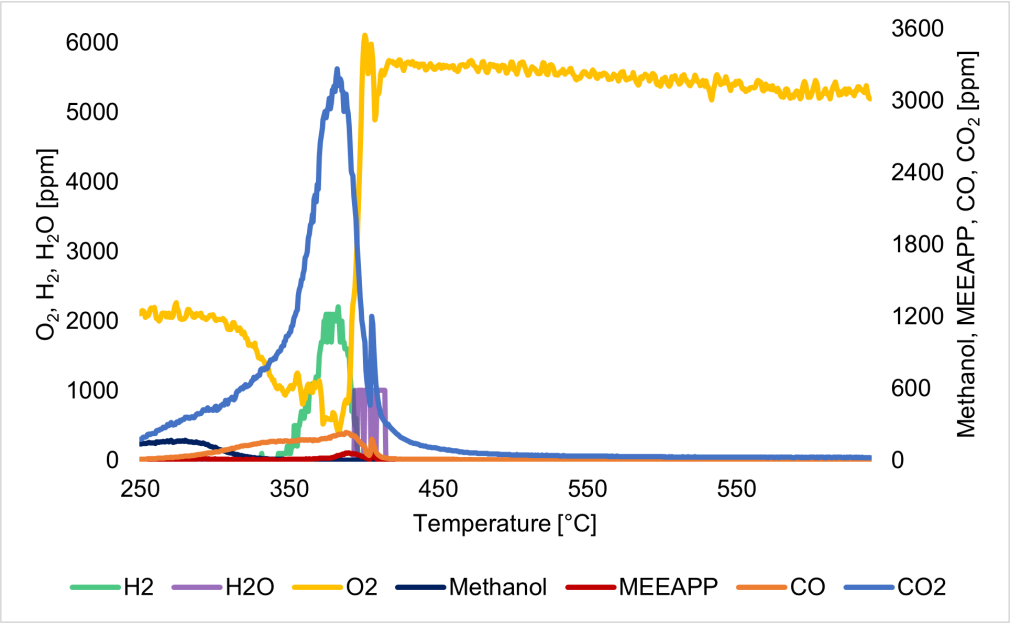

Figure 4.4: FTIR off-gas analysis uniaxial briquettes (1)

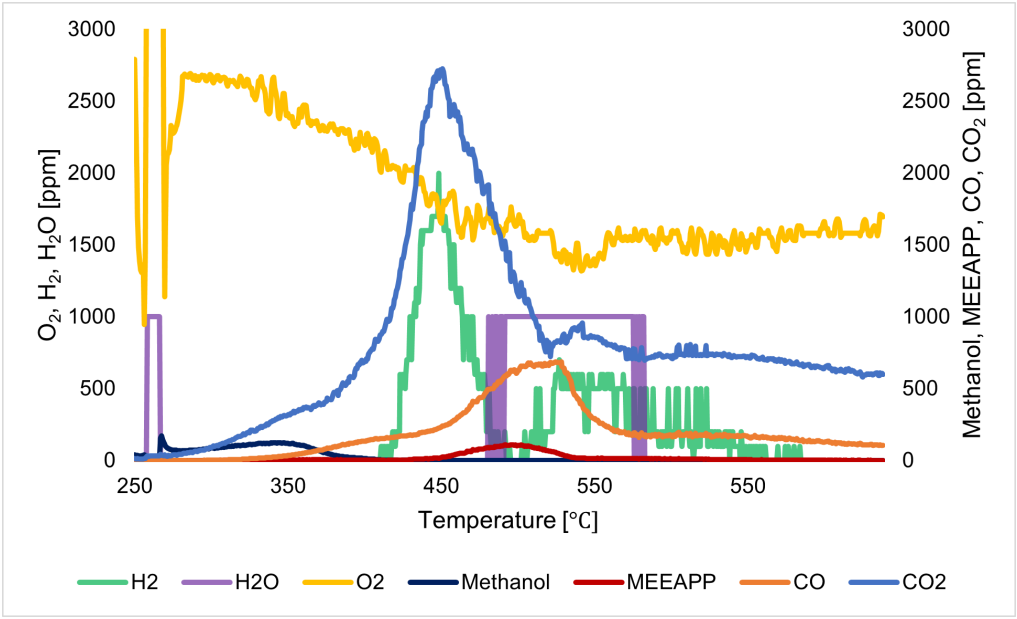

Figure 4.5: FTIR off-gas analysis uniaxial briquettes (2)

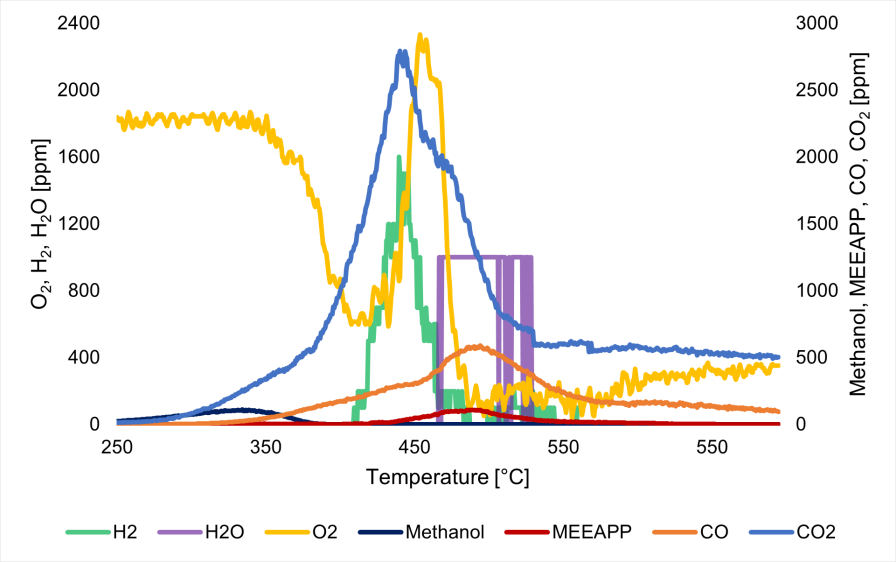

Figure 4.6: FTIR off-gas analysis uniaxial briquettes (3)

Table 4.3: Total integrated gas values for uniaxial briquettes in the reaction interval. Av. = Average. Vol.frac. = Volume fraction

Gas	Uniaxial1 [Total ppm]	Uniaxial2 [Total ppm]	Uniaxial3 [Total ppm]	Av.±STD% [ppm±%]	Vol.frac. [%]
O_2	$361.4 \cdot 10^4$	$181.7 \cdot 10^4$	$76.6 \cdot 10^4$	$206.5 \cdot 10^4 \pm 56.9$	71.07
CO_2	$27.9 \cdot 10^4$	$62.4 \cdot 10^4$	$58.1 \cdot 10^4$	$49.5 \cdot 10^4 \pm 31.0$	17.03
CO	$2.8 \cdot 10^4$	$15.1 \cdot 10^4$	$14.2 \cdot 10^4$	$10.7 \cdot 10^4 \pm 52.4$	3.69
H_2O	$2.5 \cdot 10^4$	$16.5 \cdot 10^4$	$9.4 \cdot 10^4$	$9.5 \cdot 10^4 \pm 60.4$	3.26
H_2	$8.5 \cdot 10^4$	$18.1 \cdot 10^4$	$8.4 \cdot 10^4$	$11.7 \cdot 10^4 \pm 39.0$	4.01
Methanol	$1.4 \cdot 10^4$	$0.4 \cdot 10^4$	$1.5 \cdot 10^4$	$1.6 \cdot 10^4 \pm 13.5$	0.54
MEEAPP	3568.0	13708.8	15072.0	10782.9 ± 47.6	0.37
Methane	257.6	4165.4	5730.8	3384.6 ± 68.0	0.12
Ethane	801.1	3747.0	4446.1	2998.1 ± 52.7	0.10
Propane	0.0	175.2	161.0	112.1 ± 70.9	< 0.00
Ethene	2421.8	4989.4	4460.0	3957.1 ± 28.0	0.14
Propene	0.0	27.4	0.7	9.4 ± 136.2	< 0.00
Acetylene	87.5	604.4	273.4	321.8 ± 66.4	0.01
N_2O	380.3	903.3	911.0	731.5 ± 34.0	0.03

Some notable observations:

- The first trial deviates from the second and third with profoundly lower integrated gas generation values and narrow peaks. The first trial also experiences a quick stop in gas formation at about 400 °C. This leads to large standard deviations on the averages.
- Absolute values for CO_2 were obtained at 388 °C (3265 ppm), 471 °C (2728 ppm), and 464 °C (2793 ppm) for trials one, two, and three respectively.

- The average integrated oxygen amount is 205 % if compared to the loose chips. The average integrated CO_2 amount is 73 % compared to chips.
- The average generation of short-chained hydrocarbons (MEEAPP) is only 69 % if compared to the amount from loose chips.
- The uniaxial briquettes were fragile, and in the first trial, only 87.1 % of the feed was still intact briquettes while 12.9 % of the feed was loose chips which had fallen off the briquettes.

Graphical representation of major gas compounds from off-gas analysis of the MPT briquettes trial in the reaction interval can be observed in Figure 4.7. Corresponding integrated values and volume fractions can be found in Table 4.4. As only one trial was conducted, averages with standard deviations were impossible to calculate. The volume fractions are based on numbers from the one trial, not the average, such as for the chips and uniaxial briquettes.

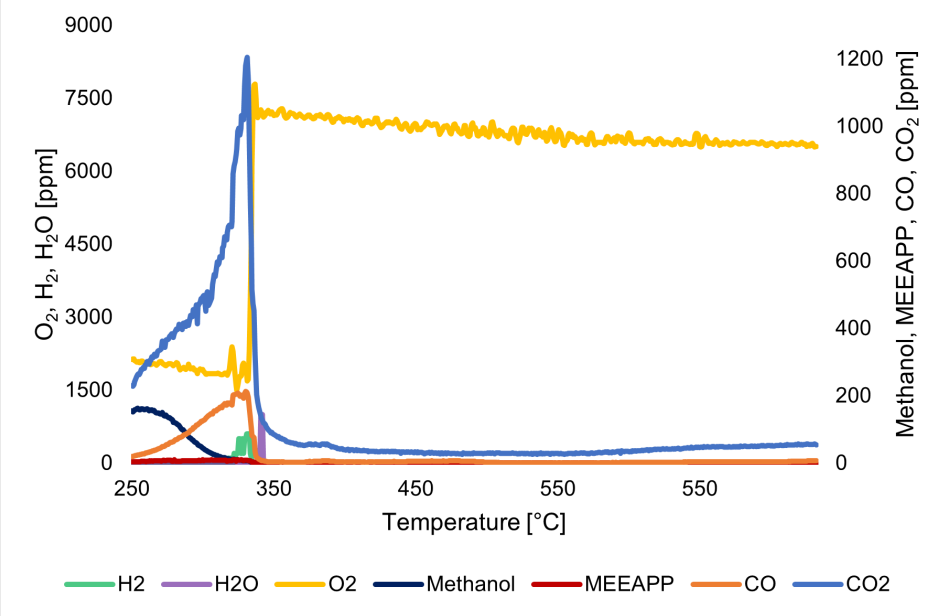

Figure 4.7: FTIR off-gas analysis MPT briquettes (1)

Table 4.4: Total integrated gas values for MPT briquettes in the reaction interval. Vol.frac. = Volume fraction

Gas	MPT1 [Total ppm]	Vol.frac. [%]
O_2	$490.5 \cdot 10^4$	97.44
CO_2	$9.3 \cdot 10^4$	1.84
CO	$1.6 \cdot 10^4$	0.32
H_2O	$0.2 \cdot 10^4$	0.04
H_2	$0.7 \cdot 10^4$	0.14
Methanol	$1.0 \cdot 10^4$	0.20
MEEAPP	1210.3	0.02
Methane	415.7	0.01
Ethane	0.0	0.00
Propane	0.0	0.00
Ethen	783.8	0.02
Propen	0.0	0.00
Acetylen	10.8	< 0.00
N_2O	91.2	< 0.00

Some notable observations:

- The total integrated CO_2 amount from the MPT trial is only 14 % if compared to the average amount in the chips' trials and only 19 % if compared to the average amount from uniaxial briquettes.
- Absolute value for CO_2 generation was obtained at 333 °C (1204 ppm).
- The integrated oxygen concentration for the MPT trial is 488 % if compared to the average for chips and 238 % compared to the average amount from uniaxial briquettes.
- Integrated methanol concentration in the first MPT trial is 59 % if compared to the average amount for chips and 63 % compared to the amount for uniaxial briquettes.
- Compared to peak position and shape for chips and uniaxial briquettes, the MPT trial is shifted towards lower temperatures, and the peaks have steep finishes.
- The MPT briquettes were more compact than the uniaxial briquettes, and during the first trial, 98.4 % of the feed was still intact briquettes while 1.6 % of the material had fallen off as chips.
- As only one trial of MTP briquettes was conducted, this trial can give a false impression of the briquette's behaviour.

4.2.2 Temperature development

The temperature development did not occur in the same precise manner for the different trials as observed in Figure 4.8. The first trial of chips had a step-by-step slow incline as the target temperature was adjusted during the trial. This also resulted in a prolonged treatment time, and the line is thus longer. The six other trials had more similar temperature developments. The second trial of uniaxial briquettes experienced the highest temperatures.

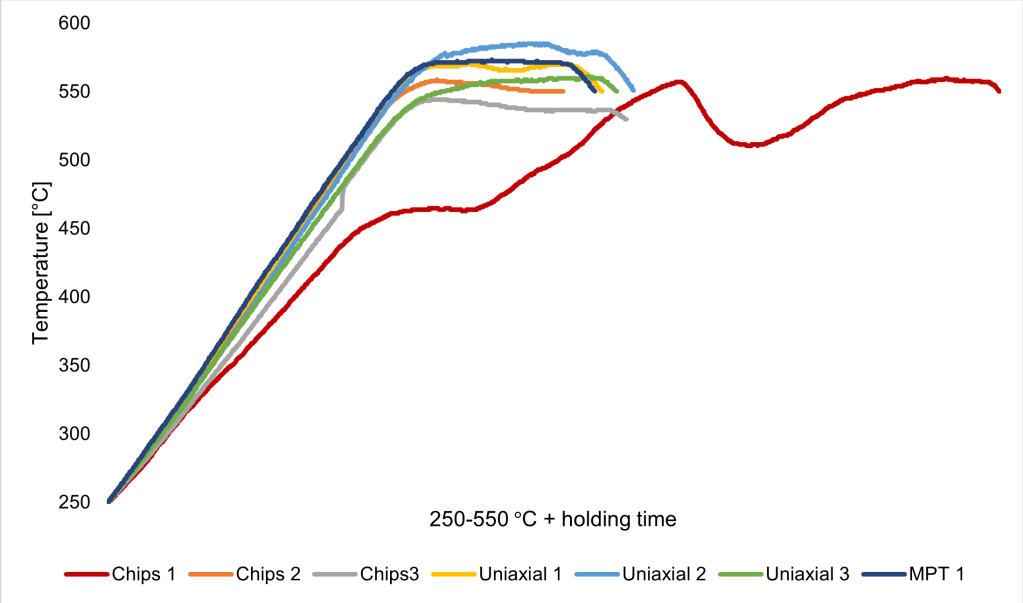

Figure 4.8: Temperature development in reaction interval

4.2.3 CO/CO_2 ratios

The CO/CO_2 ratio for each thermal treatment series was calculated in the reaction interval by dividing each measured CO-value by the corresponding CO_2-value. Plots of the CO/CO_2 ratios for development through the reaction interval for the three trials of loose chips can be seen in Figure 4.9. Ratios for the three trials of uniaxial briquettes can be found in Figure 4.10, and for the MPT briquettes trial in Figure 4.11. Exact numbers for maximum values and average ratios can be found in Table 4.5.

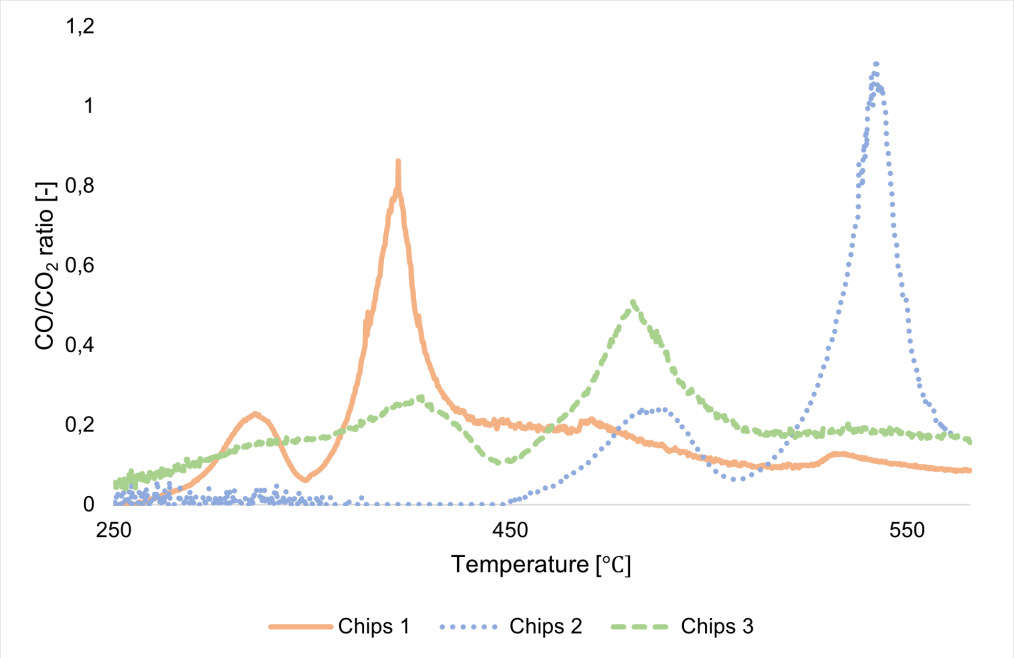

Figure 4.9: CO/CO_2 ratios for loose chips

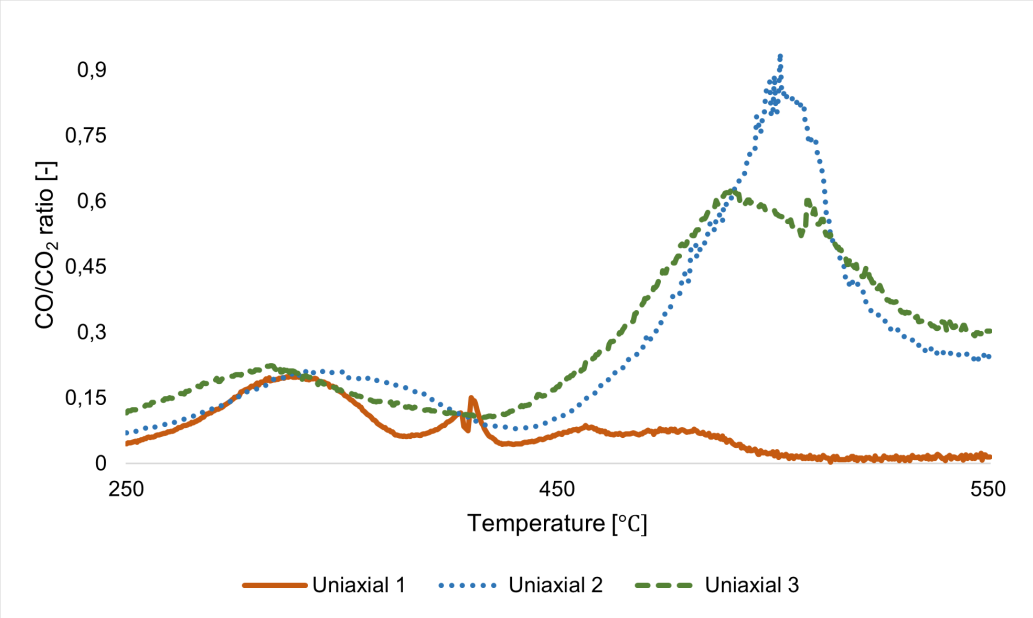

Figure 4.10: CO/CO_2 ratios for uniaxial briquettes

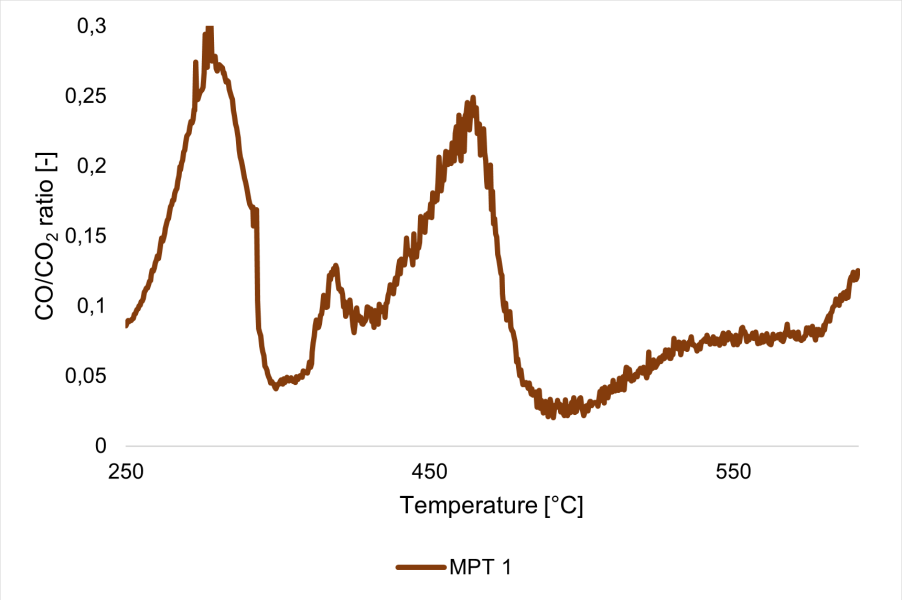

Figure 4.11: CO/CO_2 ratios for MPT briquettes

Table 4.5: Maximum CO/CO_2 ratio values and average ratios in reaction interval

Sample	Maximum value	Average ratio
Chips 1	0.86	0.17
Chips 2	1.12	0.19
Chips 3	0.51	0.22
Uniaxial 1	0.20	0.06
Uniaxial 2	0.94	0.22
Uniaxial 3	0.63	0.23
MPT 1	0.30	0.11

Some notable observations:

- The maximum CO/CO_2 ratio positions of chips are spread throughout approximately 100 °C, and the third trial has a lower average ratio.
- The first trial of uniaxial briquettes has a maximum ratio being 79 % and 68 % lower than the maximum ratios of the second and third trials, respectively. The second and third trials have similar peak positions and more similar values.
- The MPT trial has an uneven development of CO/CO_2 ratio in the reaction interval, and the two main peaks are similar in shape and value. The maximum peak value is 64 % lower than the average maximum ratio value for loose chips.
- It is observed that the CO/CO_2 ratios develop as wave-like functions. Especially the chips have two clear peaks, one small and then a larger one.

4.2.4 Global warming potentials

Global warming potentials for some species in the off-gases (CO_2, CO, N_2O, methane, ethane, and propane) were calculated with values from Table 2.2. GWP values for each species were multiplied by the detected off-gas amount (in ppm) in each data point and summed for all species. Plots showing the development of GWP for the different sample materials in the reaction interval can be found in Figure 4.12, Figure 4.13 and Figure 4.14 for chips, uniaxial briquettes and MPT briquettes respectively. Tabulated values for maximum peak value and total integrated value in the reaction interval for all trials can be found in Table 4.6.

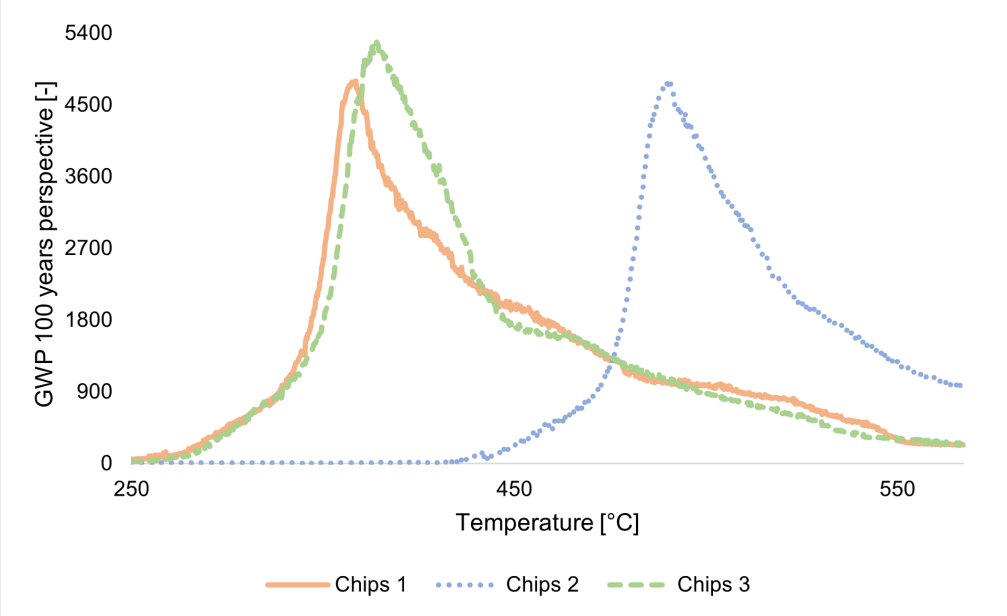

Figure 4.12: Global warming potential in chips off-gases

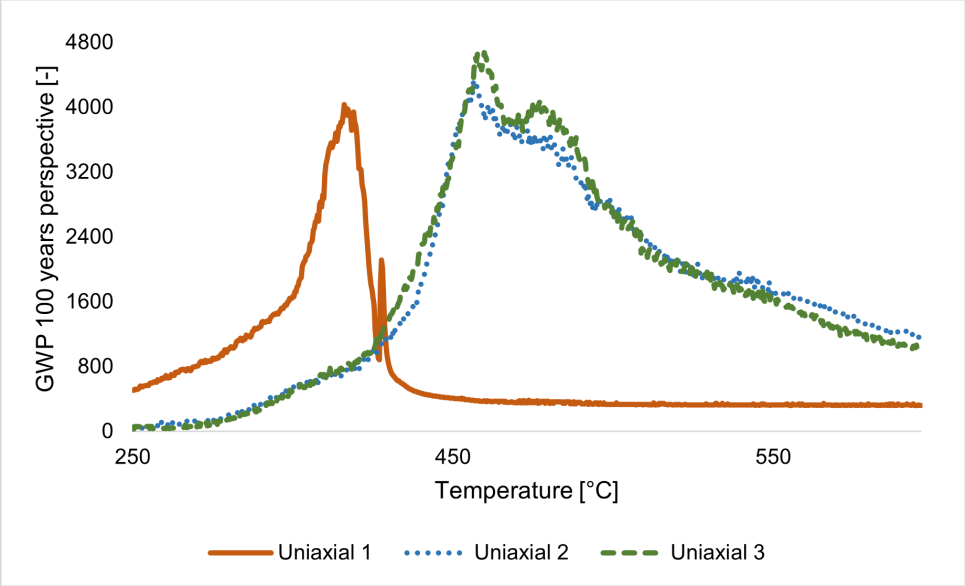

Figure 4.13: Global warming potential in uniaxial briquettes off-gases

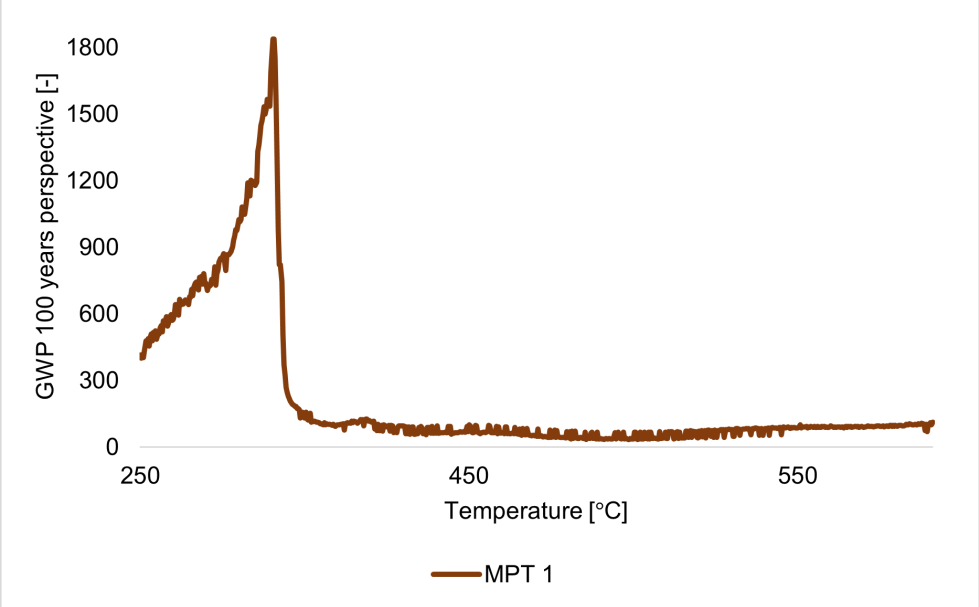

Figure 4.14: Global warming potential in MPT briquettes off-gases

Table 4.6: Maximum and integrated values for GWP in the reaction interval

Sample	Maximum value	Integrated value
Chips 1	4799.4	1,637,766.4
Chips 2	4826.4	1,089,158.4
Chips 3	5285.7	1,457,057.6
Uniaxial 1	4034.8	562,894.8
Uniaxial 2	4303.0	1,305,512.1
Uniaxial 3	4672.0	1,291,761.6
MPT 1	1839.0	160,360.1

Some notable observations:

- The trials of chips have both the highest average maximum value of total GWP and the highest average integrated value of total GWP if compared to uniaxial and MPT briquettes.
- The uniaxial briquettes have more similar integrated and maximum GWP values to the loose chips than to the MPT briquettes.
- The same shift in peak position observed for the chips and uniaxial briquettes for CO/CO_2 ratios can be observed for the GWP.

4.2.5 Heat of combustion

The heat of combustion for some species in the off-gases (CO, methane, ethane, propane, ethene, and propene) were calculated with values from Table 2.3. The heat of combustion for each species was multiplied by the off-gas amount (in ppm) in each data point, and the values were summed. Plots showing the development of heat of combustion for the different sample materials in the reaction interval can be found in Figure 4.15, Figure 4.16 and Figure 4.17 for chips, uniaxial briquettes and MPT briquettes respectively. Tabulated values for maximum peak value and total integrated value in the reaction interval for all trials can be found in Table 4.7.

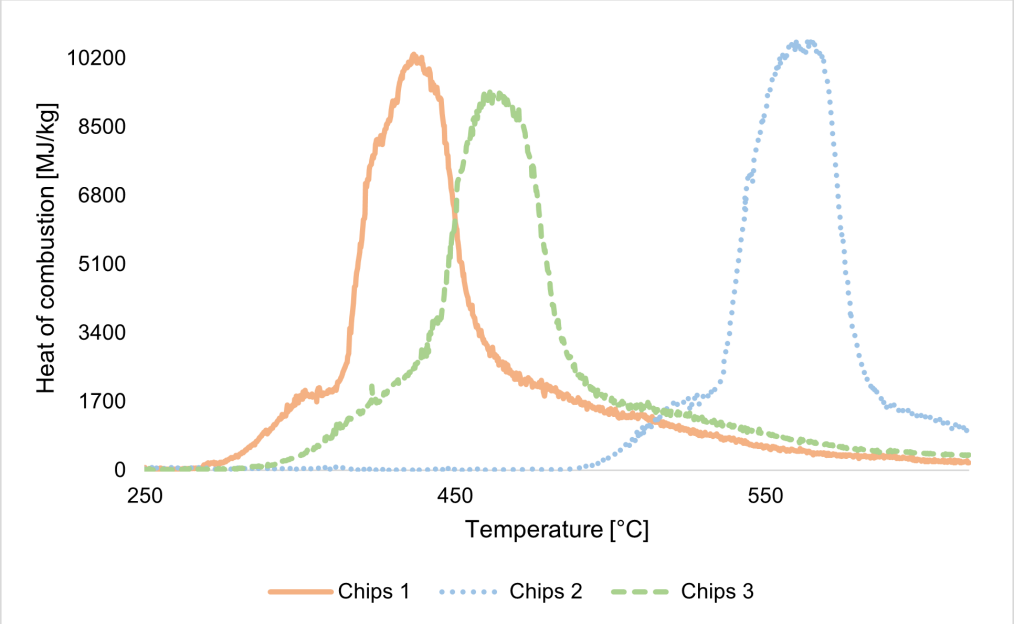

Figure 4.15: Heat of combustion in chips off-gases

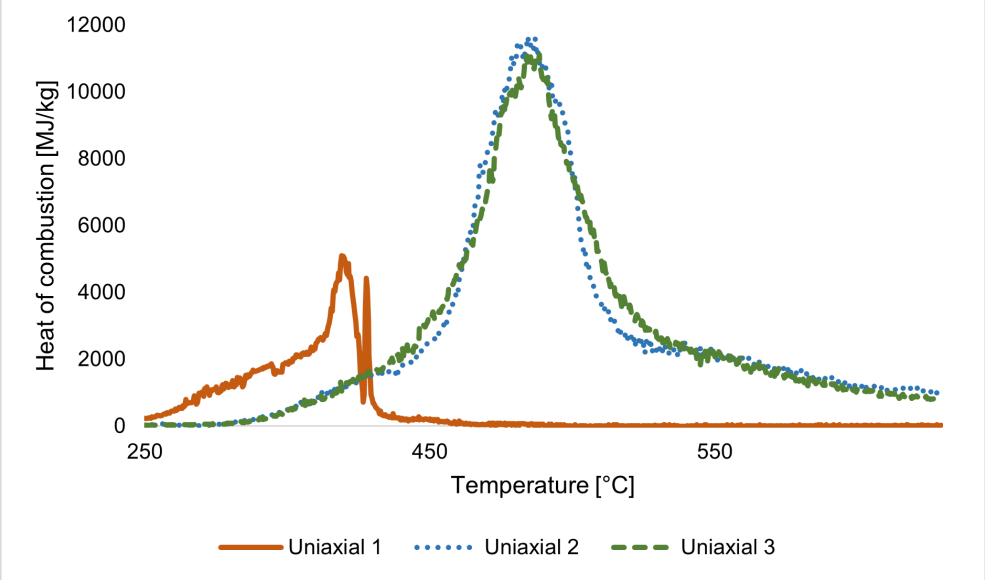

Figure 4.16: Heat of combustion in uniaxial briquettes off-gases

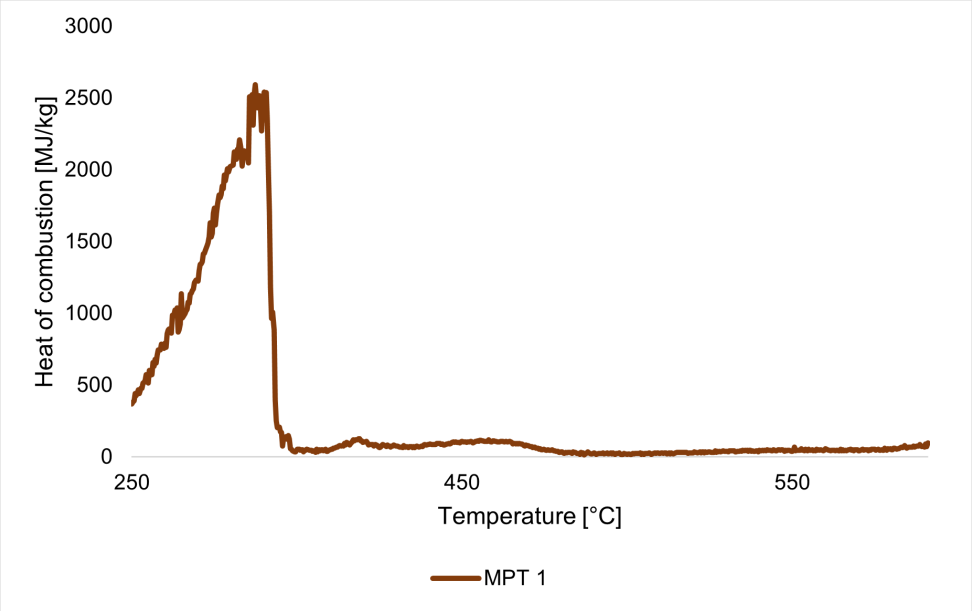

Figure 4.17: Heat of combustion in MPT briquettes off-gases

Table 4.7: Maximum and integrated values for heat of combustion in the reaction interval

Sample	Maximum value [MJ/kg]	Integrated value [MJ/kg]
Chips 1	10,306.0	2,445,777.3
Chips 2	10,688.1	1,943,305.1
Chips 3	9363.1	2,128,727.0
Uniaxial 1	5101.7	447,089.9
Uniaxial 2	11,668.0	2,158,925.8
Uniaxial 3	11,111.5	2,155,210.2
MPT 1	2593.2	218,042.3

Some notable observations:

- The second and third trials of uniaxial briquettes have higher values for maximum heat of combustion than the trials of loose chips. The MPT trial has lower values for maximum heat of combustion and integrated value.
- The peak shape for uniaxial and MPT briquettes is more pointy than the loose chips, which are rounded on top.
- The peaks are shifted in temperature position such as the CO/CO_2 ratios and GWP.

4.2.6 Weight changes

One batch of each sample material was weighed before and after thermal treatment, and the percentage weight change was calculated. The project work before this master's thesis found that the coated material had 0.0241 (g of coating/ g of sample material) and the decoating efficiency of the trials could thus be calculated by Equation 4.4.

$$\text{Decoating efficiency} = \frac{\text{Weight change of sample}}{\text{Initial sample weight} \cdot 0.0241} \cdot 100\ \% \tag{4.4}$$

Table 4.8 shows weight changes and decoating efficiencies from FTIR thermal treatment trials.

Table 4.8: Weight changes and decoating efficiencies after thermal treatment

Sample	Weight change [%]	De.c efficiency [%]
Chips	-1.55	64.2
Uniaxial	-1.43	59.5
MPT	-1.32	54.9

4.2.7 Colour changes

A distinguished colour change was observed on the sample surfaces after thermal treatment. Figure 4.18 illustrates untreated and thermally treated chips from different trials. The chips treated only up to 450 °C are very dark. In one of the trials reaching 550 °C, the chips in the upper layer of the crucible obtained bright colours of grey and yellow, while chips in the bottom of the crucible obtained a darker colour. The coating was loose.

(a) Untreated chips **(b)** Chips treated at 450 °C **(c)** Chips treated at 550 °C

Figure 4.18: Colour changes of untreated chips and chips thermally treated at 450 and 550 °C

The briquettes of both compaction types also changed colours upon thermal treatment, which is illustrated in Figure 4.19. The colour changes were somewhat variegated, with some areas being darker than the original coating and some areas being lighter grey and yellow. The colour changes were only observed on the outside surface of the briquettes.

(a) Untreated unaixial briquettes

(b) Uniaxial briquettes treated at 550 °C

(c) MPT briquettes treated at 550 °C

Figure 4.19: Colour changes on thermally treated briquettes compared to untreated briquettes

4.2.8 Formation of pyrolysis condensate

The thermal treatment resulted in a pyrolysis condensate condensing on colder surfaces in the furnace; the lid and upper part of the furnace, the filters, and all gas outlets. The condensate on the furnace lid and in the filter is shown in Figure 4.20. The residue condensate on the lid had a brown-yellow colour and was sticky. The residue in the filter was also yellow-brown but was more powdery. Both condensates were easily washed off with ethanol.

(a) Condensate on lid

(b) Condensate on filter inlet

Figure 4.20: Condensate on furnace lid and filter inlet

4.3 Analysis

4.3.1 Analysis of pyrolysis condensate

The GC/MS analysis found a variety of pyrolysis condensate components. Each component obtained a match factor and a component area, and the species with the highest component areas, of magnitudes above seven and match factors above 90.0, can be found in Table 4.9.

Table 4.9: Main detected components of the pyrolysis condensate

Component	Chemical formula	Component Area	Match Factor
Phthalimide	$C_8H_5NO_2$	206,820,086.1	99.4
1,2-Benzenedicarboxylic acid	$C_8H_6O_4$	30,474,859.2	99.5
1H-isoindole-1,3(2H)-dione, 2,2'-(1,2-ethanediyl)bis-	$C_{18}H_{12}N_2O_4$	20,510,328.6	95.9
1H-Isoindole-1,3(2H)-dione,2-(2-hydroxyethyl)-	$C_{10}H_9NO_3$	13,847,362.6	98.5
1H-Isoindole-1,3(2H)-dione, 2,2'-methylenebis-	$C_{17}H_{10}N_2O_4$	12,825,888.0	95.2
Benzoic acid, 2-methylpropyl ester	$C_{11}H_{14}O_2$	4,999,681.7	90.1
N-(2-Hydroxypropyl) phthalimide	$C_{11}H_{11}NO_3$	1,617,147.4	90.5
Phthalic acid, neopentyl 2-pentyl ester	$C_{18}H_{26}O_4$	1,607,891.8	92.6
1H-Isoindole-1,3(2H)-dione, 2-methyl-	$C_9H_7NO_2$	1,251,205.9	98.8

4.3.2 TGA and DSC analysis

Maximum relative mass change for each TGA trial, and the average with standard deviations, are presented in Table 4.10. The deviation between trials is slight.

Table 4.10: Relative mass change in TGA analysis

-	Trial 1	Trial 2	Trial 3	Average ± STD
Mass change [%]	-1.66	-1.67	-1.73	-1.69 ± 0.03

Figure 4.21 illustrates the mass loss peaks of the TGA analysis. The relative mass change was highest at temperatures between approximately 100 and 250 °C, and it is observed only one mass loss peak per trial. Note that above this temperature, the mass is not

increasing by oxidation e.g., even though the curve is declining but the relative mass loss is smaller.

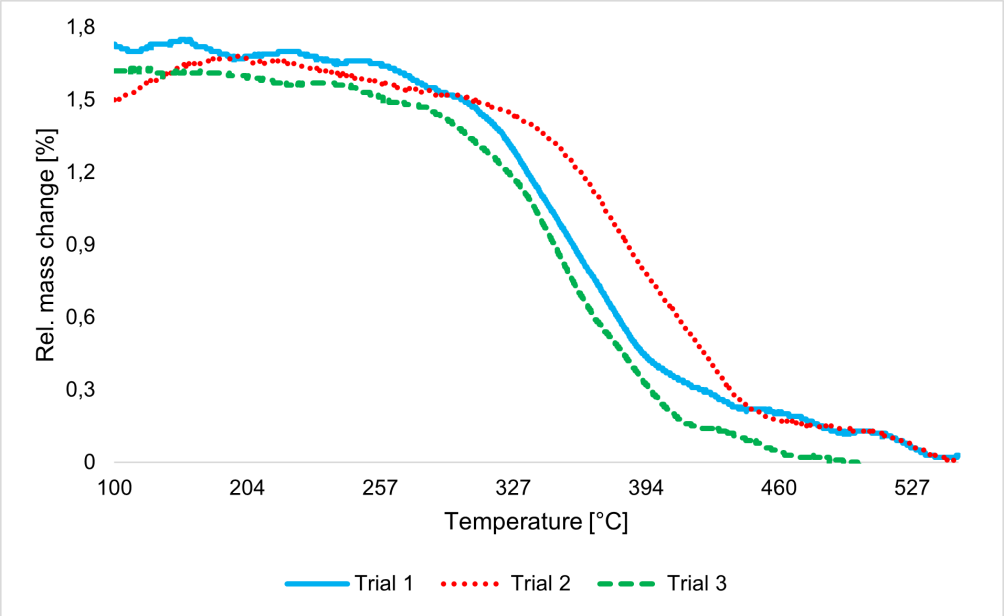

Figure 4.21: TGA analysis of coated material

Figure 4.22 illustrates the development of detected changes in heat flux with respect to temperature during DSC analysis. The peaks indicate one endothermic peak followed by one exothermic peak for each trial. The second trial is shifted towards higher temperatures and lower values, but overall the lines are relatively similar.

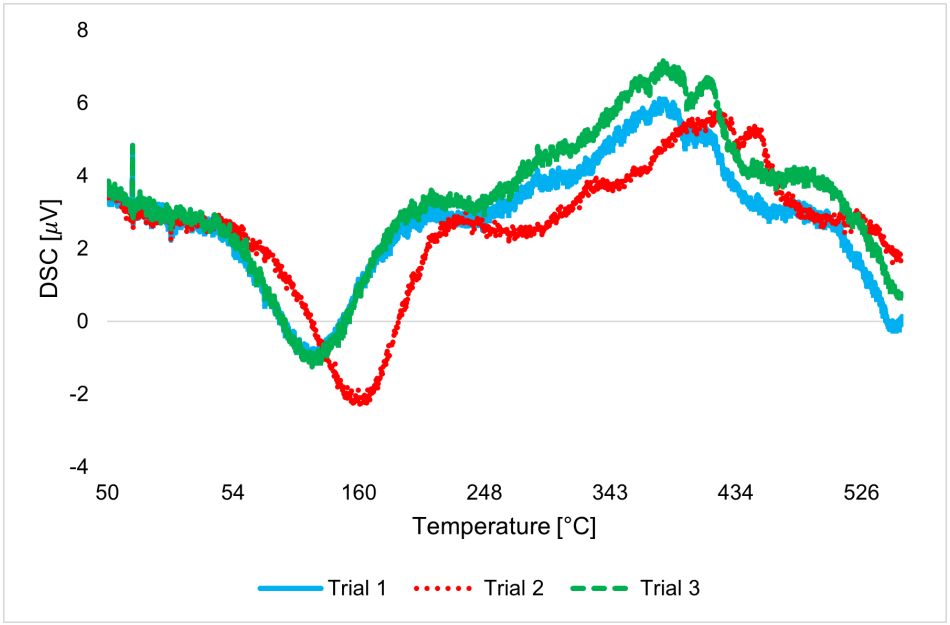

Figure 4.22: DSC analysis of coated material

The raw file plot for TGA and DSC analysis can be found in Appendix D.

4.4 Remelting trials

4.4.1 Dross weights and remelting yield

Each remelting trial resulted in dross skimmed off the molten metal, one batch before charging and one batch before casting. The dross which was skimmed before casting originated from the heel itself, and out of nine remelting trials, the average heel dross amount was 18.52 g ± 2.92, corresponding to 1.73 % ± 0.26. Specific numbers for the trials can be found in Appendix C. Figure 4.23 illustrates the average dross values obtained for each sample group, resulting from the skimmed dross after charging. The dross values were calculated by Equation 2.12, where the dry scrap input is the weight of the specific sample material charge.

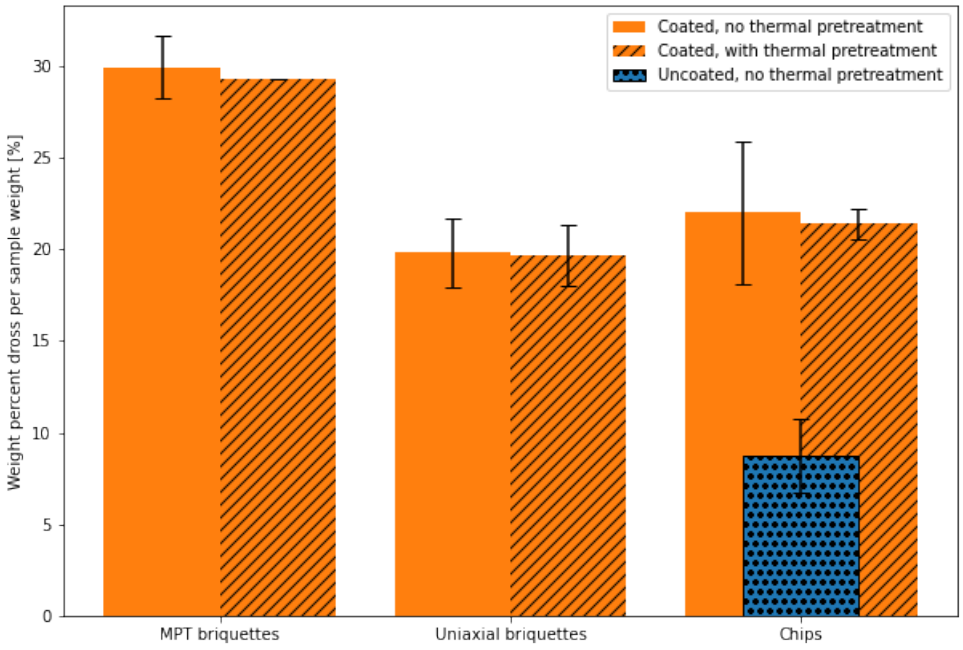

Figure 4.23: Average dross weights from remelting trials with standard deviations

A metal yield for each charge of sample material was calculated by Equation 4.5. Dross weighs and percentages, and calculated sample yields for the different trials can be found in Table 4.11.

$$\text{Yield}_{\text{sample}} = \frac{\text{Initial sample weight - Dross weight}}{\text{Initial sample weight}} \tag{4.5}$$

Table 4.11: Dross weighs and percentages and sample yields from remelting trials

Sample	Dross [g]	Dross %	Av. dross %	Sample yield
Chips unc	59.1	5.91	-	-
Chips unc	100.9	10.09	-	-
Chips unc	102.0	10.20	8.73 ± 2.00	0.91 ± 0.02
MPT	322.6	32.18	-	-
MPT	296.9	29.66	-	-
MPT	280.0	27.94	29.92 ± 1.74	0.70 ± 0.02
Uniax	202.1	20.28	-	-
Uniax	218.8	21.82	-	-
Uniax	171.8	17.28	19.79 ± 1.89	0.80 ± 0.02
Chips c.	274.3	27.42	-	-
Chips c.	184.4	18.44	-	-
Chips c.	201.7	20.16	22.01 ± 3.89	0.78 ± 0.04
MPT tt	278.5	29.24	29.24	0.71
Uniax tt	171.8	18.03	-	-
Uniax tt	201.6	21.32	19.67 ± 1.65	0.80 ± 0.02
Chips c. tt	202.5	20.55	-	-
Chips c. tt	207.9	22.21	21.38 ± 0.83	0.79 ± 0.01

Some casting residue was collected from the crucible after each remelting, and out of nine remelting trials, the amount of crucible residue was, on average, 14.96 g ± 1.85. Specific numbers can be found in the Appendix C. The yield for the whole charge was calculated from Equation 4.6. Sample and cast ingot weights, and calculated charge yields can be found in Table 4.12. Differences in stated decimals vary due to different weights being used for measurements.

$$\text{Yield}_{\text{charge}} = \frac{\text{Cast ingot weight}}{\text{Initial sample weight} + \text{Initial heel weight}} \tag{4.6}$$

Table 4.12: Sample, heel and cast ingot weighs, and charge yields from remelting trials

Sample	Sample [g]	Heel [g]	Cast ingot [g]	Charge yield
Chips unc	1000.09	1030.1	1934	-
Chips unc	1000.03	1062	1922	-
Chips unc	1000.03	1100	1956	0.94 ± 0.01
MPT	1002.45	1080.18	1710	-
MPT	1001.17	1084.9	1744	-
MPT	1002.23	1084.6	1754	0.83 ± 0.01
Uniax	996.55	1087.9	1818	-
Uniax	1002.57	1070.7	1804	-
Uniax	994.33	1068	1804	0.87 ± 0.00
Chips c.	1000.40	1065.9	1748	-
Chips c.	1000.08	1066.3	1836	-
Chips c.	1000.40	1057.7	1812	0.87 ± 0.02
MPT tt	952.40	1040.8	1680	0.84
Uniax tt	953.10	1074.8	1818	-
Uniax tt	945.40	1036.5	1746	0.89 ± 0.01
Chips c. tt	985.50	1051	1796	-
Chips c. tt	936.00	1074	1803	0.89 ± 0.01

Some notable observations:

- The uncoated chips resulted in small amounts of dross compared to the coated materials, regardless of thermal pretreatment for the coated materials.

- For coated material groups, the remelting trials generated, on average, less dross if the samples were thermally treated before remelting. However, the difference was small and standard deviations were profound. Thus the coated and decoated materials in each material group cannot be distinguished.

- For coated materials, it is observed that the MPT briquettes generate more dross than the uniaxial briquettes and the loose chips. On average, the uniaxial briquettes generate the least dross.

- Calculated yields, both sample-based and charge-based, are highest for the uncoated material. The charge yields are higher than the sample yields.

- As there was only conducted one remelting trial of thermally treated MPT briquettes, it was not possible to calculate averages with standard deviation. However, variation would have occurred if three trials had been conducted. The variation is calculated from only two data points for thermally treated chips and uniaxial briquettes.

4.4.2 Dross appearance

In Figure 4.24, one example of collected dross from each material type can be seen.

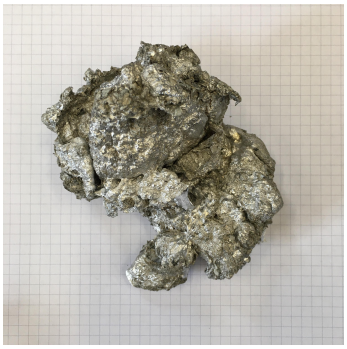

(a) MPT briquette without thermal treatment

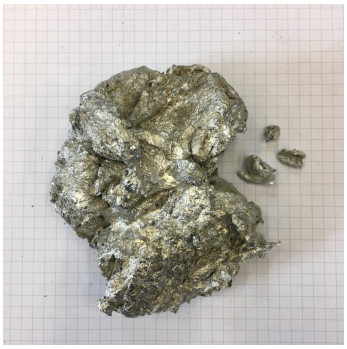

(b) MPT briquette with thermal treatment

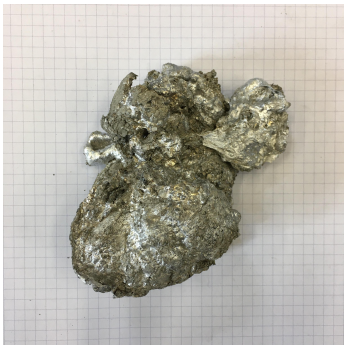

(c) Uniaxial briquette without thermal treatment

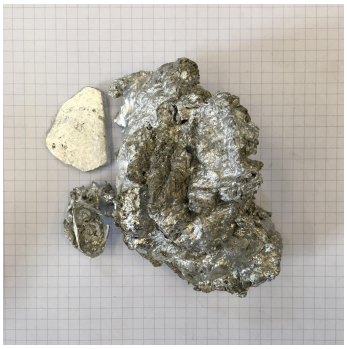

(d) Uniaxial briquette with thermal treatment

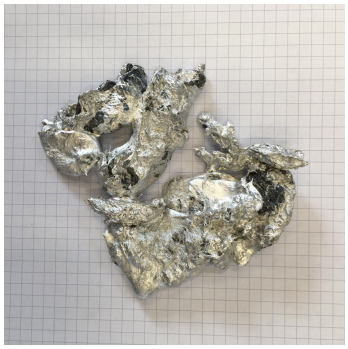

(e) Uncoated chips

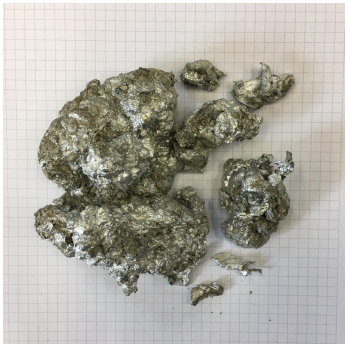

(f) Coated chips without thermal treatment

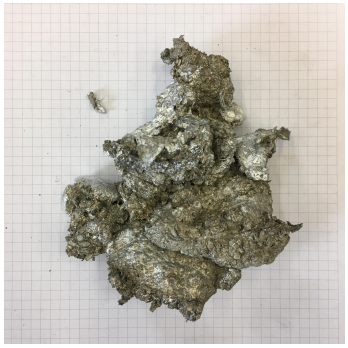

(g) Coated chips with thermal treatment

Figure 4.24: Appearance of sample dross from remelting trials

It was observed that the dross looked dry and spongy for the coated materials, while for the uncoated material, it appeared to be more metallic and hard. The dross from coated material samples had similar appearances regardless of the former thermal treatment. Each square on the white paper is 0.5x0.5 cm as a size reference.

4.4.3 Observations regarding process control

Another observation from the remelting trials was that the coated and not thermally treated samples caused intense smoke and flames upon charging to the molten heel. The chips had the most excessive flaming in terms of flame intensity, followed by uniaxial briquettes and then MPT briquettes. The MPT briquettes had, however, more intense smoking. Charging of the thermally treated samples resulted in neither smoke nor flames. The uncoated material did not cause smoke or flames, and it was also easier to charge than the coated chips since they melted faster. All material, loose chips and briquettes, floated on the molten metal surface before it melted, rather than submerging into the melt. A white powder sticking to the crucible after casting was observed.

5 Discussion

5.1 Thermal treatment with FTIR analysis

5.1.1 Generation of detected gases through pyrolysis and combustion

The FTIR off-gas analysis showed the most significant gas formation of CO_2, CO, shorter hydrocarbons, H_2O, H_2, N_2O, and methanol. All of these gases must originate from the coating on the aluminium surface. As inorganic pigments in the coating cannot vaporise, the detected gases must, more specifically, originate from the organic mass of the coating. Since the organic vehicle in the coating was unknown, it was assumed to consist of common coating compounds such as BADGE epoxy, polyester, and PET monomer. Typical decomposition products of these organic materials were stated in Section 2.6.2 to include acetaldehyde, water, carbon monoxide, carbon dioxide, compounds with acid and anhydride end-groups, phenolic decomposition products, propane, propene, ethane, ethene, butene, hexene-1, and butene-1. Some of these compounds were detected in the FTIR off-gas analysis, while others were not. From the stated list of possible decomposition products above, only water, carbon monoxide, carbon dioxide, propane, propene, ethane, and ethene were chosen for detection. The results reflect the chosen detection parameters, and some essential components could thus have been overseen. Other components than those stated above were detected in FTIR, such as heptan-n and toluol, but uncertainty resulted in them being cut from the results.

The fact that there were detected other compounds than just CO_2, CO and water vapour shows that the thermal treatment, as desired, did not result in complete combustion. The controlled oxygen flow must have resulted in some pyrolysis, proved by detectable condensable and non-condensable primary gases, observed as pyrolysis condensate on the equipment and by gas detection in the FTIR. However, it was assumed during the calculation of needed oxygen amounts that emissions of hydrocarbons would not occur. The formation of these gases can thus have resulted in too high amounts of oxygen in the reaction interval. With no observed liquid products and with the chosen process parameters of slow heating rate and prolonged treatment time, it is probable that slow pyrolysis has occurred. Taking this into consideration, the chosen temperature was too low to achieve maximised gas production. Nevertheless, proper temperature control was necessary in this case to prevent aluminium oxidation and reduce the possibility of melting the aluminium during thermal treatment.

Methanol was also detected during FTIR as one of the main phases, and the peak for methanol occurred before any other peak. The amount of methanol was also relatively

high in the MPT trial compared to other gasses. For instance, the integrated methanol amount in the MPT trial was 59 % of that of chips, while the CO_2 amount was only 14 %. In Section 2.6.2, methanol is not reported as a typical decomposition product of any of the suggested organic vehicle compounds. However, the coating could have consisted of other compounds as well. It was investigated if the methanol could originate from impurities in the washing ethanol, but the detected generated amounts are too high and the formation at too high temperatures to make this reasonable. Hydrogenation of CO-gas is the main production route of methanol, and the methanol could thus have emerged this way[38]. However, this is unlikely as the pressure is too low. It is thus still a question of where the methanol is coming from and if it is really methanol or instead another compound confused with methanol in the FTIR set-up. Due to equipment repairs, it was impossible to recalculate or re-calibrate the results to examine this.

The temperature development differed between the trials. Especially the first trial of chips differs from the others with a step-by-step incline and prolonged treatment, as observed in Figure 4.8. The longer treatment at a higher temperature may be the reason for increased integrated off-gassing in this trial, if compared to the other trials of chips, observed in Table 4.2. Looking at the graphical representation of the first trial of chips, in Figure 4.1, compared to the second and third in Figures 4.2 and 4.3, it is observed that the second and third trials have higher CO_2 concentrations at the end of the reaction interval than the first trial. This indicates that the second and third trials were not finished in off-gassing and could thus have obtained higher off-gassing values if the reaction interval was extended. The second trial of uniaxial briquettes experienced the highest temperatures during treatment. Out of the three uniaxial trials, this second trial has the highest total integrated values of both CO_2 and CO, which may be due to the higher temperature. However, the third trial has higher total integrated amounts of short-chained hydrocarbons (MEEAPP). Higher temperatures can thus result in more combustion, and prolonged heating time can result in increased off-gassing.

5.1.2 Comparison between sample materials

Some trends stand out when observing the off-gassing from the three types of coated sample materials, with graphical representation and integration in the reaction interval, from Section 4.2. First, the loose chips material generates much more gas than the other materials. In integrated values, the total off-gassing from chips was 1.137.330,8 ppm, from uniaxial briquettes 840.805,7 ppm, and from MPT briquettes 129.111,4 ppm. These values are without O_2 and calculated from Tables 4.2, 4.3, and 4.4. Looking at levels of CO_2 gas generation, the average integrated value for the chips is 138 % larger than

the average for uniaxial briquettes. Compared to the MPT briquettes, the difference is 733 %. Regarding volume fractions of each gas in the gas mix, 31.85 % of the total gas amount for chips is CO_2 gas. In contrast, the amounts are 17.03 % and 1.84 % for the uniaxial and MPT briquettes, respectively. Considering absolute values, the maximum peak values for CO_2 are similar for trials of chips and uniaxial briquettes with maximum values around 3000 ppm. On the contrary, the trial of MPT briquettes only exceeds 1200 ppm.

Also, for CO, MEEAPP, N_2O, H_2, and H_2O, the average integrated generation of gas from loose chips is more significant than for briquettes. In contrast, briquettes' gas formation is generally lower for MPTs than uniaxial briquettes. Regarding uniaxial briquettes, the only integrated average gas formations larger than for loose chips is for H_2 and propene, but the standard deviation for propene is above 100 %. Looking at off-gassing from the MPT briquettes, all detected integrated gas formation values are smaller than for the chips and uniaxial briquettes.

On the other hand, oxygen consumption follows the opposite trend, whereas larger integrated oxygen gas amounts are detected for the briquettes than for the chips. Compared to loose chips, the integrated oxygen amount for uniaxial briquettes is 205 %, meaning that less oxygen is consumed during thermal treatment. For MPT briquettes, the integrated oxygen amount is 488 % of that of chips. The differences in oxygen detection can be related to the λ-ratio, where compaction has led to ratios above 1, meaning that oxygen is more available than needed[24]. This can further be why an excessive generation of CO_2 and H_2O combustion products are happening. At the same time, it is observed that the oxygen concentration decreases simultaneously with the gas formation, indicating oxygen usage, which hence could result in λ-ratios below 1 and further result in the formation of CO and CxHy in addition to the H_2O and CO_2. This possible trend is observed for the third trial of chips in Figure 5.1.

It is also observed that the first uniaxial and the MPT trial, Figures 4.4 and 4.7, are shifted towards lower temperatures. As Meskers described it, higher oxygen concentrations can lead to combustion at a lower temperature, which may be the case in these trials[29]. Nevertheless, oxygen amounts were calculated to be stoichiometrically adjusted and should thus be consumed completely. This only occurs at short temperature intervals during the first and second trials of chips and the second trial of uniaxial briquettes. The reduced oxygen concentration down to 0 ppm can also be observed in Figure 5.1.

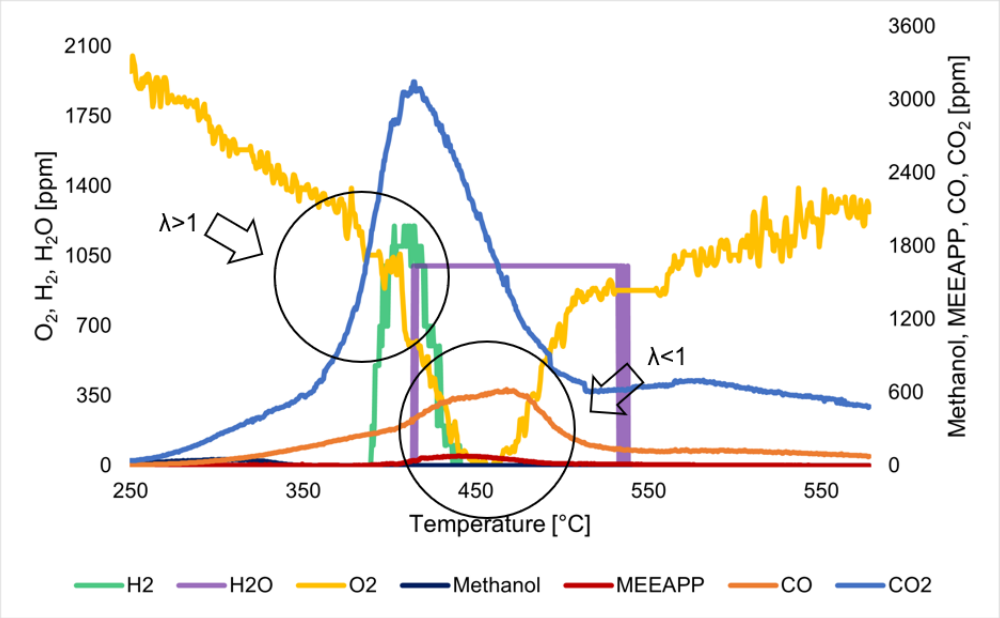

Figure 5.1: Relation between oxygen concentration and possible λ-ratio for chips (3)

The reason for lower gas evolution and lower oxygen consumption from the briquettes than for the loose chips can be related to the compaction and thus higher density of these briquettes. The higher compaction can make thermal decoating more challenging due to unavailable coating. If only the briquette's outer surfaces are de-coated, not the interior, this will lead to a lower burn-off during thermal treatment. The assumption of 2 wt% of organic matter for all trials might thus not be correct if some material is trapped and not accessible. Both briquette types are denser than loose chips, and as the MTP briquettes have a higher density than the uniaxial briquettes, it is reasonable that the off-gassing is even lower for the MPT trial. Unfortunately, only one MPT trial was conducted, and thus no variation could be calculated. Due to the less available organic mass in the briquettes, the possible lower hydrocarbon combustion for the compacted material can be a reason for smaller amounts of combustion gases. The briquettes' higher integrated remaining oxygen levels, indicating less combustion, can substantiate this. On the other hand, less detected hydrocarbons could have indicated complete combustion if the number of combustion products had been higher. Nevertheless, the ratios of CO_2, CO, and H_2O are also smaller for briquettes than for chips, both regarding the total volume and volume fractions.

The standard deviations for CO_2 and CO generation of uniaxial briquettes are large compared to those of chips, and overall, the standard deviations of uniaxial briquettes are more significant than those of chips. The uniaxial briquettes were fragile, verified by the significant amount of loose chips that had fallen off the briquettes before thermal treatment. This inhomogeneous material mix, with varying amounts of briquette and chip material in the charge, can be the reason for the large standard deviations. The

first trial varies most regarding lower CO_2 and CO generation and no detected propane and propene. In contrast, the third trial has much lower integrated oxygen amount than the two first. In addition to the uniaxial briquettes being fundamentally more loosely compacted than MPTs, the inhomogeneity can also be why the uniaxial briquettes have more similar values to the loose chips than to the MPT briquettes. If only regarding the second and third trials, the STD% for average integrated CO_2 formation would be 3.5 % and for CO 3.0 %, compared to 31.0 % and 52.4 % respectively if regarding all three trials. The average integrated CO_2 amount would further be 88 % compared to that of chips instead of 73 %. These numbers show the impact that the first trial had on the variation for the uniaxial trials.

Regarding the MPT briquettes, the material mix was more homogeneous than the uniaxial briquettes since the MPT briquettes did not fall apart as extensively as the uniaxial briquettes. This could have resulted in lower variation between the trials, such as for the chips, but as only one trial was conducted due to the equipment repair this is just speculations. With their high compaction, the MPT briquettes could just as well be a very complex material that could have had significant variations between trials.

5.1.3 Comparison to similar studies

The study of Gökelma et al. on the recyclability of used coffee capsules shows both similarities and differences to the present study. Process parameters of target temperature, heating rate, and off-gas flow deviate, but the goal of off-gas detection with FTIR agrees. Gökelma et al. detected two periods of reactions, first dehydration and then degradation. However, it must be specified that some of the samples were wet; therefore, only the second period is relevant for comparison. If investigating the trials of the present study below 250 °C, only one trial showed water vaporisation. This could also be confused with air in the system before full zeroing of the system and will thus not be investigated further. In the second period of Gökelma's study, the organic material degraded into volatile components and char, and methane, ethane, ethylene, and butane were detected as off-gases. Ethane was detected between 300 and 470 °C, while hydrogen and methane were detected at higher temperatures[23]. Methane alone had the highest peak value at approximately 650 ppm and propane at approximately 12,000 ppm, as observed in Figure 2.12.

The present study's combination of short-chained hydrocarbons (MEEAPP) never exceeded these values. The highest peak value was obtained during the second chips trial with a value of 123 ppm. The generation of short-chained hydrocarbons was thus much smaller in the present study. The peak position of the MEEAPP curve, regarding tem-

perature, also varied between the trials. The maximum CO_2 value of Gökelma et al. was obtained at approximately 3200 ppm and CO at 920 ppm[23]. These values correspond better to the present study, especially for loose chips and uniaxial briquettes' second and third trials. Again, significant differences in materials are present where the coffee capsules used in FTIR analysis only had a metal content of 6.8 wt%, due to large amounts of water and coffee residue.

In comparison, the coated alloy sheets in the present study were assumed to have an organic mass of 2 wt%. Therefore, it is difficult to compare these trials. It is, nevertheless, notable that the CO_2 and CO levels are similar despite the significant differences in organic matter and generation of hydrocarbons. It might be so that the organic matter in the present study has combusted more thoroughly than in the study by Gökelma et al., resulting in relatively higher amounts of combustion products and lower amounts of pyrolysis products. However, this would be reasonable as the samples of Gökelma et al. were pyrolysed in argon while the samples in the present study were treated by stoichiometric pyrolysis. A section of off-gassing in the study by Gökelma et al. and the FTIR off-gassing for the first trial of chips in this study are compared in Figure 5.2.

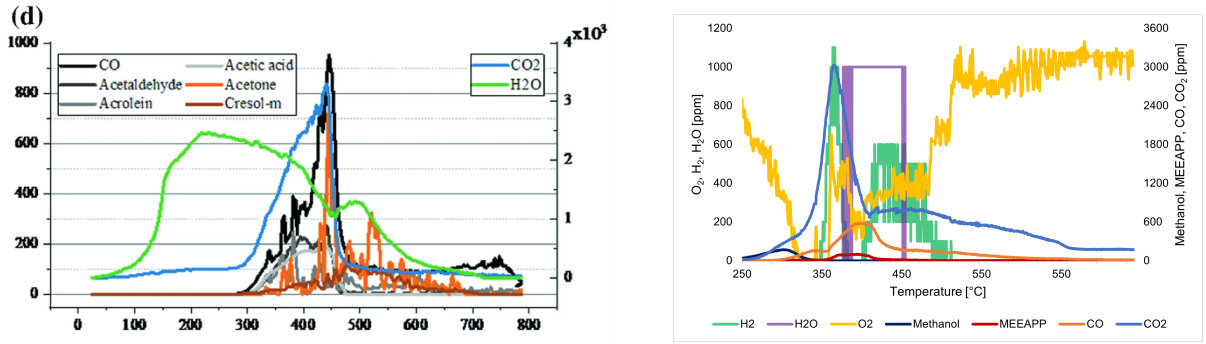

(a) Section of off-gasing figure from Gökelma et al.[23]

(b) FITR off-gassing loose chips (1)

Figure 5.2: Comparison off-gassing: Gökelma et al. and present study

Meskers et al. found that the thermal treatment of coated magnesium did not complete the decoating if the material was treated in a pure argon atmosphere. In contrast, the materials were virtually completely decoated in an air atmosphere[29]. An issue with the sample materials in the present study was their compaction, which might have led to difficulties of complete pyrolysis due to coated material being trapped inside the briquettes. The coating exposed to the reaction gas might thus have experienced a higher relative oxygen concentration than what was desired through the calculations, leading to complete combustion rather than pyrolysis. This can be why higher CO_2 and CO concentrations and lower levels of short-chained hydrocarbons are detected in this study and why the peaks are shifted towards lower temperatures for the first trial of uniaxial briquettes and MPTs.

5.1.4 Effect of possible side reactions

In addition to combustion and pyrolysis reactions, several possible side reactions might have occurred during the thermal treatment. The exothermic WGSR yields CO_2 and H_2 while consuming CO and H_2O[31]. As all needed compounds were present during treatment, the reaction has probably adjusted the ratios of CO and H_2O to CO_2 and H_2, following Le Châteliers principle. With significant amounts of CO_2, the principle predicts a shift of the reaction to the left, yielding CO and H_2O. As the chips had more available CO_2 this system could have been more shifted, making it reasonable to have higher hydrogen amounts for the uniaxial briquettes as less hydrogen is consumed together with CO_2 in WGSR. Both methanation and Boudouard reaction might have occurred, but it is difficult to interpret to which extent and in what favour[32] [7].

5.1.5 Differences in CO and CO_2 formation and CO/CO_2 ratios

As previously stated, generated CO and CO_2 levels vary between the sample groups, whereas the trials of chips generate the most gas. In Figure 4.8 the temperature development of the different trials was presented. It was observed that the first trial of loose chips varied profoundly from the others. However, if only looking at the second and third trial of chips, the STD% of CO_2 is still 19.02 %, 1 % lower than for the three trials combined. For CO the STD% for the second and third trials became 18.63 %, 1 % higher than for the three trials combined. Hence, the first trial did not seem to increase the variation. Numbers are obtained from Tables 4.2 and 4.3.

Compared to uniaxial briquettes, the average CO_2 formation from all three trials of chips is 138 % and compared to MPT briquettes, the amount is 733 %. Looking at the graphical representations of FTIR raw data in Section 4.2, it is observed that all materials have a rapid increase in CO_2 generation occurring around 300 °C, and all materials generate one prominent peak. However, the decrease in CO_2 formation is more differentiated between the materials. All trials of loose chips and the second and third trials of uniaxial briquettes have a rapid decrease followed by a slack decline. The first trial of uniaxial briquettes and the MPT trial have an instant stop in CO_2 generation with gas levels dropping fast. Regarding CO generation, the generation from chips is 133 % if compared to uniaxial briquettes and 888 % if compared to MPT briquettes. Numbers are obtained from Tables 4.2, 4.3, and 4.4.

Investigating the CO/CO_2 ratios for the different material groups, the average ratio is lowest for the MPT briquettes, followed by the uniaxial briquettes. The loose chips had the highest average ratio, as observed in Table 4.5. The integrated oxygen levels had the

opposite trend with 205 % oxygen in the uniaxial briquettes trials and 488 % oxygen in the MPT briquettes trials if compared to loose chips trials. Therefore, in the briquettes trials, there must have been relatively more oxygen per available organic mass and amount of produced gas. The abundance of oxygen can have led to an oxidative atmosphere in the furnace where CO gas can be oxidised to CO_2, further lowering the CO/CO_2 ratio. The loose chips, having a higher availability of organic mass, could produce more CO gas, which would not be oxidised due to less available oxygen. This can result in higher CO/CO_2 ratios for the briquettes than for the loose chips.

There was also some variation between the CO/CO_2 ratios in between the trials of the same sample materials. For the uniaxial briquettes, the maximum peak value varied between 0.20 and 0.94. One reason for this could be the variation in how fragile these briquettes were. Some fell apart, partly and thoroughly, before and during the treatment, resulting in material conditions more or less like the loose chips, which had higher CO/CO_2 ratios. However, the ratios for the chips varied as well, with the highest ratios between 0.51 and 1.12. Packing the chips in the crucible could be a reason since variation in filter placement when making the doughnut could have occurred. The filter was also reused for all trials and could have gotten clogged even if this was not observed. The highest peak value for the MPT briquette trial was only 0.30.

For all graphical representations of the CO/CO_2 ratios, in Figures 4.9, 4.10, and 4.11, it is observed wave-like graphs. For the trials of chips, it is clear that each trial first has one small peak, followed by a valley and another larger peak. Even though the difference in scission and combustion regimes was difficult to observe in the raw data plots, it becomes clearer through the CO/CO_2 ratios. However, the first peak of CO_2 in the raw data plot corresponds to the scission regime, described in Section 2.6.2, the second slow decline could correspond to the combustion regime even if it is not showing as a peak. These trends are compared in Figure 5.3.

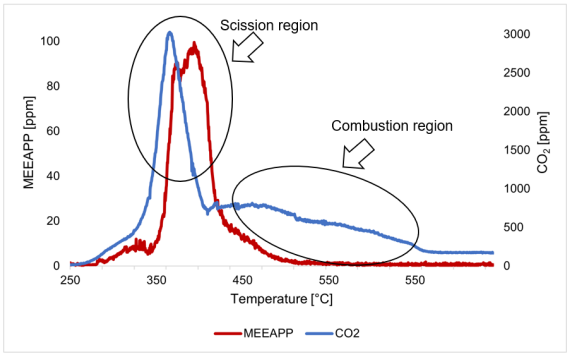

(a) CO_2 and MEEAPP for chips (1)

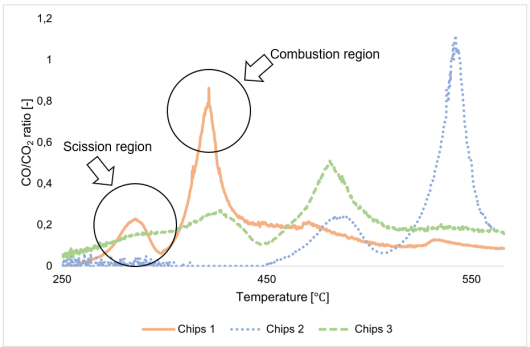

(b) CO/CO_2 ratio chips

Figure 5.3: Possible scission and combustion regimes

The wave-like graph indicates that two-stage combustion may have occurred throughout the thermal treatment, with scission followed by combustion. The first peak is less prominent for the uniaxial briquettes, observed in Figure 4.10, and for the first trial of uniaxial briquettes, the first peak is larger than the second. For all trials, the uniaxial waves are more uniform than in the trials of chips. This indicates a more consistent behaviour in gas formation. For the MPT briquettes, in Figure 4.11, two similar peaks are observed in terms of maximum value and width. In addition to the more oxidative environment for treating these briquettes, the small scission peak for the uniaxial briquettes indicates less scission, perhaps in relation to the less available coating. An equal ratio between the gas evolution makes the regimes similar for the MPTs.

5.1.6 Global warming potential and heat of combustion in off-gases

Thermochemical conversion converts organic mass to valuable and convenient gaseous fuels with useful heating values, denoted by the possible heat of combustion. At the same time, the global warming potential of these gases is typically higher than for CO_2 and hence are undesired as off-gases if released into nature. Thus it is desirable to yield products with low GWP if they are to be emitted, while it is preferred to yield products with a high heat of combustion if captured and used. The GWP was calculated from the amounts of CO_2, CO, N_2O, methane, ethane, and propene in the off-gases of each trial. The combined heat of combustion was calculated from generated amounts of CO, methane, ethane, propane, ethene, and propene.

Regarding GWP, it would be preferred to have complete combustion of the organic material and yield CO_2, as CO_2 has lower GWP than both CO and the hydrocarbons[35]. It is also preferred to get a generation of ethane and propane rather than methane due to the higher GWP of methane. It would thus be very undesirable to get methanation leading to an improved methane formation. The methanation reaction can be fuelled by both CO_2 and CO; hence it would also lower the number of combustion products with the lowest GWPs[32]. If possible, reduced hydrogen formation would also be feasible to decrease methanation, for instance, by reversed WGSR[31].

If CO_2 is preferred over CO, the MPT briquettes would be better than uniaxial briquettes and chips. This is due to a more significant available oxygen concentration, resulting in both complete combustion and also oxidation of generated CO gas, giving a lower CO/CO_2 ratio. Results from the trials, in Table 2.3, showed that the MPT briquettes obtained the lowest maximum and integrated values for GWP. However, the MPT briquettes generated small amounts of gas, and 34 % of the MEEAPP generated was methane, while the generation of ethane and propane was 0. This is undesired as

methane has a higher GWP than ethane and propane. For the uniaxial briquettes, the methane fraction of the MEEAPP was 31 %, and for the chips, 32 %, so the fraction of methane formation was most significant for the MPT briquettes.

Looking at the formation of N_2O, which has the highest GWP of the compounds investigated, the chips generated, as a total integrated average, 971.6 ppm ± 18.1 %, the uniaxial briquettes generated 731.5 ppm ± 34.0 %, and the single MPT briquettes trial generated 91.2 ppm. Lower amounts of N_2O would be highly desired. However, the lower value for MPT briquettes does not necessarily mean that this material is preferred due to the lower overall gas formation where the relative N_2O amount was < 0 % due to very high amounts of oxygen. Uniaxial briquettes, which had more similar off-gassing amounts compared to chips, obtained lower N_2O concentrations than chips which are feasible. The standard deviation was, however, twice the STD% of chips. Nevertheless, it must be pointed out that after-burning of gases is standard procedure in the industry. Hence, these gases would not have been emitted in a real system[3]. The calculations on GWP are thus only presented to give a perspective on the potential harm if they were discharged.

Regarding heat of combustion, which is relevant for after-burning, hydrocarbons are preferred above carbon monoxide and significantly above carbon dioxide due to higher heat values. Out of the compounds in consideration, methane has the highest heat of combustion and would therefore be preferred. It would thus be desirable with a reducing atmosphere so that CO gas is not converted to CO_2 and also desirable with methanation and methane formation. This is conflicting advice compared to process parameters for lowering the GWP. From the resulting values of heat of combustion, the chips had both the highest average maximum value and the highest integrated value, observed in Table 4.7. However, the second and third trials of uniaxial briquettes had the highest maximum values for single trials and the second and third highest integrated values.

The higher values can be due to the second trial of uniaxial briquettes having higher generated gas values for ethene than the third trial of chips. The third trial of uniaxial briquettes generated higher amounts of methane than the third trial of chips, observed in Tables 4.2 and 4.3. As methane and ethene have the highest values for the heat of combustion, the amounts of these gases contribute more significantly to the total heat of combustion than, for instance, the amount of propene. The second trial of uniaxial briquettes had, nevertheless, the highest generation of propene of all trials, and this can also have contributed to the high total heat of combustion. The MPT briquettes generated a small number of gases with useful heating values due to low overall gas production. In an ideal system, it could be desirable to use the combustion heat of the generated gases to operate the pyrolysis by providing the needed energy. Calculations

regarding the energy demand during pyrolysis have not been conducted here.

5.1.7 Weight and colour changes during thermal treatment

As a result of the thermal decoating in the FTIR trials, the samples changed colours and experienced a mass reduction. Regarding colour, the material transformed from dark grey-brown and light grey to black, white, and yellow. In the project work before this master's thesis, which treated the same material as sheets in air, bright yellow and white colours were only obtained for materials either treated for a prolonged time at 550 °C or high temperature. It was concluded that the bright colours were a sign of complete decoating due to their close correlation to the weight reduction. On the other hand, dark brown colours were a sign of incomplete combustion, and shades of black were not observed. In the present study, the chips generally resulted in more bright colour changes. The interior was not possible to investigate for the briquettes, but the outside surfaces of the briquettes were generally darker than the chips.

Kvithyld et al. observed coatings turning black during the scission regime of thermal treatment and concluded that the black phase was char or tar with inorganic particles[6]. The black material observed in the present study was probably also chars resulting from incomplete combustion after the scission. These results indicate that the chips observed a more complete decoating due to the brighter colour. However, it was also observed that the chips placed higher up in the crucible obtained more significant colour changes. This can indicate that chips closer to the top experienced a more thorough decoating than chips further down. This can also be related to lower oxygen availability down in the crucible as the chips there were shielded from the process gas by the chips above.

Regarding the weight changes, only one batch of each material type was weighted before and after FTIR thermal treatment, but these results indicate a similar trend to the decoating experiments of Vallejo-Olivares et al. which explored the decoating of compacted briquettes in air[28]. The MPT briquettes had the lowest weight decrease both in that study and the present study. In the present study, the chips experienced the most significant weight decrease, while in the study of Vallejo-Olivares, the uniaxial briquettes had the highest weight reduction. A significant difference between the studies is the amount of treated sample material. Each briquette in the Vallejo-Olivares study weighed 20 g, while each briquette in the present study weighed 50 g, and 500 g of sample was treated simultaneously. If the compaction was one of the reasons for decreased gas formation, this could correlate with reduced weight reduction. With more material in each briquette, it is also reasonable that more organic material was trapped, resulting in a lower relative decrease.

Regarding decoating efficiencies for sheets, calculated in the project work, the highest efficiency was obtained after treatment for 20 minutes at 550 °C resulting in 72.52 %, while the lowest efficiency was 45.03 % obtained after 5 minutes of treatment at 450 °C. From the present study, the highest efficiency was obtained for the chips with 64.2 %. Thus, all materials in the present study have lower efficiencies than the highest efficiency found by the project work. However, the lowest efficiency in this study was 54.9 % which is higher than the lowest efficiency previously found. This shows that the stoichiometric thermolysis in the present study was more efficient than thermal treatment in air at 450 °C for 5 minutes but less effective than thermal treatment in air at 550 °C for 20 minutes.

5.1.8 Effects of pyrolysis as decoating strategy

Industrial decoating is typically conducted in a rotary kiln with temperatures between 450 and 600 °C, with a short heating time and oxygen concentration below 8 % to reduce the risk of oxidation[25] [3]. The trials of the present study show some similarities to this but had small amounts of material treated simultaneously. The material was at rest during treatment, and two material groups were compacted. In the FTIR trials, it was detected that almost all gas formation occurred before reaching the 30 minutes holding time at 550 °C, so that shorter holding time could have been applicable even at this temperature. At the same time, it was observed that for some trials, the CO_2 concentration was still high (about 500 ppm) at the end of the reaction interval and thus, a higher CO_2 amount could have been achieved for more extended treatment time. However, if the goal is to collect gases with useful heating value, collecting CO_2 is no use.

After treatment, it was observed residues on the coating surface. Some of this has to originate from inorganic particles, which are known to be in the coating. However, the black colour can indicate incomplete removal of organic material and carbon residue. Compared to previous trials with the same material and the TGA analysis, the weight change and decoating efficiencies have lower values, indicating less coating removal.

Previous decoating trials with this material have been executed in air. The TGA analysis had a relative higher oxygen concentration than the FTIR trials, despite the same oxygen percentage, due to a smaller amount of material in treatment. The presence of oxygen can thus lead to higher decoating, but the compromise between higher decoating and possible oxidation must be considered. The amount of material treated in the FTIR thermal treatments was much higher than in previous studies and during TGA. This can affect the coating removal regarding oxygen availability and ease of gas transportation through the sample mass. Another factor to consider is the usefulness of the evolved pyrolysis gases compared to the lower decoating efficiency. If the gases can be collected,

used constructively, and have useful heating values, this can be favourable to pyrolysis as a decoating method.

Other decoating methods could have been chosen. Wang, Rabah, and Li and Qui introduced leaching methods and combined thermal treatment and leaching, resulting in decoating efficiencies up to 100 %[34] [33] [21]. With results of decoating efficiencies around 60 % in the present study, pyrolysis alone sounds unfeasible. However, higher decoating efficiencies would be probable also in this study if leaching had been applied after pyrolysis. The methods are thus not wholly comparable. To consider best practices, oxidation, decoating efficiency, and valuable byproducts must be considered.

5.2 Remelting trials

5.2.1 Process control and oxidation

Remelting of coated, not thermally treated material resulted in excessive formation of soot and smoke, a typical problem and safety hazard when remelting coated and greased scrap. Combined with the flaming during charging, this resulted in difficult process control due to challenges in keeping a stable temperature. Since it was difficult to see the melt through the smoke, charging also became more difficult. Charging times thus became longer for coated material. From an operational perspective, the thermally treated samples were much preferred due to easier charging conditions as the decoating process was finished in advance.

Another problem with the flaming and thus varying temperature during charging of coated materials is that higher temperatures can result in excessive oxidation of the aluminium, and aluminium in the form of oxides cannot be reprocessed into metallic aluminium. Aluminium melts will be highly reactive with oxygen and oxidise, significantly above 727 °C and firmly above 780 °C[1]. During the remelting trials in the present study, the molten aluminium metal was heated to 780 °C before de-drossing and 750 °C before charging, which are temperatures where oxidation can be substantial. However, the trials were executed below a protective argon atmosphere which can have protected the melt from oxidation. During charging and heating before de-drossing, the dross itself could work as protection, but it could just as easily have contributed to metal loss through the entrapment of metal. Trials at lower temperatures were not executed, so oxidation due to high temperature and flaming during the charging of coated material can not be concluded.

On the other side, the materials being de-coated during the controlled FTIR thermal

treatments had a stricter temperature control and a maximum temperature of 550 °C, which is at the recommendation temperature of Steglich for successful decoating and reduced oxidation possibilities[25]. In comparison, the material being de-coated during remelting experienced a more varied temperature regime. During sample charging, the melt had a temperature of 750 °C, 200 °C higher than the controlled thermal treatments at recommended temperatures. The exact surface temperature of the melt was not measured, but the high melt temperature indicates high temperatures also on the surface. Stevens found that carbon powder on the aluminium surface seemed to protect from oxidation, indicating reduced oxidation in the thermal treatment FTIR trials as a carbon residue was observed after treatment[37]. This would be feasible compared to the uncontrolled burning of the coating during charging, where it is difficult to say if coating residues, or the coating itself, could serve as protection against oxidation. Note that the magnesium concentration of Stevens' trials was relatively high and could have been a reason for improved oxidation.

Oxidation during remelting could also occur due to reactions between the molten aluminium and oxides in the melt or oxygen-containing gases in the melting chamber, as described in Section 2.3.5[1]. The project work found that the coating on the aluminium sheets contained both silicon- and titanium oxides. These oxides could have reacted with the aluminium melt during remelting, resulting in aluminium oxides and dissolved silicon and titanium. These elements have a lower affinity to oxygen than aluminium, as seen in the Ellingham diagram, making oxidation of these elements possible. After casting is was observed a white powder in the crucible. The powder could originate from the coating, perhaps from titanium oxide, which is known to be white. The powder was, however, not analysed.

In the FTIR analysis, both carbon monoxide and carbon dioxide were detected, and these gases were probably generated when the coating burned during charging. The aluminium melt could thus react with the carbon gasses, resulting in aluminium oxide and dissolved carbon. As the remelting was executed in an electrical resistance furnace, no combustion gases other than the ones generated by the coating itself could have reacted with the molten aluminium metal. Thus, only the untreated samples could have been oxidised by combustion gases, and not all sample trials, as if the remelting had been executed in a gas-fired furnace, which is sometimes the case in the industry[3].

The prepared briquettes obtained average densities of 2.04 and 2.22 g/cm^3 for uniaxial and MPT briquettes, respectively. Compared to the values stated in Section 2.3.4 these fit quite well. It was observed that the briquettes of this study floated on top of the melt when charged. However, they also had smaller densities than the average aluminium alloy density stated in Section 2.3.4. However, the briquettes had much larger densities than

those reported by Steglich for remelting trials of UBCs[20]. The advantages of briquetting should include reduction in the area-to-volume ratio, which can further decrease the possibility of oxidation and burn-off during thermal treatment, charging and remelting. In these trials, this effect was not specifically investigated by trials of different thermal treatments and analysis of oxides. However, with higher density, the MPT briquettes also had a smaller area-to-volume ratio which could influence the remelting.

5.2.2 Impact of thermal treatment for dross formation

The thermal pretreatment showed little impact on dross formation as thermally treated and not thermally treated samples generated an approximately equal amount of dross. Even though the average values for dross generation were smaller for the thermally treated samples, the standard deviations were large, and differentiation between the trials is not valid. Excess flaming and smoking were observed during the remelting of non-thermally treated samples. The flames can only originate from the coating burning, which happens during the material charging and remelting. The uncontrolled decoating can further be the reason for the similar dross values as both material groups, in practice, were de-coated before remelting, whether controlled or not.

Coatings are, in remelting operations, regarded as contamination and must be removed not to cause impurities in the melt. However, as observed in the present study's thermal treatment, the project work, and from the results of Vallejo-Olivares et al., the coating would not be entirely removed by thermal treatment as possible phases of inorganic particles, and char remained on the surface[28]. These phases may have contributed to the dross generation, regardless of pretreatment or organic burning during charging. In addition to impurities, oxides formed during oxidation significantly contribute to dross formation. As described above, the non-thermally treated samples could have experienced excessive oxidation during the burning of the coating, resulting in oxidation and larger average dross values. However, the difference in dross between the samples is slight. The possible oxidation during the burning of the coating had thus little impact, if it occurred at all.

5.2.3 Differences in dross formation between material groups

Some variation in dross generation between the different material groups can be observed. While the loose chips and uniaxial briquettes have similar values for dross generation, the MPT briquettes stand out with larger dross weights, as seen in Figure 4.23. This difference can be related to the variation in off-gassing during thermal treatments, where

a reduced off-gassing was observed from the MPT briquettes if compared to the other two material groups. Also, the weight loss from thermal treatment was lower for the MPT briquettes. As described earlier, this might be related to the higher compaction of these briquettes making thermal decoating difficult due to unavailable coating, further resulting in a lower burn-off. The reduced decoating would result in more organic material being fed to the melt, increasing the impurity input and oxidation possibilities and resulting in an increased dross formation.

The uncoated loose chips resulted in considerably lower dross amounts than the samples of the coated material. As discussed above, the improved dross formation for the coated material could be caused both by the coating itself and oxidation during thermal treatment and burning of the coating. Since the uncoated material had no coating and experienced no thermal treatment or burning off the coating, it is reasonable that the dross generation is lower. The first trial of uncoated material has 40 % lower dross amount than the dross from the second and third trials. This first trial of uncoated material was the first to be executed of all trials. Thus the dedrossing procedure was less familiar than in the following trials, which could have resulted in too little dross being skimmed off the melt.

It is also worth noting that even though the uncoated material consisted of only pure alloy, it resulted in some notable dross formation. The two aluminium alloys did not have the same composition, even if they were from the same alloy group. The unocated alloy had, for instance, a considerably higher content of magnesium, as seen in Table 3.1. Magnesium has an even higher affinity to oxygen than aluminium, as observed on the Ellingham diagram in Figure 2.1, and will thus oxidise more extensively. Hence, the uncoated alloy sheet could have experienced increased oxidation before use and during charging of the material, resulting in more oxides and improved dross amounts. These observations demonstrate how difficult it is to obtain a high yield and no metal losses during remelting.

5.2.4 Comparison to similar studies

Compared to Steglich's trials on remelting of UBCs and their dross generation, the present trials obtained lower dross amounts. While Steglich reported dross percentages for UBC A and B between 50 and 70 % relative to the sample weight, no trials in the present study exceeded amounts above 30 %. All the dross percentages were calculated with Equation 2.12. The 30 minutes holding time in Steglich's remelting trials and differences in organic content and possible coating composition can be reasons for varying results [24]. In Steglich's trials, the UBC with the highest organic composition (UBC B) resulted in

the most dross. At the same time, it also experienced the most considerable reduction in carbon content and an increase in oxygen content after thermal treatment.

The present study achieved the most considerable dross amounts for the MPT briquettes, which also experienced the least mass reduction through thermal treatment. With the assumptions of a higher organic concentration in these briquettes upon charging, due to lower burn-off, these results correlate even though the exact values vary. Steglich observed a significantly reduced dross formation for UBC material A when the material was treated by thermolysis before remelting[24]. In the results of the present study, this relationship between thermal treatment and dross generation was, unfortunately, not observed. A comparison between dross amounts from this study and UBC material A from Steglich can be observed in Figure 5.4. Numbers for Steglich's trials are read from Figure 2.15 and may be slightly inaccurate.

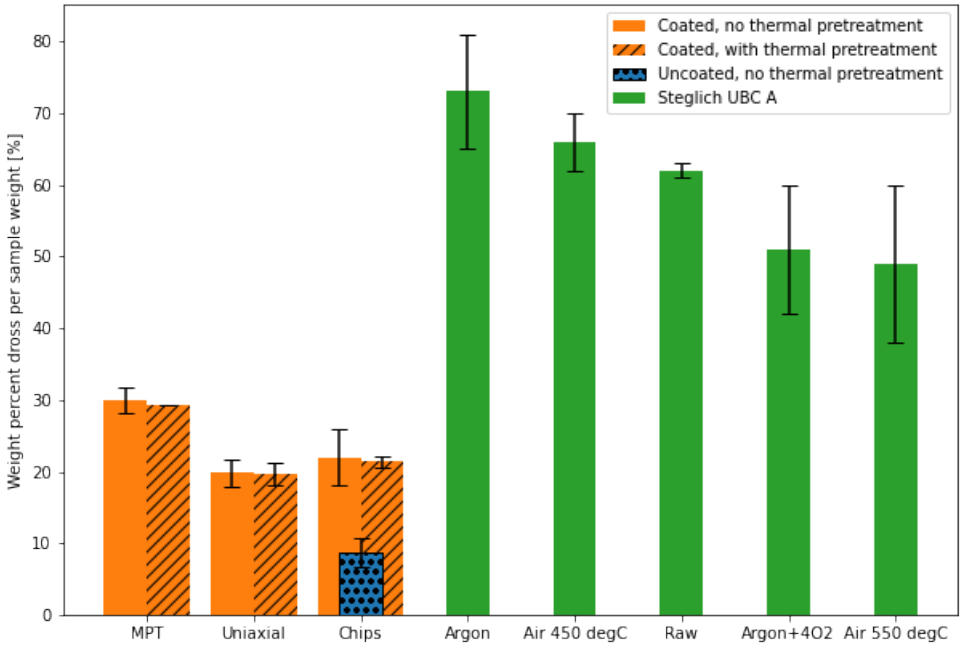

Figure 5.4: Differences in dross formation between the present study and UBC A from Steglich et al.

The level of compaction on Steglich's materials was, however, less intense than in the trials of this study. Where the MPT and uniaxial briquettes of this study had densities of 2.22 and 2.04 g/cm^3, Steglich's UBC A and B had densities of 0.45 and 0.91 g/cm^3 respectively, and UBC C densities of 1.11, 0.81, and 0.69 g/cm^3 [20]. The organic content of the UBC materials was also higher (2.8, 8.4, and 10.0 wt%) compared to the 2 wt% in this study. Also, the size of the samples varied a lot, where Steglich's samples weighted 100 g $\pm$ 1, and the samples in the present study weighed 50 g in addition to being fed in

batches of 1000 g.

5.2.5 Comparison between dross formation and coalescence

In a previous study conducted by Vallejo-Olivares et al., with the same material used in this master's thesis, remelting was conducted under a salt flux and not in molten heel [28]. In that case, dross formation was not used as a measure of effective remelting, but it was observed that the coalescence was highly positively affected by thermal treatment. Compaction alone did not improve the coalescence, and the coalescence was better for thermally treated chips and uniaxial briquettes than for MPT briquettes. This trend can be correlated to the dross generation, where the MPT briquettes generated more significant dross amounts than uniaxial briquettes and chips. Cappuzzi et al. also found a positive effect on thermal decoating for improved coalescence as the thermal treatment removed organics in the material [4].

While the thermal treatment improved coalescence, thermal treatment did not reduce dross generation in this study. However, improved coalescence could also be due to the salt flux itself and especially the oxide-stripping fluorides in the salt mix [19]. For further investigations, it could be interesting to remelt the dross generated in the present study under a salt-flux to extract possible trapped metal, as or in oxides. The uncoated material showed good coalescence and metal yield for all compaction and thermal treatment combinations in the Vallejo-Olivares study and had the least dross generation in these trials.

5.2.6 Remelting yields

The two presented equations for yield were made with some assumptions. For the sample yield in Equation 4.5, it was assumed that since the heel was de-drossed separately before charging of sample material, the sample material caused all dross formation. For the charge yield in Equation 4.6, it was assumed that the casting residue could originate both from the aluminium in the sample and from the aluminium in the heel and thus lower the yield calculated from Equation 4.5.

The obtained numbers for sample yields and charge yield varied, as seen in Tables 4.11 and 4.12. The charge-based yields were higher for all trials, which is reasonable due to small amounts of heel dross resulting in a relative higher aluminium output. The difference is smallest between the yields of uncoated material, which is rational as the sample dross weight for these trials was low, resulting in higher metal outputs. The difference in

yields was highest for not thermally treated MPT briquettes. This can be reasonable as the sample dross weights were largest for the MPT trials, resulting in relatively small amounts of aluminium output after remelting. The high aluminium output from the heel itself profoundly increases the total aluminium yield. To be able to calculate a whole mass balance for the aluminium in the trials, values for aluminium metal content in the dross would be required. However, dross remelting for aluminium extraction has not been conducted at this point.

Calculations on sample yield, which were based on dross values, showed the opposite trend between the samples than what the dross showed. The highest value for sample yield was 0.91 $\pm$ 0.02 obtained for uncoated chips, and the lowest value was 0.71, which was obtained for the single trial of not thermally treated MPT briquettes. The yields show that aluminium is, in fact, not 100 % recyclable in these trials, as there was always a metal loss. The reported 98 % yield in scrap-based aluminium recycling does not seem to fit with the data from these trials, especially not for coated scrap. Not even for uncoated material, the yield was reaching 98 %. However, as Yang described it, cleanliness will improve recovery rates. Therefore, it is reasonable with the highest yield for the uncoated material even if it is lower than the desired [16]. One reason for the yields being lower than what has previously been reported can be the size of the trials. With only 2 kg of material per charge, too much aluminium could have been removed during de-drossing, giving lower yields. It would thus be interesting to remelt the dross and examine the metal content. Extracting the metal in the dross would then increase the total yield.

Some refiners have reported 2-7 % higher yields when remelting compressed material [5]. Regarding the coated material, the increase in yield from chips to uniaxial briquettes of not thermally treated samples was 2 %. However, the average values had overlapping standard deviations and thus cannot be differentiated. Comparing chips with MPT briquettes, the compaction decreased the yield by -8 % on average. Considering standard deviations, the slightest difference in yield was -2 %. Regarding thermally treated materials, the difference in yield between chips and uniaxial briquettes was, on average, 1 % but with overlapping standard deviations. The difference in yield between chips and MPT briquettes was, once again, on average -8 %, with the slightest difference of -7 % when regarding standard deviation. Thus a positive effect cannot be concluded concerning uniaxial compaction, while MTP compaction negatively affected the yield.

Figure 5.5 compares the sample yields of the trials in the present study to the metal yields achieved for the dense (1.1 g/cm^3) trials of UBC material C in the studies of Steglich [24]. It is observed that the yields for uniaxial briquettes and chips of the present study have similar values to those for the stoichiometric thermally treated samples (Thermo) of

Steglich. This corresponds well due to similar treatment parameters. On the other hand, the yield for MPT briquettes is more similar to the yield of samples without thermal treatment (Raw) or samples treated in air (Pyro), but the MPT yields are even lower. This indicates a less effective decoating or possible excessive oxidation leading to metal loss and lower yields. However, the metal yields from Steglich include the metal extracted from the dross and are thus reasonably higher. Note that the values from Steglich were read from Figure 2.16 and can thus be slightly inaccurate.

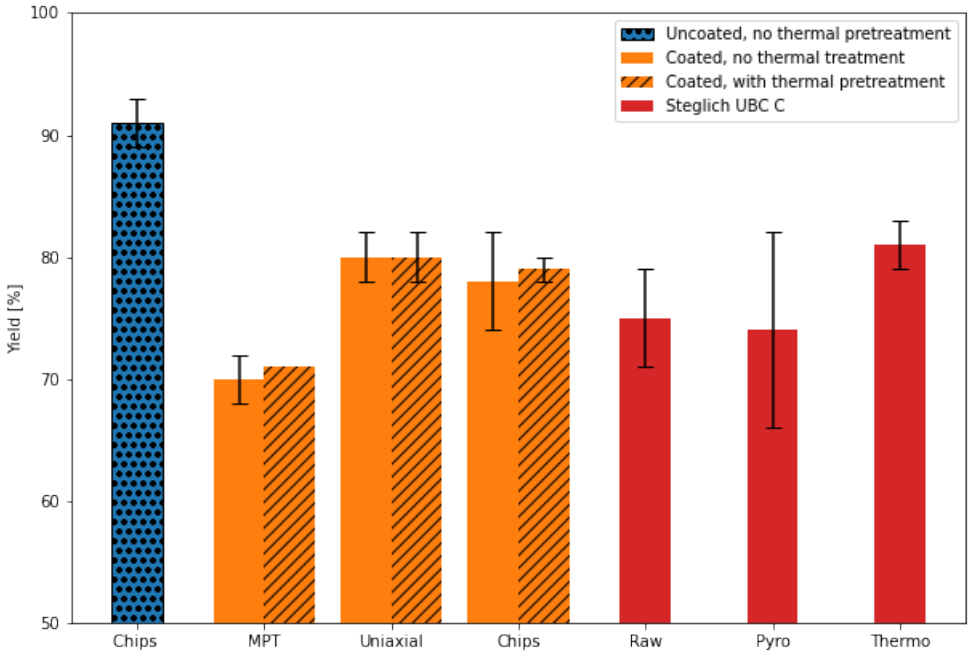

Figure 5.5: Sample yields from present study and metal yields for UBC C from Steglich et al.

Looking at differences in sample yields between thermally treated and not thermally treated samples in the present study, the uncertainty of standard deviations makes it difficult to conclude if thermal treatment is constructive before remelting. Even though coating removal before remelting is both standard and recommended, the results of this study cannot substantiate these previous observations, as the yield does not necessarily increase after thermal treatment.

5.3 Analysis

5.3.1 Analysis of pyrolysis condensate

The GC/MS analysis detected a variety of long-chained hydrocarbons as components of the pyrolysis condensate. All components in the condensate must originate from the pyrolysis gases, which again originate from the coating. Thus, the coating must have been composed of several complex long-chained components, or components which can have decomposed into the ones detected. In Section 2.5 it was described how condensable gases could experience secondary cracking resulting in non-condensable gases and an off-gas mix of primary and secondary gases[7]. The observed condensate and its components show that secondary cracking has not occurred to a full extent. This results in a lower amount of off-gases and further reduces the total heat value of the gaseous products.

If the goal is to use the evolved gases, for instance, in the pyrolysis process itself, it would be desirable with an as high gas amount as possible, which is not obtained in these trials. As discussed in Section 5.1.1 a higher gas formation might have demanded higher temperatures, which was not applicable in this case due to possible oxidation of the aluminium. The gas-sweep transporting gas into the FTIR analysis machine could also have reduced the possibilities of secondary cracking. A lower gas flow could thus have been feasible for increased secondary cracking and further increased gas formation. When the condensable gasses condense on the equipment outlets, this can challenge the pyrolysis operation, which will be another undesired result of the condensate generation.

5.3.2 TGA analysis

The TGA analysis showed an average mass change of -1.69 % $\pm$ 0.03. Compared to the achieved mass change of the FTIR trials, this is a more considerable decrease, by 0.14 % compared to chips, 0.26 % compared to uniaxial briquettes, and 0.37 % compared to MPT briquettes. Compared to the previous study of Vallejo-Olivares, the achieved mass change from TGA is somewhat smaller than the maximal mass change of the 20 g uniaxial briquettes[28]. However, the TGA mass change is more significant than the mass change of chips and MPT briquettes in the Vallejo-Olivares study. As previously discussed, the reduced mass change during FTIR thermal treatment may be caused by increased sample amount, reduced access to oxygen, and larger briquettes, making decoating more challenging. The TGA analysis was executed with reduced oxygen accessibility when compared to the study of Vallejo-Olivares et al. but with more extensive accessibility when compared to the FTIR thermal treatment as the samples were smaller. However,

the oxygen concentration and flow were the same. The TGA mass change shows that even with a reduced oxygen amount, the coated material could have achieved a higher mass change than the FTIR thermal treatment showed, substantiating a reduced decoating during these trials.

Kvithyld et al. measured the DTG curve and evolved gases from a typical hydrocarbon for acrylic coated aluminium with mass spectrometer [30]. In Figure 5.6, Kvithyld's results are compared with evolved CO_2 and MEEAPP signals from the first trial of chips in the present study. In both studies, the CO_2 and hydrocarbon formation occurred simultaneously, and while the hydrocarbon peaks end in steep declines, the CO_2 signals have slow declines.

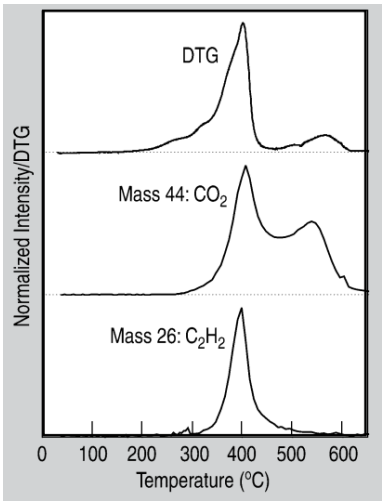

(a) DTG and CO_2 and C_2H_2 signals [6]

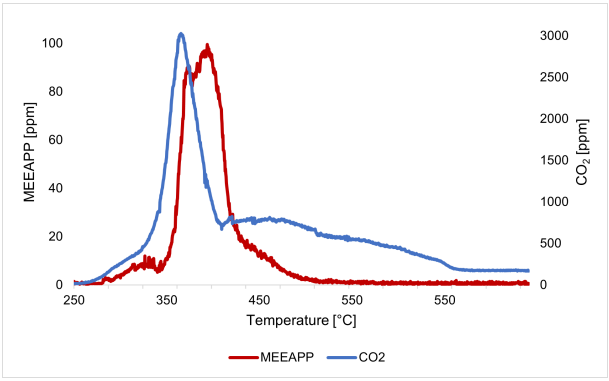

(b) CO_2 and MEEAPP signal loose chips (1)

Figure 5.6: Comparison between the study of Kvithyld et al. and the present study

The decline of CO_2 in the study of Kvithyld results in another second peak, which is not observed in the present study. Regarding mass loss, the DTG curve from Kvithyld has two peaks, while it is impossible, or at least challenging, in the TGA trials of this study (Figure 4.21), to determine if these regimes can be differentiated. However, looking back at the FTIR raw data graphs for the chips and second and third trials of uniaxial briquettes, a slight decrease in CO_2 levels was observed after the prominent peak. This can also be observed for the first chips trial in Figure 5.6. The slow decline, rather than a second peak, could correspond to the combustion regime as illustrated in Figure 5.3.

The plots of CO/CO_2 ratios, in Figures 4.9, 4.10, and 4.11, made the differentiation between the regimes more prominent. Why this is not observable on the mass loss peak could be due to secondary cracking of gases rather than combustion of char which, therefore, is not observed as a second mass loss peak. Note that TGA and DTG are two different analysis methods, where DTG is the derivative of TGA, but a comparison between the

number of peaks should be applicable.

5.3.3 DSC analysis

Section 2.5 presented that pyrolysis reactions are endothermic and occur at relatively low temperatures between 300 and 650 °C. DSC trials indicate one endothermic peak followed by one exothermic peak. However, the endothermic peak in DSC occurs at even lower temperatures than the detectable pyrolysis gas formation in FITR. During DSC analysis, artificial air was used, but the reaction gas was not dried in a gas dryer before usage, and some water vapour might, therefore, have been present in the system. The vaporisation of water is an endothermic reaction and the endothermic peak at low temperature can hence be due to the presence of water in the system.

In Section 2.5 it was also described that combustion reactions are exothermic processes typically occurring at higher temperatures, which could fit with the exothermic peak of the DSC. On one side, the missing combustion TGA mass peak challenges this hypothesis. Conversely, the clear double peaks in the CO/CO_2 ratios can substantiate the relationship between combustion and the exothermic peak. This comparison is illustrated in Figure 5.7.

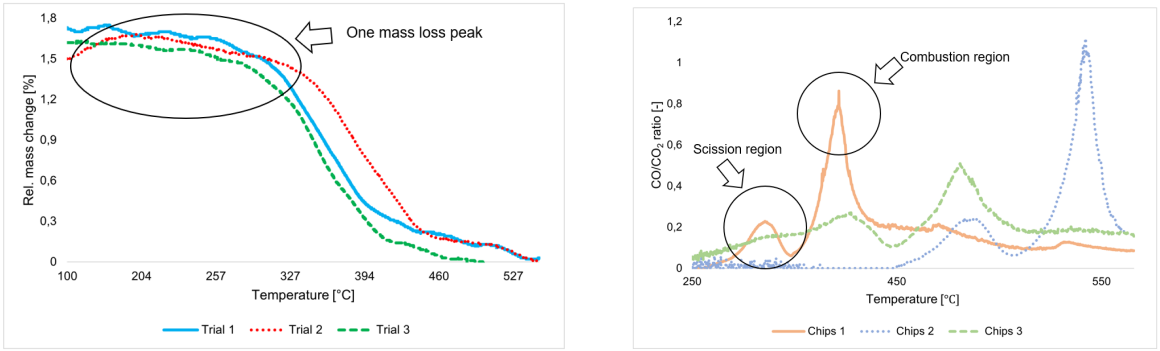

(a) TGA mass loss peak[6] **(b)** CO/CO_2 ratio

Figure 5.7: Comparison between single TGA peak and double peaks in CO/CO_2 ratios

The exothermic peak could also originate from side reactions in the furnace chamber, whereas the WGSR, Boudouard, and methanation reactions are exothermic. However, it was discussed in Section 5.1.4 that the reverse WGSR was more probable, leading to an endothermic reaction. Nevertheless, the endothermic peak in DSC was observed at too low temperatures to correspond to the FTIR off-gassing leading to WGSR. The exothermic peak and possible reactions could lead to increased temperature and harmful oxidation of the aluminium.

The endothermic and exothermic peaks can also be related to the furnace chamber's

lambda ratio and oxygen accessibility. A ratio below 1, having less available oxygen than the required stoichiometric amount, will result in endothermic thermolysis and formation of CO, CxHy, H_2O, and CO_2. A ratio above 1 will, on the other hand, lead to exothermic combustion and CO_2 and H_2O formation. Looking at the FTIR raw data plots, one can observe variation in oxygen amounts which can correspond to variation in the lambda ratio. However, the results vary a lot both in amounts of oxygen and at which temperature it is lowest. The lowest concentration seems to vary between approximately 350 and 550 °C, while the DSC peaks do not seem to be shifted, even if they are more shifted than the mass loss curves of the same trials.

6 Conclusion

This master thesis has investigated the combination of thermal treatment and compaction for optimised aluminium recycling. A coated 8111-alloy material was shredded into chips, whereas some material was kept as chips, and some were compacted to briquettes with uniaxial pressure or with uniaxial pressure and torque (MPT). FTIR thermal treatment off-gas analysis was conducted for half of the coated chips and briquettes samples under a heating rate of 350 °C/h, a target temperature of 550 °C, and a nitrogen atmosphere with 5 % oxygen. Thermally treated and not thermally treated samples were remelted in an argon atmosphere under a molten aluminium heel and dedrossed before casting. Remelting of uncoated chips was also conducted. Pyrolysis condensate from the thermal treatment was analysed with GC/MS. TGA and DSC analyses of mass and heat flux change were also conducted.

6.0.1 Conclusions on thermal treatment

- Thermal treatment of chips resulted in increased amounts of gas formation compared to treatment of uniaxial and MPT briquettes. The total integrated sum of generated gases for chips was 168 % compared to the amount from uniaxial briquettes and 1092 % compared to that of MPT briquettes. These numbers do not include oxygen amounts.
- In absolute values of CO_2 formation, the trials of chips and uniaxial briquettes had maximum generation at approximately 3000 ppm while the MPT briquette trial had 1204 ppm.
- The reason for improved gas formation for chips can be better availability of organic mass. The compaction of the briquettes may have resulted in unavailable organic mass trapped inside the briquette, reducing the possibility of gas formation. Since MPT briquettes had higher compaction than uniaxial briquettes, this trend is more profound for the MPT trial.
- The total integrated values of oxygen show that there was more available oxygen in the trials of briquettes. This can substantiate the reduced combustion due to lower consumption of oxygen.
- The enlarged oxygen amounts can have led to an oxidising atmosphere in the furnace resulting in oxidation of CO to CO_2, further lowering the CO/CO_2 ratios.
- The wave-like appearance of the CO/CO_2 ratios indicate two-stage combustion. This trend was difficult to observe from FTIR raw data and mass change peaks

from TGA.

- Mass change from FTIR was lower than the relative mass loss from TGA analysis. Smaller samples and improved oxygen availability were possible reasons for the increased TGA mass loss.
- The generated gases and their values of GWP and heat of combustion result in conflicting advice for preferred gas emissions. Since after-burning is standard industry practice, gases with high heating value, such as methane, will be preferred.

6.0.2 Conclusions on remelting and dross generation

- The similar dross amounts from remelting trials of coated material showed no substantial reduction in dross generation as a result of thermal pretreatment.
- There was no substantial difference in dross formation between the coated chips and the uniaxial briquettes, but the MPT briquettes generated average higher dross amounts. Higher organic content due to lower burn-off during thermal treatment was presented as a reason.
- The series of uncoated chips resulted in lower dross amounts than the coated materials due to no impurities from the coating and possible lower oxide amounts due to no thermal pretreatment or burning during charging. The relative high dross amount was probably due to higher magnesium concentration in the uncoated alloy.

6.1 Future work

For future work, the last remaining trials of FTIR and remelting should be conducted to obtain more certain data sets. The dross from remelting trials should also be remelted under a salt flux to extract possible trapped metal and further calculate a whole mass balance for the aluminium in the system. The chemical composition of the cast ingots can also be interesting to analyse to see if the presence of coating influences the resulting remelted composition. Another interesting feature would be to investigate the interior of the thermally treated briquettes to check if there is intact organic material inside the briquettes. This could, for instance, be conducted by cutting the samples and analysing the insides with optical microscopy or SEM.

References

[1] D. Raabe, D. Ponge, P. Uggowitzer, M. Roscher, M. Paolantonio, C. Liu, H. Antrekowitsch, E. Kozeschnik, D. Seidmann, B. Gault, F. De Geuser, A. Dechamps, C. Hutchinson, C. Liu, Z. Li, P. Prangnell, J. Robson, P. Shanthraj, S. Vakili, C. Sinclair, L. Bourgeois, and S. Pogatscher. Making sustainable aluminum by recycling scrap: The science of "dirty" alloys. *Progress in Materials Science*, 2022. ISSN 0079-6425. doi: https://doi.org/10.1016/j.pmatsci.2022.100947. URL `https://www.sciencedirect.com/science/article/pii/S0079642522000287`.

[2] O. Edenhofer, R. Pichs-Madruga, Y. Sokona, E. Farahani, S. Kadner, K. Seyboth, A. Adler, I. Baum, S. Brunner, P. Eickemeier, B. Kriemann, J. Savolainen, S. Schlömer, C. von Stechow, T. Zwickel, and J.C. Minx (eds.). *Climate Change 2014: Mitigation of Climate Change. Contribution of Working Group III to the Fifth Assessment Report of the Intergovernmental Panel on Climate Change*. Cambridge University Press, Cambridge, United Kingdom and New York, NY, USA, 2014.

[3] M.E Schlesinger. *Aluminum recycling 1st ed.* CRC Press Taylor & Francis Group, Broken Sound Parkway, NW, 2007. ISBN 0-8493-9662-X.

[4] S. Capuzzi, A. Kvithyld, G. Timelli, A. Nordmark, E. Gumbmann, and T.A. Engh. Coalescence of clean, coated, and decoated aluminum for various salts, and salt-scrap ratios. *Journal of Sustainable Metallurgy*, 4:343–358, 2018. doi: https://link.springer.com/article/10.1007\%2Fs40831-018-0176-2.

[5] C. Hamers and A. Jessberger. Aluminium cycle: Machining, briquetting, melting. `https://global-recycling.info/archives/2354`, 03.2018. Date: 18.05.2022

[6] A. Kvithyld, C.E.M Meskers, S. Gaal, M. Reuter, and T.A Engh. Recycling light metals: Optimal thermal de-coating. *The Journal of The Minerals, Metals & Materials Society*, 60(8):47–51, 2008. doi: https://doi.org/10.1007/s11837-008-0107-y.

[7] P. Basu. *Biomass Gasification and Pyrolyisis*. Elsevier Inc., 2010. ISBN 978-0-12-374988-8.

[8] J.K. Solberg. *Teknologiske metaller og legeringer*. NTNU Institutt for materialteknologi, 2017.

[9] B. Gleeson. Thermodynamics and theory of external and internal oxidation of alloys. *Shreir's Corrosion*, pages 180–194, 12 2010. doi: 10.1016/B978-044452787-5.00012-3.

[10] W.J. Rankin. *Minerals, Metals and Sustainability*. CRC Press/Balkema, 2011. ISBN 978-0-415-68459-0.

[11] S. Senanu, A. Solheim, and E. Skybakmoen. Sju veier til grønnere aluminium. https://www.sintef.no/siste-nytt/2021/sju-veiertilgronnere-aluminium/, 02.07.2021. Date: 18.05.2022

[12] M. Stacey. Aluminium recyclability and recycling, 2015.

[13] European Aluminium. Recycling circular economy. https://european-aluminium.eu/policy-areas/recycling-circular-economy/, 2021. Date: 11.12.2021

[14] M.J. Wang. The environmental footprint of semi-fabricated aluminium products in north america, 2022.

[15] European Aluminium. Recycling rate of aluminium beverage cans. https://european-aluminium.eu/data/packaging-data/recycling-rate-of-aluminium-beverage-cans/, 2021. Date: 12.12.2021

[16] M. Nilmani and W.J. Rankin, editors. *Aluminium Recycling: Scrap Melting and Process Simulation*, July 2005. John Floyd International Symposium. doi: https://www.researchgate.net/profile/Markus-Reuter/publication/270431103_Aluminium_Recycling_Scrap_Melting_and_Process_Simulation/links/54aa4b0c0cf257a6360d65e8/Aluminium-Recycling-Scrap-Melting-and-Process-Simulation.pdf.

[17] A.J.R. Bauer and C. Laska. Libs for automated aluminium scrap sorting, 2018.

[18] SECOPTA. Mopalibs. https://www.secopta.com/products/mopalibs-recycling. Date: 18.05.2022

[19] S. Besson, A. Pichat, E. Xolin, P. Chartrand, and B. Friedrich. Improving coalescence in al-recycling by salt optimization. *European metallurgical conference*, pages 1–16, 2011. doi: http://www.metallurgie.rwth-aachen.de/new/images/pages/publikationen/besson_emc2011_id_5418.pdf.

[20] J. Steglich, R. Dittrich, G. Rombach, M. Rosefort, B. Friedrich, and A. Pichat. Dross formation mechanisms of thermally pre-treated used beverage can scrap bales with different density. In A.P. Ratvik, editor, *Light Metals 2017*, pages 1105–1113, Cham, 2017. Springer International Publishing. ISBN 978-3-319-51541-0.

[21] N. Li and K. Qui. Study on delacquer used beverage cans by vacuum pyrolysis for recycle. *Environmental Science & Technology*, 47(20):11734–11738, 2013. doi: https://pubs.acs.org/doi/10.1021/es4022552.

[22] A.A. Tracton. *Coatings Technology Handbook, Third Edition*. CRC Press Taylor & Francis Group, Broken Sound Parkway, NW, 2006. ISBN 1-57444-649-5.

[23] M. Gökelma, F. Diaz, I.E. Öner, B. Friedrich, and G. Tranell. An assessment of recyclability of used aluminium coffee capsules. In A. Tomsett, editor, *Light Metals 2020*, pages 1101–1109, Cham, 2020. Springer International Publishing. ISBN 978-3-030-36408-3.

[24] J. Steglich, B. Friedrich, and M. Rosefort. Dross formation in aluminum melts during the charging of beverage can scrap bales with different densities using various thermal pretreatments. *JOM*, 72:3383–3392, 2020. doi: https://doi.org/10.1007/s11837-020-04268-4.

[25] J. Steglich, C. Matthies, M. Rosefort, and B. Friedrich. Behavior of mg-si-rich phases in aluminum can sheets and their impact on metal oxidation during industrial thermal pre-treatment. In O. Martin, editor, *Light Metals 2018*, pages 1123–1130, Cham, 2018. Springer International Publishing. ISBN 978-3-319-72284-9.

[26] C. Beyler and M. Hirschler. Thermal decomposition of polymers. *SFPE Handbook of Fire Protection Engineering*, 2:112–143, 01 2002.

[27] S. Capuzzi, A. Kvithyld, G. Timelli, A. Nordmark, and T.A. Engh. Influence of coating and de-coating on the coalescence of aluminium drops in salt. *Light Metals 2017*, pages 1115–1121, 2017. doi: https://doi.org/10.1007/978-3-319-51541-0_134.

[28] A. Vallejo-Olivares, S. Høgåsen, G. Tranell, and A. Kvithyld. Effect of compaction and thermal de-coating pre-treatments on the recyclability of coated and uncoated aluminium. *Light Metals 2022, The Minerals, Metals & Materials Series*, 2022. doi: https://doi.org/10.1007/978-3-030-92529-1_134.

[29] C.E.M Meskers, M.A Reuter, U. Boin, and A. Kvithyld. A fundamental metric for metal recycling applied to coated magnesium, 2008.

[30] A. Kvithyld. The recycling of contaminated al scrap, 2011.

[31] Science Direct. Water gas shift reaction. `https://www.sciencedirect.com/topics/engineering/water-gas-shift-reaction`, 2018. Date: 04.05.2022

[32] Science Direct. Methanation. `https://www.sciencedirect.com/topics/engineering/methanation`, 1984. Date: 04.05.2022

[33] M. Rabah. Preparation of aluminum-magnesium alloys and some valuable salts from used beverage cans. *Waste Management*, 23(2):173–182, 2003. doi: https://www.sciencedirect.com/science/article/pii/S0956053X02001526.

[34] M. Wang, K. Woo, D. Kim, and L. Ma. Study on de-coating used beverage cans with thick sulfuric acid for recycling. *Energy Conversion and Management*, 48(3):819–825, 2007. doi: https://www.sciencedirect.com/science/article/pii/S0196890406002810?via\%3Dihub#bib16.

[35] S. Solomon, D. Qin, M. Manning, Z. Chen, M. Marquis, K.B. Averyt, M. Tignor, and H.L. Miller. *Climate Change 2007: The Physical Science Basis. Contribution of Working Group I to the Fourth Assessment Report of the Intergovernmental Panel on Climate Change*. Cambridge University Press, Cambridge, United Kingdom and New York, NY, USA, 2007.

[36] Science Direct. Heat of combustion. `https://www.sciencedirect.com/topics/earth-and-planetary-sciences/heat-of-combustion`, 2019. Date: 20.05.2022

[37] D. Stevens, A. Kvithyld, T.A. Engh, and S. Wilson. *Oxidation of AlMg in Dry and Humid Atmospheres*, pages 719–724. Springer International Publishing, Cham, 2016. ISBN 978-3-319-48160-9. doi: 10.1007/978-3-319-48160-9_125. URL `https://doi.org/10.1007/978-3-319-48160-9_125`.

[38] K. Ghasemzadeh, S. Tilebon, M. Nasirinezhad, and A. Basile. Chapter 23 economic assessment of methanol production. In A. Basile and F. Dalena, editors, *Methanol*, pages 613–632. Elsevier, 2018. ISBN 978-0-444-63903-5. doi: https://doi.org/10.1016/B978-0-444-63903-5.00023-6. URL `https://www.sciencedirect.com/science/article/pii/B9780444639035000236`.

[39] A.G Aylward. *SI Chemical Data*. ISBN 9780730302469.

A Calculations of needed oxygen amounts for stoichiometric thermolysis

The calculations for oxygen input in the stoichiometric thermolysis FTIR trials are presented below. The organic content of the input material was estimated to be 2 wt%, based on weight losses obtained during the project work before this thesis, and it was assumed that it consisted of equal amounts of either polyester and epoxy (P/E), or polyester, epoxy, and PET monomer (P/E/PET). With molar masses of these compounds being 166 g/mol, 356 g/mol, and 192 g/mol for polyester, epoxy and and PET monomer, respectively, the average molar masses for these combinations would be 261 g/mol for P/E and 238 g/mol for P/E/PET.

It was further assumed that in the case of thermolysis the following chemical reactions (Equations A.1, A.2, and A.3) would occur with the formation of $\frac{2}{3}$ CO_2 and $\frac{1}{3}$ CO in addition to water vapour. Emission of hydrocarbons were neglected. For the P/E this would result in a need of 13.5 mol O_2 per mol of organic material while for the P/E/PET 11.7 mol O_2 per mol of organic material would be required.

$$\text{Epoxy: } C_{21}H_{24}O_5 + 21O_2 \longrightarrow 14CO_2 + 7CO + 12H_2O \tag{A.1}$$

$$\text{Polyester: } C_8H_6O_4 + 6O_2 \longrightarrow 5CO_2 + 3CO + 3H_2O \tag{A.2}$$

$$\text{PET monomer: } C_{10}H_8O_4 + 8O_2 \longrightarrow 6CO_2 + 4CO + 4H_2O \tag{A.3}$$

Each thermal treatment had an input material of 500 g, corresponding to 10 g of organic material. To calculate the needed amount of oxygen the following equations were used for the P/E combination.

$$\text{Organic material} = \frac{10g}{261g/mol} = 0.038 \text{ mol}$$

$$\text{Required oxygen} = 0.038 \text{ mol} \cdot 13.5 \text{ mol/mol} = 0.517 \text{ mol} = 16.552 \text{ g} = 12.621 \text{ L}$$

The conversions of oxygen input in mol to grams and litres were calculated using the molar mass of oxygen (32 g/mol) and ideal gas volume (24.4 L/mol).

For the P/E/PET combination the calculations were as follows,

$$\text{Organic material} = \frac{10g}{238g/mol} = 0.042 \text{ mol}$$

$$\text{Required oxygen} = 0.042 \text{ mol} \cdot 11.7 \text{ mol/mol} = 0.490 \text{ mol} = 15.686 \text{ g} = 11.961 \text{ L}$$

Process parameters for the thermal treatment included expected start of decomposistion (250 °C), target temperature (550 °C), holding time (0.5 h), and furnace heating rate (350 °C/h). The time frame for reactions through oxygen exposure were calculated as

$$\text{Exposure time} = \frac{550°C - 250°C}{350°C/h} + 0.5 \text{ h} = 1.357 \text{ h} = 81.429 \text{ min}$$

Using an input gas flow of 3 L/min the total gas input in the critical time frame would be

$$\text{Total gas input} = 3 \text{ L/min} \cdot 81.249 \text{ min} = 244.286 \text{ L}$$

This would correspond to oxygen concentrations of

$$\frac{12.621L}{244.286L} \cdot 100\% = 5.17 \text{ \% for P/E}$$

$$\frac{11.961L}{244.286L} \cdot 100\% = 4.90 \text{ \% for P/E/PET}$$

An oxygen concentration of 5 % was chosen.

B Calculations for heat of combustion

Chemical data for calculations for heat of combustion, ΔH_c can be found in Table B.1. Numbers were obtained from the SI Chemical Data 7th edition [39]. Equations B.1 and B.2 were used for calculations. Resulting values for heat of combustion was given in Table 2.3.

Table B.1: Chemical data used for calculations for heat of combustion

Compound	Δ H_f [kJ/mol]	M [g/mol]	mol/kg
O_2	0	-	
H_2O	-242	-	
CO_2	-394	-	
CO	-111	28.01	35.70
CH_4	-74	16.04	62.34
C_2H_6	84	30.07	33.26
C_2H_4	52	28.05	35.64
C_3H_8	-105	44.09	22.68
C_3H_6	20	42.08	23.77

$$\Delta H_c = \Sigma \Delta H_f(\text{products}) - \Sigma \Delta H_f(\text{reactants}) \tag{B.1}$$

$$\Delta H_c[\text{kJ/kg}] = \Delta H_c[\text{kJ/kg}] \cdot \text{mol/kg} \tag{B.2}$$

Combustion reactions for the species in consideration are given in Equations B.3, B.4, B.5, B.5, B.7, and B.8.

$$\text{Carbon monoxide: } CO(g) + 0.5O_2(g) \longrightarrow CO_2(g) \tag{B.3}$$

$$\text{Methane: } CH_4(g) + 2O_2(g) \longrightarrow CO_2(g) + 2H_2O(g) \tag{B.4}$$

$$\text{Ethane: } C_2H_6(g) + 3.5O_2(g) \longrightarrow 2CO_2(g) + 3H_2O(g) \tag{B.5}$$

$$\text{Ethene: } C_2H_4(g) + 3O_2(g) \longrightarrow 2CO_2(g) + 2H_2O(g) \tag{B.6}$$

$$\text{Propane: } C_3H_8(g) + 5O_2(g) \longrightarrow 3CO_2(g) + 4H_2O(g) \tag{B.7}$$

$$\text{Propene: } C_3H_6(g) + 4.5O_2(g) \longrightarrow 3CO_2(g) + 3H_2O(g) \tag{B.8}$$

C Heel dross and casting residue weights

Weights of heel dross and casting residues, and heel dross percentages can be found in Table C.1.

Table C.1: Heel dross weights and percentages and weight of casting residues

Sample	Heel dross [g]	Heel dross [%]	Casting residue [g]
Chips unc	24.0	2.2	18.0
MPT	15.3	1.4	14.1
MPT	18.2	1.7	18.1
Uniax	19.0	1.8	14.3
Uniax	21.1	2.0	13.4
Chips c.	14.4	1.4	13.4
Uniax tt	21.1	2.0	13.3
Uniax tt	16.8	1.6	13.8
Chips c. tt	16.8	1.6	16.2

D TGA and DSC raw plot

Figure D.1 illustrates the raw plot from TGA and DSC analysis.

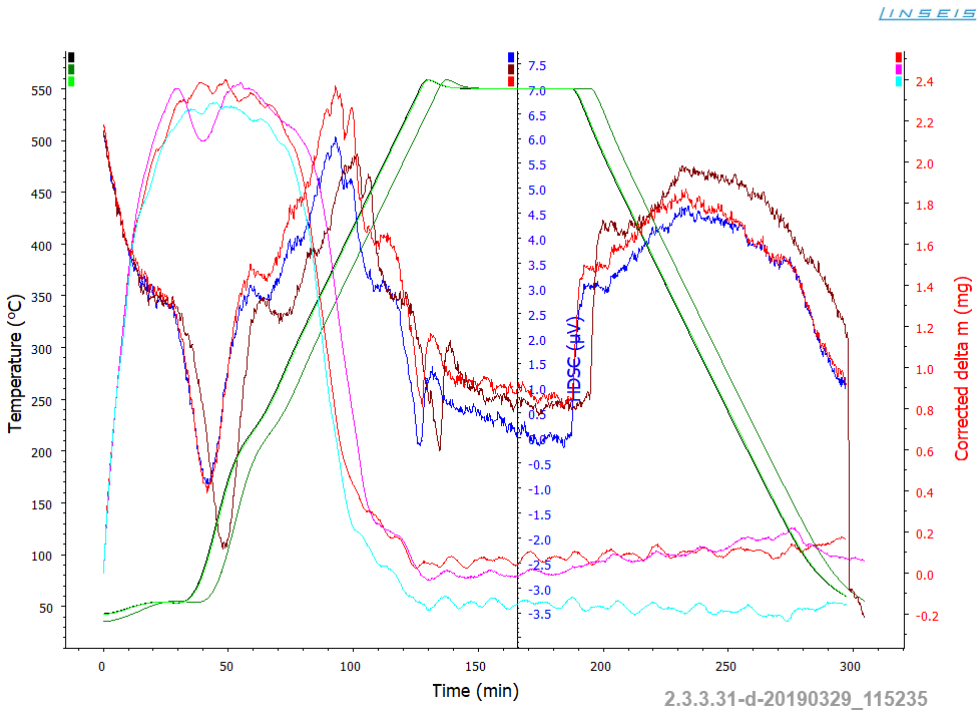

Figure D.1: Raw file of TGA and DSC plot

Solveig Høgåsen

The effect of compaction and thermal treatment in the recovery of coated aluminium scrap

NTNU
Norwegian University of
Science and Technology